

NCAT Report 06-03

METHODOLOGY AND CALIBRATION OF FATIGUE TRANSFER FUNCTIONS FOR MECHANISTIC-EMPIRICAL FLEXIBLE PAVEMENT DESIGN

By

Angela L. Priest
David H. Timm

December 2006



**METHODOLOGY AND CALIBRATION OF FATIGUE TRANSFER
FUNCTIONS FOR MECHANISTIC-EMPIRICAL FLEXIBLE PAVEMENT
DESIGN**

by

**Angela L. Priest¹, Kimley-Horn and Associates, Inc.
David H. Timm, PhD, P.E., Gottlieb Assistant Professor of Civil Engineering
National Center for Asphalt Technology
Auburn University, Alabama**

NCAT Report 06-03

December 2006

“The contents of this report reflect the views of the authors who are solely responsible for the facts and the accuracy of the data presented herein. The contents do not necessarily reflect the official view and policies of the National Center for Asphalt Technology of Auburn University. This report does not constitute a standard, specification, or regulation.”

¹ The majority of the research documented herein was accomplished while A. Priest was a graduate research assistant at Auburn University

ACKNOWLEDGEMENTS

The authors wish to thank the Alabama Department of Transportation, the Indiana Department of Transportation and the Federal Highway Administration for their support and cooperation with the Structural Study at the Test Track. Further, the contributions of R. Buzz Powell, Thomas McEwen, Jennifer Still, Suresh Immanuel, Nicole Donnee, Tara Liyana, Seckin Ozkul and Hunter Hodges were imperative to the completion of this work.

TABLE OF CONTENTS

	<u>Page</u>
CHAPTER 1 – INTRODUCTION	1
Background	1
Objectives	3
Scope	4
Organization of Report	6
CHAPTER 2 – LITERATURE REVIEW	7
Introduction	7
General M-E Design Procedure	8
Fatigue Transfer Function Development	10
Fatigue Failure Mechanism	10
Fatigue Performance	13
General Model Development Procedure	15
Existing Transfer Functions	18
Regression Constant Relationship	20
Dynamic Data and Instrumentation	20
Mn/ROAD	20
Virginia’s Smart Road	22
CHAPTER 3 – TEST FACILITY	24
NCAT Test Track	24
NCAT Structural Study	24
Instrumentation	25
In Situ Conditions	26
Dynamic Pavement Response	28
Data Collection Efforts	30
Dynamic Data Collection	30
Environmental Data Collection	31
FWD Testing	31
Performance Data Collection	32
Concluding Remarks on Test Facility	34
CHAPTER 4 – DYNAMIC STRAIN DATA	35
Introduction	35
Strain Trace Investigation	35
Strain Trace Processing	39
Strain Characterization	44
Data Storage	45
Concluding Remarks on Dynamic Data	46
CHAPTER 5 – METHODOLOGY AND PARAMETER CHARACTERIZATION	47
Introduction	47
Methodology	48
Traffic Characterization	49
Weight Data	49
Lateral Distribution of Loads	50

	<u>Page</u>
Traffic Volume.....	54
Concluding Remarks on Traffic Characterization	54
HMA Stiffness Characterization.....	54
Backcalculated Stiffness Data.....	54
Seasonal Trends	55
Stiffness Prediction Models.....	56
Concluding Remarks on HMA Characterization.....	58
Strain Response Characterization	59
General Trends.....	59
Comparison Between Sections	62
Strain Prediction Models.....	65
Strain Distributions and Endurance Limit	67
Concluding Remarks on Strain Characterization.....	69
Fatigue Performance Characterization.....	69
Observed Fatigue Distress	69
Crack Mapping.....	72
Data Processing and Characterization	74
Failure Criteria.....	76
Concluding Remarks on Methodology and Characterization.....	77
CHAPTER 6 – FATIGUE MODEL DEVELOPMENT	78
Introduction.....	78
Methodology.....	78
Fatigue Model.....	80
Thin Model.....	81
Rich Bottom Model.....	84
Thick Model.....	86
Concluding Remarks on Model Development.....	88
CHAPTER 7 – CONCLUSIONS AND RECOMMENDATIONS	89
Conclusions.....	89
Recommendations.....	90
REFERENCES	92

LIST OF TABLES

	<u>Page</u>
Table 5.1 Axle Weight Data by Truck.....	50
Table 5.2 Regression Analysis for HMA Stiffness – Temperature Relationship	58
Table 5.3 Triple-Trailer Regression Analysis for Strain – Temperature Relationship	67
Table 5.4 Box Trailer Regression Analysis for Strain – Temperature Relationship	67
Table 5.5 Section Failure Data.....	77

LIST OF FIGURES

	<u>Page</u>
Figure 1.1 M-E Design Schematic.....	2
Figure 1.2 NCAT Test Track Facility.....	4
Figure 1.3 Test Section Layout.....	5
Figure 1.4 Truck Fleet a) Triple-trailer b) Box Trailer Test Vehicles.....	5
Figure 2.1 M-E Design Flow Chart.....	9
Figure 2.2 Schematic of Fatigue Cracking Mechanism in Pavement Cross Section.....	11
Figure 2.3 Photograph of Fatigue Cracking.....	12
Figure 2.4 Influence of VFB on Fatigue Life (Monismith et al., 1985).....	14
Figure 2.5 Schematic of Third Point Beam Fatigue Test (Monismith et al., 1985).....	15
Figure 2.6 Error (Predict – Measured Percent Cracking) vs. Damage % (El-Basyouny and Witczak “Calibration,” 2005).....	17
Figure 2.7 Mn/ROAD Facility (“About Minnesota,” 2005).....	20
Figure 2.8 Map of Virginia’s Smart Road (“Virginia’s Smart,” 2005).....	22
Figure 3.1 Aerial Photo of NCAT Test Track.....	24
Figure 3.2 Structural Study Test Section Layout.....	25
Figure 3.3 Schematic of Instrumentation (Timm et al., 2004).....	26
Figure 3.4 In Situ Instruments a) Thermistor Bundle b) TDR.....	27
Figure 3.5 Roadside Box and Datalogger (Timm et al., 2004).....	28
Figure 3.6 Dynamic Gauges a) Asphalt Strain Gauge b) Earth Pressure Cell.....	29
Figure 3.7 Dynamic Data Acquisition Scheme (Timm et al., 2004).....	30
Figure 3.8 FWD Testing and Data Collection.....	31
Figure 3.9 a) Pavement Inspection b) Crack Marking.....	32
Figure 3.10 Camera Apparatus for Crack Record.....	32
Figure 3.11 Crack Map Example.....	33
Figure 3.12 Rut Depth Measurements a) Dipstick b) Automated Pavement Survey Vehicle.....	33
Figure 4.1 Longitudinal Strain Trace – Example 1.....	36
Figure 4.2 Longitudinal Strain Trace – Example 2.....	37
Figure 4.3 Transverse Strain Trace – Example 1.....	38
Figure 4.4 Transverse Strain Trace – Example 2.....	38
Figure 4.5 Transverse Strain Trace – Example 3.....	39
Figure 4.6 Longitudinal Strain Trace a) Before and b) After Moving Average.....	40
Figure 4.7 Strain Amplitude Illustration – Example 1.....	41
Figure 4.8 Strain Amplitude Illustration – Example 2.....	42
Figure 4.9 Strain Amplitude Illustration – Example 3.....	43
Figure 4.10 Strain Processing Window.....	44
Figure 4.11 Effect of Lateral Offset.....	45
Figure 5.1 Illustration of Transfer Function Development.....	48
Figure 5.2 Triple-Trailer Weight Distribution.....	50
Figure 5.3 Statistical Summary of Wheel Wander Data (Timm and Priest “Wheel Wander,” 2005).....	51
Figure 5.4 Wheel Wander Data – AM (Timm and Priest “Wheel Wander,” 2005).....	52

	<u>Page</u>
Figure 5.5 Wheel Wander Data – PM (Timm and Priest “Wheel Wander,” 2005).....	52
Figure 5.6 Average Strain by Truck and Pass.....	53
Figure 5.7 Actual and Backcalculation Cross Section.....	55
Figure 5.8 Seasonal Trend in HMA Stiffness.	56
Figure 5.9 HMA Stiffness vs. Mid-depth Temperature.....	57
Figure 5.10 Seasonal Trends in Longitudinal Strain Data.....	60
Figure 5.11 Transverse vs. Longitudinal Strain.....	61
Figure 5.12 Cumulative Distribution of Strain Ratio.....	62
Figure 5.13 Temperature-corrected Strain Data by Test Section	64
Figure 5.14 Triple-Trailer Strain – Temperature Relationship.....	66
Figure 5.15 Box Trailer Strain – Temperature Relationship	66
Figure 5.16 Strain Distributions.....	68
Figure 5.17 Transverse Cracking in Wheelpath – Section N8.....	70
Figure 5.18 Progressed Fatigue Cracking.....	70
Figure 5.19 Water Ponding Due to Rutting – Section N8	71
Figure 5.20 Extensive Fatigue Cracking in Section a) N1 b) N2	71
Figure 5.21 N2 Crack Map 6/21/2004.....	72
Figure 5.22 N2 Crack Map 6/28/2004	73
Figure 5.23 N2 Crack Map 8/02/2004.....	73
Figure 5.24 N2 Crack Map 10/18/2004.....	74
Figure 5.25 Percent Fatigue Cracking by Date.....	76
Figure 6.1 Strain Cycles for Triple-Trailer and Box Trailer Trucks.....	79
Figure 6.2 Damage Accumulation for Sections N1 and N2	82
Figure 6.3 Monismith and Epps (1969) Laboratory Model Predictions for Sections N1 and N2.....	83
Figure 6.4 AI MS-1 Model Predictions for Sections N1 and N2.....	84
Figure 6.5 Damage Accumulation for Section N8.....	85
Figure 6.6 Damage Accumulation for Section N6.....	87
Figure 6.7 Mean Air Temperature	87

CHAPTER 1 – INTRODUCTION

BACKGROUND

Research and development in the structural design of hot mix asphalt (HMA) pavements over the past fifty years has focused on a shift from empirical design equations to a more powerful and adaptive design scheme. Mechanistic-empirical (M-E) design has been developed to utilize the mechanical properties of the pavement structure along with information on traffic, climate, and observed performance, to more accurately model the pavement structure and predict its life. Although M-E design still relies on observed performance and empirical relationships, it is a much more robust system that can easily incorporate new materials, different traffic distributions, and changing conditions.

The M-E design process is more accurately described as an analysis procedure which is used in an iterative manner. The procedure is used to determine the appropriate materials and layer thicknesses to provide the structural capacity for the required performance period. For flexible pavements, this includes considering the main load-related structural distresses: fatigue cracking and structural rutting.

The M-E design and analysis process, shown conceptually in Figure 1.1, integrates the environmental conditions and material properties of the HMA and underlying layers into the pavement structure. The structure is then modeled using a mechanical analysis program, and the pavement responses are calculated given the axle load and tire configuration. The pavement response is then correlated to performance or cycles to failure, N , through empirically derived transfer functions. The expected traffic or load cycles for the given design life, n , is then included to calculate a damage factor for that particular condition (i.e., particular truck load and configuration along with in situ pavement and climatic conditions). The damage for each condition is typically added together using Miner's hypothesis, shown in Equation 1.1, where the failure criteria is reached when the ratio approaches unity (Miner, 1959):

$$D = \sum_{i=1} \frac{n_i}{N_i} \quad (1.1)$$

where: n_i = Number of load applications at condition, i

N_i = Number of load applications at failure for condition, i

Because the design process is modular, varying degrees of accuracy and sophistication can be used at each step depending on the needs of the design. For example, very specific traffic data can be incorporated, or a crude approximation of equivalent single axle loads (ESAL) can be used. Further, average material property values (i.e., stiffness, Poisson's ratio) can be used, or the design can be divided into seasons with differing properties due to environmental changes and material aging. The process can also incorporate sophisticated mechanical models like finite element models, if so desired.

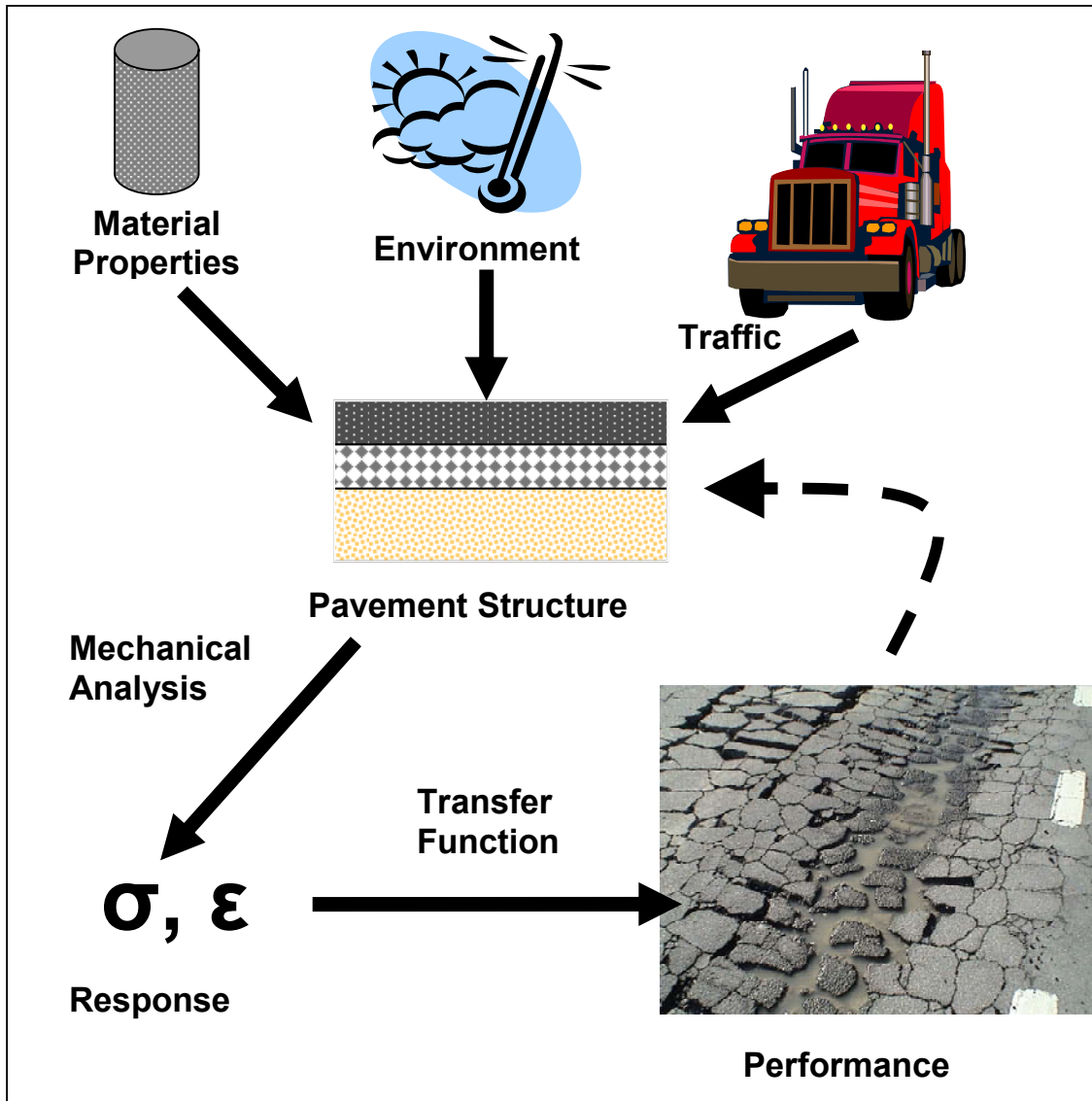


Figure 1.1 M-E Design Schematic.

A particularly challenging piece of the design process is developing the transfer function, or performance equation, that is needed to relate the calculated pavement response (stress, strain) to performance (amount of cracking, rut depth). Fatigue cracking and rutting transfer functions, respectively, typically follow the form of:

$$N_f = k_1 \left(\frac{1}{\epsilon_t} \right)^{k_2} \quad (1.2)$$

$$N_r = k_3 \left(\frac{1}{\epsilon_v} \right)^{k_4} \quad (1.3)$$

where: N_f = Number of cycles until fatigue failure
 ϵ_t = Horizontal tensile strain at the bottom of the HMA layer
 N_r = Number of cycles until rutting failure

ϵ_v = Vertical compressive strain at the top of the subgrade layer
 k_1, k_2, k_3, k_4 = Empirical constants

This research focuses on accurately modeling fatigue distress and developing fatigue transfer functions.

The transfer function is the key to a successful M-E pavement design, and much effort has been devoted to developing useful transfer functions (e.g., Monismith and Epps, 1969; Shook et al., 1982; Timm et al., 1999). Transfer functions can be mix and climate dependent; therefore, local calibration or development is required to account for local materials and conditions.

Most fatigue transfer functions have been developed using laboratory fatigue tests that are then calibrated or shifted to match observed field performance. This process accurately measures the response in the loaded specimen, but is often shifted based on limited field data. Further, the performance equations developed in the lab are dependant on the mode of loading, rest periods, and type of apparatus. In fact, some researchers have argued that there is no accurate way to shift laboratory performance equations to direct field performance because there are too many discrepancies between the field and the laboratory (Romero et al., 2000).

Other functions have been developed using purely observed field performance and calculated pavement response (i.e., Timm et al., 1999). This process, too, has its pitfalls because it relies on the accuracy of the mechanical models and mixture characterization tests. Additionally, the test sections must be closely monitored over a long period of time. Therefore, engineers attempt to speed the process with accelerated load facilities. These facilities use loaded wheels and test strips of varying size to simulate vehicular loading at a controlled and accelerated rate. Yet, even with loaded wheel devices, there are still differences between full-scale conditions and the experiment. Consequently, there is a need to develop transfer equations under representative conditions with accurate response and performance measurements.

OBJECTIVES

Given the above concerns, eight test sections of the National Center for Asphalt Technology (NCAT) Test Track, a full-scale asphalt pavement testing facility, were devoted to a structural experiment to investigate the many integral parts of M-E design. Within the main objectives of the 2003 NCAT Structural Study, the goal of this research was to develop fatigue performance equations for use in M-E flexible pavement design. This included the following tasks and objectives:

- Develop a procedure for gathering, processing, and storing dynamic response data from embedded instrumentation in a useful and concise manner.
- Gather and store environmental data.
- Accurately monitor and quantify field performance.
- Characterize the material properties of the structure including seasonal trends.

- Develop a procedure for incorporating the above efforts into the development of a useful fatigue transfer function that will accurately predict fatigue life to be used in design and analysis procedures.
- Describe the effect of modified binders and thickness on fatigue performance.

SCOPE

The NCAT Test Track (Figure 1.2), located in Opelika, Alabama, is a 1.7 mile oval track designed to test asphalt mixtures and structural designs. The 2003 NCAT Structural Study consisted of eight test sections including three different HMA thicknesses and different asphalt mixtures and binders, shown in Figure 1.3. These sections were designed using the 1993 AASHTO Design Guide for flexible pavements. Further details of the design were documented by Timm et al. (2004). Instrumentation, including strain gauges, earth pressure cells, and thermistors, was installed in the pavement structure to measure pavement responses directly. The test sections were trafficked with a fleet of heavily loaded triple-trailers (gross vehicle weight = 152 kip) and one legally loaded box trailer, both shown in Figure 1.4. In other words, the Test Track was trafficked with real trucks and drivers. Therefore, similar wheel wander and traffic conditions were applied to the Test Track as open-access highways.

One million vehicle repetitions (equivalent to approximately 10 million ESAL) were applied over the 2-year test cycle which began October 2003. Dynamic response data and field performance data were collected on a weekly basis, and environmental data were collected and stored continuously. The test sections were designed to develop fatigue distress during the testing cycle so that a relationship between damage and response could be developed.



Figure 1.2 NCAT Test Track Facility.

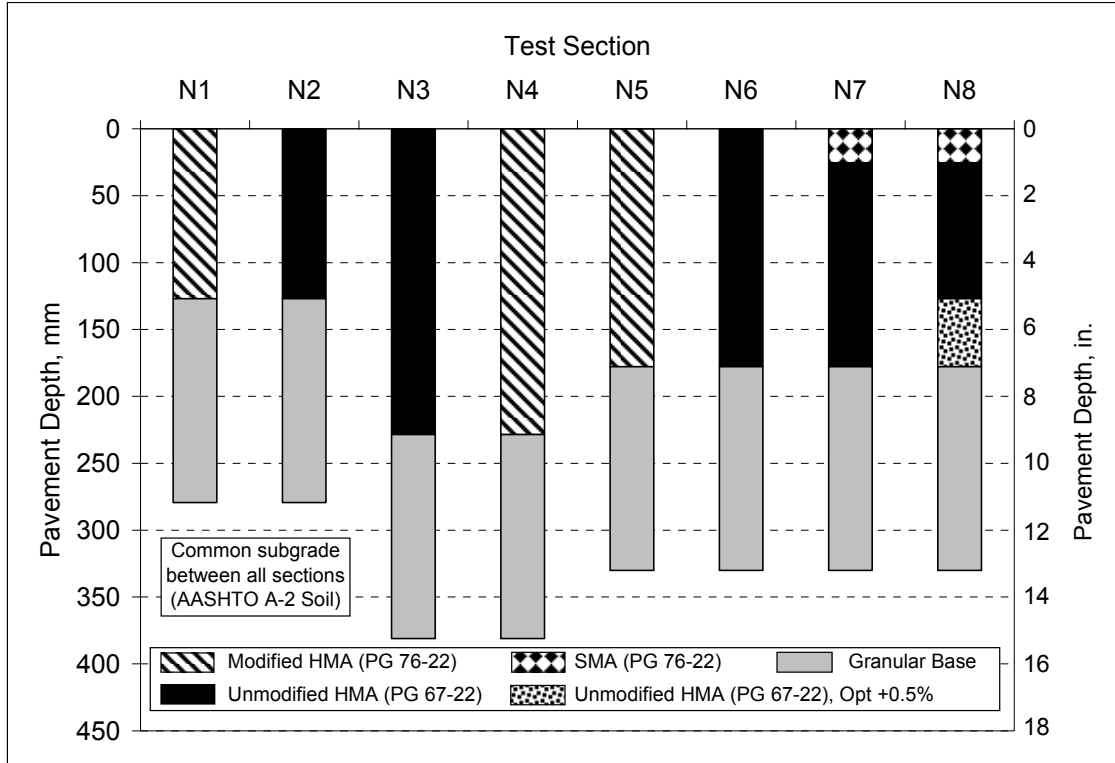


Figure 1.3 Test Section Layout.



Figure 1.4 Truck Fleet a) Triple-trailer b) Box Trailer Test Vehicles.

The structural study allowed for a direct relationship between measured mechanical response and observed field performance. One of the shortcomings of the experiment was that the testing was somewhat accelerated. Because the sections were heavily trafficked, there was not much time for the pavement to age as it might on the highway. Long-term aging will create a stiffer and often more brittle mix, which may cause the mix to be more susceptible to surface cracking. Yet, Harvey et al. (1995) found that long-term aging did not affect the fatigue life of laboratory tested specimens.

An additional limitation is that the experiment, and subsequent conclusions, are somewhat specific to the climate of the NCAT Test Track and the materials used. Thus, the equations and relationships developed are unique, yet useful, to the applicable conditions. The transfer functions developed from the 2003 test cycle will aid the Alabama Department of Transportation (ALDOT), and surrounding states, in adopting an accurate M-E design procedure. Further, the fatigue equation development process developed at the NCAT Test Track can be applied to other states and regions that may want to use full-scale accelerated testing to develop similar transfer functions for their specific climates, materials and mixtures.

ORGANIZATION OF REPORT

A literature review is first presented in Chapter 2 in order to explore the development of fatigue transfer functions and briefly report what other research efforts have discovered. The literature review also contains a section regarding full-scale pavement testing and instrumentation.

Chapter 3 provides more detailed information on the NCAT Test Track facility, 2003 Structural Study, pavement instrumentation and testing effort. Following the Test Facility, Chapter 4 explains the dynamic strain data processing and storage scheme developed for the 2003 Test Track research cycle. It is important to document how the strain measurements were obtained for reference to the rest of the work presented here. Further, detailed information regarding quantifying response from dynamic gauges is not readily available in the literature.

The methodology used to develop the fatigue transfer functions from data collected at the Test Track is then presented in Chapter 5. Also in this chapter is the parameter characterization which includes both the methodology and results.

The final fatigue transfer functions are presented and discussed in Chapter 6. This includes the developed models and discussion of damage accumulation. Additionally, the project status at the time of this report is discussed. And lastly, the conclusions and recommendations are given in the final chapter – Chapter 7.

CHAPTER 2 – LITERATURE REVIEW

INTRODUCTION

Research and development of M-E pavement design has been on-going since the 1960's. Much interest and effort has been devoted to improving the design process and encouraging adaptation by transportation agencies. The movement toward M-E design has received much attention over the past decade because of the many benefits over a purely empirical design method. Some of the advantages include, but are not limited to, the following (Timm et al., 1998; Monismith et al., 1985):

- Improved traffic characterization through load spectra
- Ability to deal with changing load types
- Enhanced definition and measurement of material properties
- Ability to relate material properties to performance
- Accommodation of material aging and environmental changes
- Modular system that allows for enhancement without disrupting the entire process
- Produces a more reliable design
- No longer dependent on the extrapolation of out-dated empirical relationships

Because of the above benefits, many state and federal agencies along with private organizations have developed M-E pavement design procedures in the U.S. and abroad. The Asphalt Institute (AI) and Shell International Petroleum Co. have both developed individual M-E design manuals. Further, other countries have produced full M-E design methods including South Africa (NITRR) and Great Britain through the University of Nottingham (Monismith, 1992). The American Association of State Highway and Transportation Officials (AASHTO) is currently working on an M-E design manual to replace the empirically-based design guide, the 1993 AASHTO Design Guide (AASHTO, 1993). This includes expanding on work done by the National Cooperative Highway Research Program (NCHRP) Report 1-10B and the AI Thickness Design Manual MS-1 (1982) to develop the M-E PDG (Eres, 2004). While this national effort is continuing, many states have developed their own procedures including, but not limited to, Minnesota, Illinois, Kentucky, and Washington State (Timm et al., 1999; "Research and Development," 1982).

The mentioned design guides are similar in their general procedure, but each is unique in how they manage the inputs, calculate pavement response, and relate response to performance. Therefore, many of the procedures were investigated and are presented in this chapter to provide background and relevance to this research, with the main focus on the development and calibration of fatigue transfer functions.

Additionally, one of the important parts of the NCAT Structural Study was the embedded instrumentation in the pavement structure. There are many challenges associated with dynamic pavement instrumentation including installation, construction, data acquisition, data processing and data organization. Other test facilities that have used similar instrumentation were examined to provide insight on how to handle the mentioned challenges. The Minnesota Road Research Project (Mn/ROAD) and Virginia's Smart

Road are both full-scale pavement test facilities with dynamic instrumentation. As a result, their operations, experiences and findings are reported within this chapter.

GENERAL M-E DESIGN PROCEDURE

The basic approach for M-E design includes computing the pavement response over the expected range of loads, i , and environmental conditions, j , using transfer functions to predict performance at each given strain level (set of traffic and environmental conditions) and summing the damage over the expected design life (Monismith, 1992). Damage is often totaled using Miner's hypothesis, where the failure criterion is reached at a value of 1 (Miner, 1959). This equation was shown previously in Equation 1.1. To calculate the pavement response, a pavement cross section must first be assumed, k , and based on the results of the analysis, it can be adjusted to fit the needed conditions. Thus, the pavement is designed with the required structural capacity for the distress mode considered (e.g., fatigue cracking). Figure 2.1 is an M-E design flow chart combining the efforts of others (Timm et al., 1998; Monismith, 1992). It is important to remember that the M-E design framework should be used in conjunction with engineering judgment and experience with specific local issues.

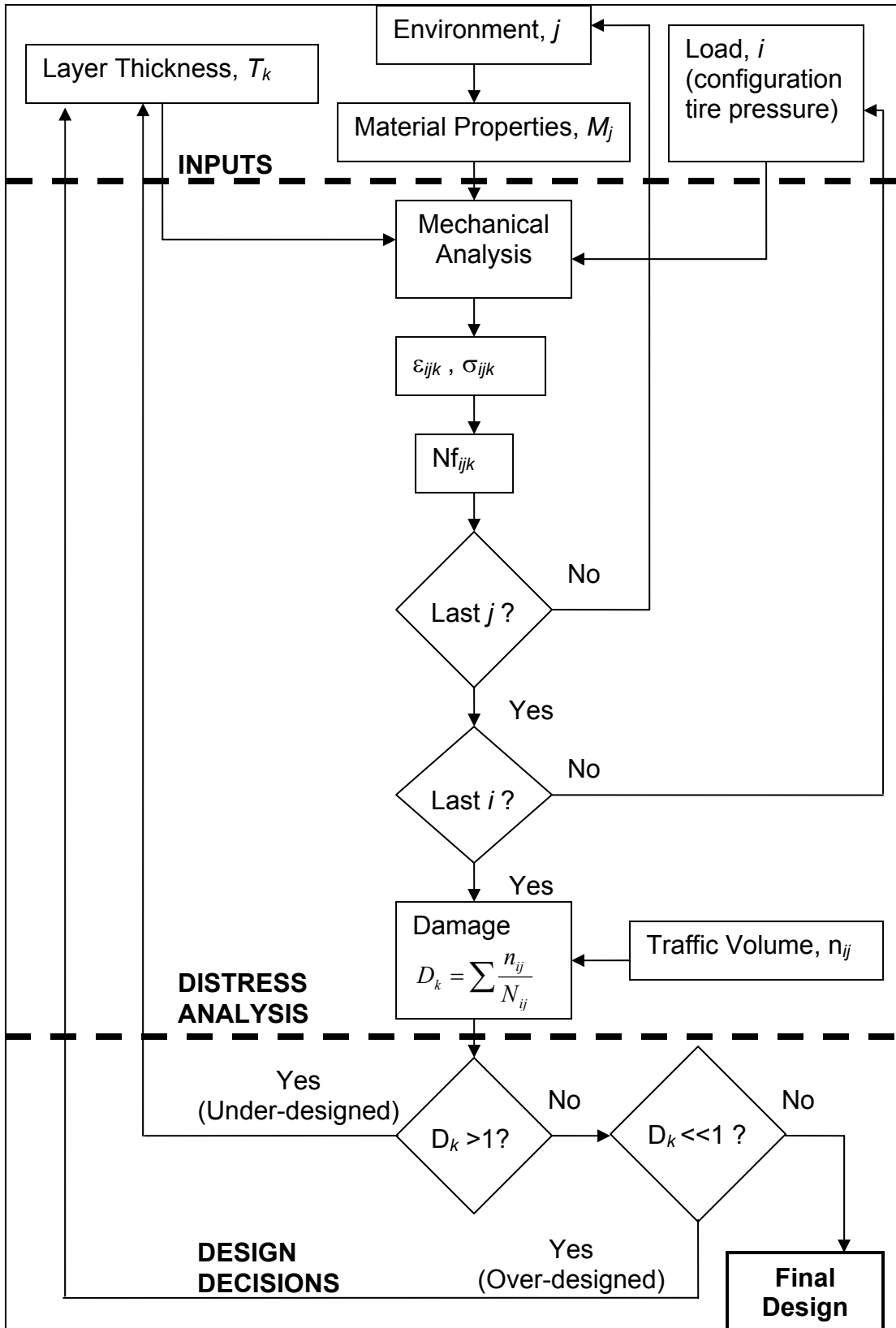


Figure 2.1 M-E Design Flow Chart.

The major components that must be quantified for design are the expected traffic over the design life including volume, configuration, and load; specific seasonal material properties for the HMA and unbound pavement layers; a mechanical model to accurately calculate the pavement response; a transfer function with local calibration for the specific distress mode; and the distress criteria considered “failure”. Refer to Figure 1.1 for a conceptual representation.

As explained prior, each part or component of M-E design is somewhat independent from the entire design process; therefore, each component can have an individual level of complexity or simplicity according to the desired outcome. Further, each component can be improved upon as M-E pavement design evolves. For example, traffic estimates in 18-kip equivalent single axle loads (ESAL) can be used, as was done with the 1993 AASHTO Design Guide and prior. Yet, converting traffic data to ESAL is no longer necessary and is often an invalid oversimplification (Ioannides, 1992). Designers can now take advantage of theoretical models and their ability to calculate response under any tire configuration, load, and tire pressure (Timm et al., 1998). Therefore, many M-E procedures utilize load spectra, which describes the modeled traffic data by axle type, frequency of load magnitude, and tire pressure.

Similar explanations can be made for the other components of M-E design including material characterization, mechanical models and transfer functions. Fatigue transfer functions are the focus of this work and will be described in detail below.

FATIGUE TRANSFER FUNCTION DEVELOPMENT

Fatigue Failure Mechanism

Fatigue cracking is one of the major modes of distress in flexible pavements along with rutting and thermal cracking. It is a significant distress because fatigue cracking propagates through the entire HMA layer, which then allows water infiltration to the unbound layers. This causes accelerated surface and structural deterioration, pumping of the unbound materials and rutting. Pumping may be better known as a rigid pavement distress, but it is observed in flexible pavements with full-depth cracking, fine unbound underlying layers and in the presence of water.

The textbook definition of fatigue theory states that fatigue cracking initiates at the bottom of the flexible layer due to repeated and excessive loading, and it is associated with the tensile strains at the bottom of the HMA layer (Huang, 1993). Shook et al. (1982) explain that the M-E structural design process must limit the tensile strain in the HMA layer in order to control or design against fatigue cracking. Further, the AI MS-1 development manual (“Research and Development,” 1982) refers to ten different M-E design procedures that use the tensile strain at the bottom of the HMA layer as the critical design criteria in regards to fatigue cracking. A schematic of fatigue cracking and the critical response are shown in Figure 2.2 along with a photograph of extensive fatigue cracking shown in Figure 2.3. Fatigue cracking is also referred to as alligator cracking

due to its distinctive pattern; the cracking often looks like the back of an alligator (Figure 2.3).

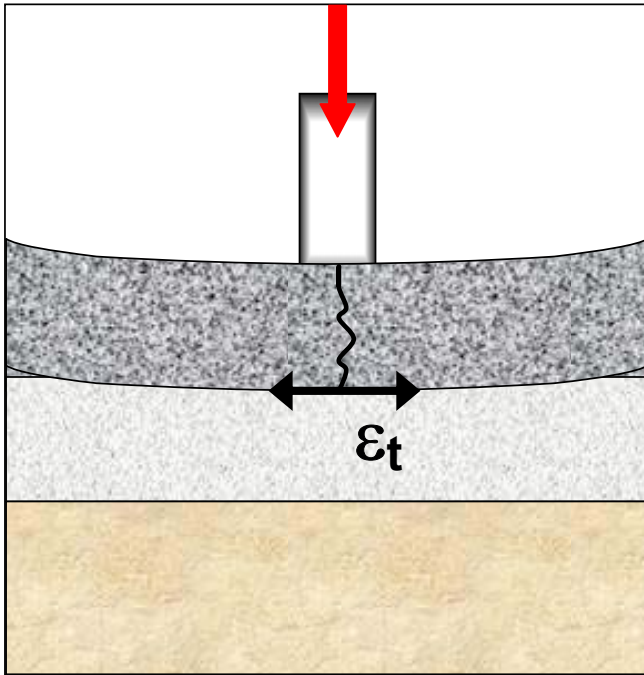


Figure 2.2 Schematic of Fatigue Cracking Mechanism in Pavement Cross Section.



Figure 2.3 Photograph of Fatigue Cracking.

Fatigue distress is defined in the field by measuring the affected pavement area. This area is then typically expressed as a percentage of the total lane area or the wheelpath area. Further, there are different levels of severity to further define the cracking. According to the Strategic Highway Research Program (SHRP) *Distress Identification Manual for the Long-Term Pavement Performance Program* (Miller and Bellinger, 2003), low severity fatigue cracking consists of individual cracks in the wheelpath with no signs of pumping. Moderate severity is reached when the cracks become interconnected, and a high severity rating is given when pumping is evident.

The SHRP distress guide gives a standard on how to measure and categorize fatigue cracking, but it does not recommend a specific failure criteria. It is important in fatigue transfer development to determine at what extent of cracking is considered failure, or in other words, at what point should the damage ratio equal one? It is also important when using established fatigue transfer functions to know what level of damage the functions were calibrated to in order to gauge expected performance.

The transfer functions developed from NCHRP 1-10B were calibrated using data from the American Association of Highway Officials (AASHO) Road Test, conducted in the late 1950's, and considered two levels of cracking as failure. The first calibrated function considered cracking of 10 percent of the wheelpath as failure, and the second considered

greater than 45 percent of the wheelpath. The second failure criterion was reached using the previous function with a multiplier of 1.38 (Monismith et al., 1985). The AI transfer functions (an adaptation of NCHRP 1-10B) were also calibrated using AASHO Road Test data and considered an area greater than 45 percent of the wheelpath or an equivalent 20 percent of the total lane as failure (Monismith et al., 1985; Shook et al., 1982). The M-E PDG used Long-Term Pavement Performance (LTPP) test sections to calibrate performance models, and 50 percent cracking of the total lane was considered failure. It is important to note that the calibration for the M-E PDG included all severities of fatigue cracking equally without any weight to the higher severities (El-Basyouny and Witczak “Calibration,” 2005). Additionally, it is important to explain the LTPP program was set up by SHRP and NCHRP to serve researchers with a large database of information regarding the construction, properties and performance of pavement sections across the U.S., with one of the goals to aid in the development of a new pavement design guide.

Fatigue Performance

Asphalt fatigue research has shown that HMA fatigue life is related to the horizontal tensile strain following the relationship of Equation 1.2. Further developments included the HMA mixture stiffness in the fatigue life relationship to account for varying temperature and loading frequency as given in Equation 2.1 (Tangella et al., 1990):

$$N_f = k_1 \left(\frac{1}{\varepsilon_t} \right)^{k_2} \left(\frac{1}{E} \right)^{k_3} \quad (2.1)$$

where: N_f = Number of load cycles until fatigue failure
 ε_t = Applied horizontal tensile strain
 E = HMA mixture stiffness
 k_1, k_2, k_3 = Regression constants

The HMA stiffness is an important parameter in the fatigue performance, and it must be considered in conjunction with the expected in situ HMA thickness and failure mode. Consider a relatively flexible mix. It will flex more, causing higher strains, yet it may be more capable of handling the strain due to its flexible nature. Further, a stiffer mix may show lower fatigue life in the laboratory at a given strain level than a more flexible counterpart. Yet, in the field, the stiffer structure will have lower strains under traffic than the flexible mixture; thus, a longer fatigue life (Hajj et al., 2005). Hajj et al. (2005) explain that mechanistic analysis should be used to understand the interaction between structure, stiffness, and laboratory testing to determine the balance for the given field and traffic conditions on a per-project basis.

Some fatigue relationships also include asphalt mixture parameters or mix volumetrics as another correction factor to the k_1 term. Typically, the effect of mix volumetrics is in the form of (Pell and Cooper, 1975):

$$VFB = \frac{V_B}{(V_B + V_V)} \quad (2.2)$$

where: VFB = void filled with bitumen
 V_B = Percent asphalt volume
 V_V = Percent air volume

This parameter is also known as voids filled with bitumen (or asphalt) noted as VFB (or VFA). Previous research showed that minimizing the air voids and maximizing the amount of asphalt was beneficial to fatigue life. Pell and Cooper (1975) expanded this work by showing that the interaction of air and binder volume to produce a high mix density was the important parameter. They showed that the lower the voids in the mix, $V_B + V_V$, the denser the mix and the better use of the available binder. At high VFB, they noted an increase in the dynamic stiffness of the mixture, and thus the fatigue performance. It was then determined that the above relationship captured the effect and interaction of aggregate gradation, air void content, and asphalt content on the mix density, stiffness and fatigue life.

Further work by Monismith et al. (1985) quantified the effect of the above ratio on laboratory fatigue response, and the results from the study are shown in Figure 2.4. The study included California asphalt mixtures using two different aggregates and one asphalt binder. From the figure, one can see an increase in fatigue life with subsequent increase in the VFB. Other parameters have also been included in fatigue life relationships, but the above are the most common and widely accepted.

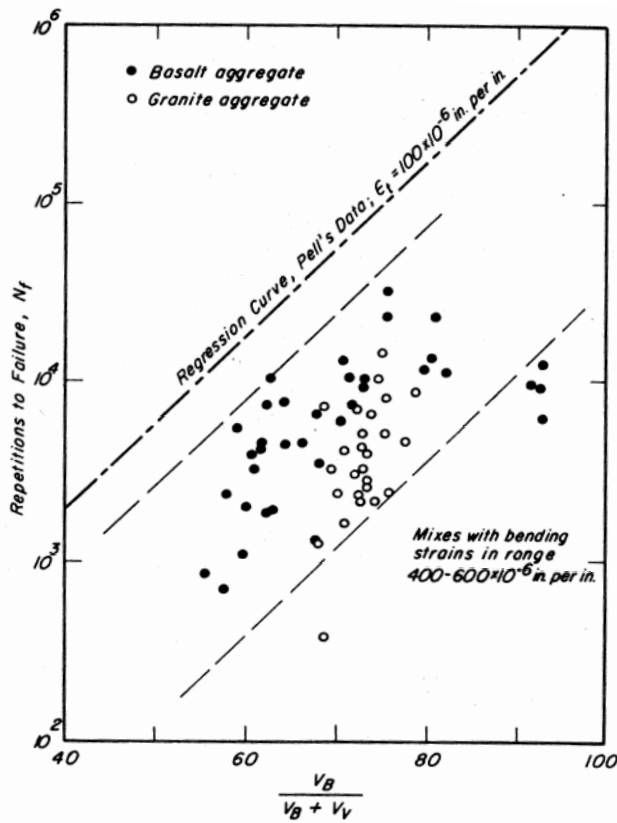


Figure 2.4 Influence of VFB on Fatigue Life (Monismith et al., 1985).

General Model Development Procedure

For the most part, fatigue life relationships or performance equations are developed in the laboratory using some form of a fatigue testing apparatus. Typically, HMA samples are cut into beams and subjected to repeated flexural loading either in a controlled strain or controlled stress mode. The most common apparatus is simple flexure with third-point loading. A schematic of the test is shown in Figure 2.5. Much research and debate has been devoted to determining whether controlled stress or controlled strain is the most appropriate. Most do agree that it depends on the conditions, mainly thickness, of the in situ pavement. Controlled stress more closely simulates the mode of loading for thicker HMA layers, while controlled strain is more appropriate for thin (i.e., less than 2 in.) asphalt pavements (El-Basyouny and Witczak "Development," 2005).

One of the main discrepancies between the two tests is the effect of mixture stiffness on the fatigue life. For controlled stress testing, stiffer mixes will have a higher fatigue life, while controlled strain testing will show that stiffer mixes have lower fatigue life. Because of the discrepancies, the mode of loading should be carefully considered and reported with beam fatigue results. Further, the observation drives the recommendation that controlled stress should be used for thicker, more robust pavements, where high stiffness is beneficial. It should also be noted that controlled stress loading will result in a more conservative fatigue life than controlled strain loading for identical mixes (Monismith et al., 1985).

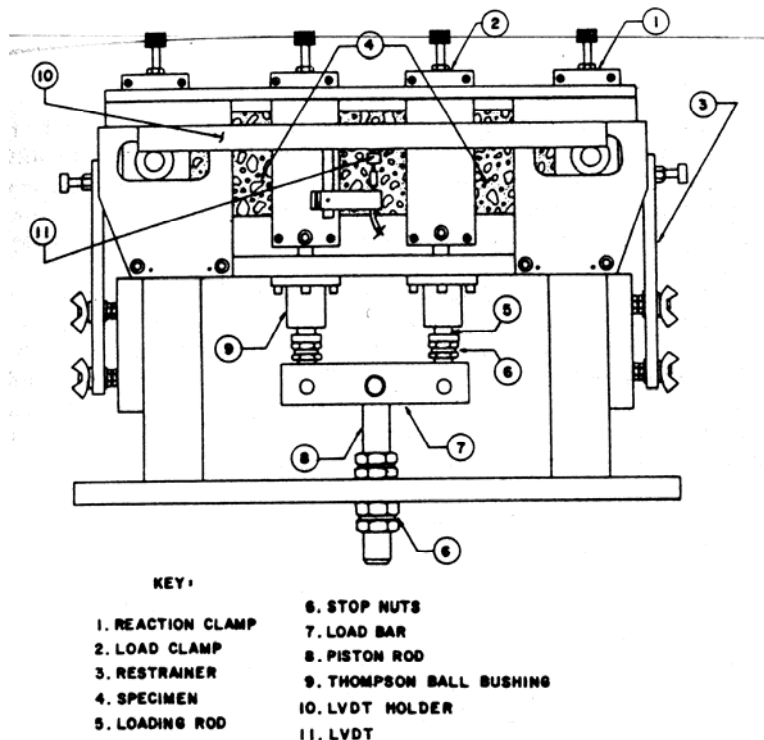


Figure 2.5 Schematic of Third Point Beam Fatigue Test (Monismith et al., 1985).

Regardless of testing method, laboratory-developed performance equations do not accurately predict the fatigue life of asphalt pavements in the field (Harvey et al., 1995). There are many reasons for the difference in laboratory and field performance, and a few are given below (Tangella et al., 1990):

- In the field, traffic loads are distributed laterally (wheel wander), so the same point of the pavement is not continually loaded.
- It is possible that in the field the HMA will sustain longer fatigue life after initial cracking due to support of underlying layers.
- Fatigue life relationships are greatly dependent on the type of fatigue test and mode of loading (i.e. flexural versus diametrical and controlled strain versus controlled stress) along with testing temperature.
- There are rest periods and the opportunity for healing in the field.
- Field performance is dependent on thickness of the in situ pavement.

Due to the differences in the laboratory and the field, fatigue life relationships must be calibrated or shifted to observed field performance. This is the empirical part of M-E design. The calibration process, or developed shift functions, is one of the more problematic elements of M-E design. The SHRP Project A-003A (Tangella et al., 1990) warned that “established correlations between laboratory data and field response are weak, [which] is a major area of concern when attempting to utilize the results of laboratory investigations to define performance criteria.” The project further reported that the range of shift factors proposed by a variety of researchers ranged from slightly over 1 to over 400.

Field calibration is necessary in defining useful transfer functions, but as mentioned above, the process can be very difficult and often inexact. Many design manuals, including the AI MS-1 (“Thickness Design,” 1982), calibrated laboratory derived equations from field performance data from the AASHO Road Test. Therefore, the calibration and subsequent transfer functions are reliant and restricted by the conditions of the AASHO Road Test, which are more than likely irrelevant for today’s conditions. As mentioned earlier, one of the main benefits of M-E design is that performance predictions will no longer be based on out-dated empirical relationships presented in the AASHTO Design Guide (1993).

The empirical relationships in the AASHTO Design Guide are considered out-dated because they were developed from the AASHO Road Test. As further background, the AASHO Road Test was limited to one subgrade soil, one environmental condition, 1950’s vehicles and tires, 1950’s materials and specifications and only a few million ESAL of traffic (Hallin, 2004). It seems that more recent performance data are warranted to produce more accurate models. Otherwise, M-E design is still limited to AASHO conditions through the calibration of the distress models. This deficiency is a major motivator for projects like the SHRP LTPP project.

As an improvement to earlier efforts, the M-E PDG calibrated the fatigue transfer function using data from the LTPP database from different pavement sections all over the U.S. (El-Basyouny and Witczak “Calibration,” 2005). A total of 82 new LTPP sections

were included in the analysis, and the M-E PDG Software (also known as the MEPDG) was run at a full matrix of assumed shift factors. The set that most closely matched the performance data was selected to calibrate the model. Another shift factor was then developed to mathematically shift the thinner asphalt sections (less than 4 in. thick).

Although this particular method may be considered to be applicable over a wider range of conditions because it was calibrated considering many conditions, one may also argue that the unspecific calibration deems the functions unsuitable to any one site. From Figure 2.6, the error between the final M-E PDG distress predictions and the observed performance reach high levels even with the field calibration. The figure shows the error in the model in terms of the percent of cracking plotted against the log of the percent damage. For example, at a damage of 0.1 or 10 percent (log damage = 1), the error between the predicted cracking and the measured cracking reaches 45 percent. Also notice that the reported error is on the un-conservative side; in other words, the model is over predicting the performance. It is also important to note that when damage reaches unity (100 percent, log damage = 2), there are no data. The equations were actually calibrated using data from test sections that had not reached the failure criteria.

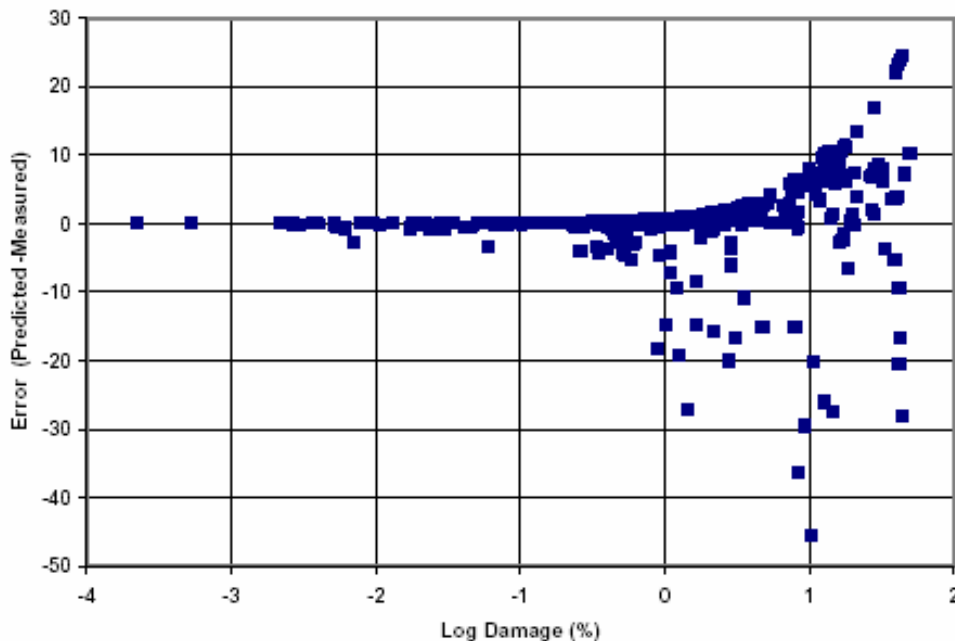


Figure 2.6 Error (Predicted – Measured Percent Cracking) vs. Damage % (El-Basyouny and Witczak “Calibration,” 2005).

Due to the above concerns, transfer functions, and M-E design as a whole, are more useful when they are specifically calibrated for their use. Local calibration more accurately includes the effects of local materials and environmental conditions. For example, the transfer functions developed in Minnesota were adjusted or calibrated to observed field performance at Mn/ROAD (Timm et al., 1998).

Existing Transfer Functions

A sampling of developed transfer functions are presented here to serve as examples and guidance for this research. Notice that many are very similar in form, with different coefficients based on their specific use and/or failure condition definition.

Asphalt Institute MS-1

Finn et al. (1977) developed a calibrated fatigue transfer function for NCHRP 1-10B based on the laboratory equation below developed by Monismith and Epps (1969):

$$\log N_f = 14.82 - 3.291 \log\left(\frac{\varepsilon_t}{10^{-6}}\right) - 0.854 \log\left(\frac{E^*}{10^3}\right) \quad (2.3)$$

where: N_f = Cycles until fatigue failure

ε_t = Initial tensile strain

E^* = Complex modulus of the HMA, psi

Equation 2.3 was calibrated using data from the AASHO Road Test to produce Equation 2.4, considering failure with 45 percent cracking of the wheelpath (20 percent of the total lane). This particular field calibration only shifted the intercept or multiplier (k_1). Notice that the other parameters did not change.

$$\log N_f = 16.086 - 3.291 \log\left(\frac{\varepsilon_t}{10^{-6}}\right) - 0.854 \log\left(\frac{E^*}{10^3}\right)$$

Or (2.4)

$$N_f = 18.4 * (0.00432 * \varepsilon_t^{-3.29} * E^{*-0.854})$$

Equation 2.4 was then adopted by the 9th edition of the AI Thickness Design Manual MS-1 ("Research and Development," 1982) and further modified to include a correction factor to account for the volumetrics of the mixture as suggested by Pell and Cooper (1975). The final MS-1 design equation was:

$$N_f = 18.4 * C * (0.00432 * \varepsilon_t^{-3.29} * E^{*-0.854}) \quad (2.5)$$

where: $C = 10^M$

$$M = 4.84 * \left(\frac{V_B}{V_B + V_V} - 0.69 \right) \quad (2.6)$$

Shell Pavement Design Manual

Shell International Petroleum Company published an asphalt design manual in 1978 and included the fatigue transfer function below following a similar pattern of AI MS-1 (Ali and Tayabji, 1998):

$$N_f = 0.0685 * \varepsilon_t^{-5.671} * E^{-2.363} \quad (2.7)$$

where: ε_t = Initial tensile strain

E = Stiffness of the HMA, psi

Equation 2.7 was developed from mainly laboratory fatigue data. Further work was done in 1980, and separate functions were developed for thin (less than 2 in.) and thick (6-8

in.) asphalt pavements, which are presented elsewhere (El-Basyouny and Witczack, “Development,” 2005).

M-E PDG

In the development of the fatigue cracking models for the M-E PDG under NCHRP 1-37A (Eres, 2004), the researchers considered both the Shell Oil and AI fatigue transfer functions as starting points. It was determined that the AI MS-1 equation was the most applicable (El-Basyouny and Witczack “Development,” 2005). Equation 2.4 was basically re-calibrated using LTPP data and included a new correction factor, K , to account for thinner pavements (less than 4 in.). The final fatigue design equation, considering failure at 50 percent cracking of the total lane area, is (El-Basyouny and Witczack “Calibration,” 2005):

$$N_f = 0.00432 * K * C * \left(\frac{1}{\varepsilon_t}\right)^{3.9492} \left(\frac{1}{E}\right)^{1.281} \quad (2.8)$$

$$\text{where: } K = \frac{1}{0.000398 + \frac{0.003602}{1 + e^{11.02 - 3.49 * h_{ac}}}} \quad (2.9)$$

h_{ac} = Thickness of HMA layer, in.

California Department of Transportation

A large laboratory effort was conducted following the recommendations of SHRP A-003A by researchers at the University of California, Berkeley to evaluate California asphalt mixtures for California Department of Transportation. The model derived from lab data included the mix stiffness, VFB and tensile strain (Harvey et al., 1995).

$$N = 2.5875 \times 10^{-8} * e^{0.053VFB} * \left(\frac{E}{145}\right)^{-0.726} * \varepsilon_t^{-3.761} \quad (2.10)$$

Further, a recommended shift factor was developed to determine design ESAL from laboratory life. The shift factor developed from the study was (Harvey et al., 1995):

$$\text{ShiftFactor} = 2.7639 \times 10^{-5} * \varepsilon_t^{-1.3586} \quad \text{for } \varepsilon_t \geq 0.000040 \quad (2.11)$$

Minnesota Department of Transportation

The Minnesota Department of Transportation (Mn/DOT) developed a fatigue transfer function following the Illinois Department of Transportation function developed for dense-graded asphalt mixtures (Alvarez and Thompson, 1996):

$$N_f = 5 \times 10^{-6} * \left(\frac{1}{\varepsilon_t}\right)^{3.0} \quad (2.12)$$

The final Mn/DOT fatigue equation was calibrated using performance data from Mn/ROAD and is given as (Timm et al., 1999):

$$N_f = 2.83 \times 10^{-6} * \left(\frac{1}{\varepsilon_t}\right)^{3.206} \quad (2.13)$$

Both the Illinois and Minnesota equations followed the simplified form of Equation 1.2.

Regression Constant Relationships

Timm et al. (1999) reported that many studies have observed trends between the regression coefficients, k_1 and k_2 , of Equation 1.2. These trends, Equations 2.14-16, can aid in calibration, because if an approximation of k_1 is determined, then k_2 can be easily calculated. The relationships can also serve as a check of reasonableness.

$$k_2 = 1.35 - 0.252 * \log k_1 \quad (2.14)$$

$$k_2 = 1.332 - 0.306 * \log k_1 \quad (2.15)$$

$$k_2 = 0.5 - 0.213 * \log k_1 \quad (2.16)$$

Equation 2.14 was developed by the Federal Highway Administration (Rauhut et al., 1984), and Equation 2.15 shows a very similar trend developed from research in Norway (Myre, 1990). The final relationship was reported by M-E design research from Nottingham, England (Cooper and Pell, 1974).

DYNAMIC DATA AND INSTRUMENTATION

Mn/ROAD

The Minnesota Road Research Project (Mn/ROAD) is a full-scale pavement testing facility located off of I-94 in Ostego, Minnesota (Figure 2.7). The facility consists of two main parts: the 3.5 mile mainline that runs parallel to I-94 and carries interstate traffic and the 2.5 mile low-volume road loop with controlled traffic. At the facility, there are 40 test sections with a wide variety of pavement structures (both flexible and rigid). The facility promotes cooperative research between Minnesota Department of Transportation (MnDOT), University of Minnesota and FHWA, as well as other state DOTs (“About Minnesota,” 2005).



Figure 2.7 Mn/ROAD Facility (“About Minnesota,” 2005).

Of most relevance to the NCAT Structural Study, is the embedded instrumentation at Mn/ROAD. There are approximately 4,500 sensors embedded in the test sections to monitor both the pavement condition and the dynamic response under loading (Alvarez and Thompson, 1998). The sensors are connected to 26 roadside boxes, and there are two main collection systems. Most of the gauges are sampled via an automated, continuous data acquisition system that is triggered by the passage of a vehicle which then records a burst of data. The condition gauges are also sampled automatically based on a routine time schedule. There are also sensors that are collected manually with an on-site system (Beer et al., 1996).

At Mn/ROAD, there are many types of dynamic response gauges. The three of most importance to flexible pavements are asphalt strain gauges, linear variable differential transducers (LVDT) and dynamic soil pressure gauges. As described by Alvarez and Thompson (1998), the asphalt strain gauges are electrical resistant strain gauges on an H-shaped bar, and they were installed at the bottom of the asphalt layer in both the transverse and longitudinal directions. Further, they were installed at the center of the wheelpath and at 1 ft transverse offsets. The gauges and array are very similar to what was used for the NCAT Structural Study. The LVDTs consist of an electromagnetic device and separate core. They were used to measure the vertical displacement at different depths within the pavement structure. Lastly, soil pressure cells were used to measure the dynamic vertical pressure due to truck loads. These gauges consisted of a liquid-filled steel cell with adjacent pressure transducer, also similar to the gauges used at NCAT.

In addition to the response gauges, there are also pavement environmental condition sensors including thermocouples and time domain reflectometers (TDR). The TDRs were installed in the soil layers, and measure the in situ moisture content. The thermocouples are used to measure the temperature profile in the pavement structure (Alvarez and Thompson, 1998; Beer et al., 1996). At NCAT, TDRs as well as temperature probes were used.

In 1996, a report was published (Beer et al.) regarding the performance of the instrumentation at Mn/ROAD, and a few suggestions were given. First, more redundancy in the asphalt strain gauges was desired due to the loss of gauges during construction and throughout the testing cycle. It was also noted that nearly twice the strain gauges orientated in the transverse direction failed as those in the longitudinal direction. In regards to the moisture content measurements, they recommended developing specific calibration equations and also reported that the gauges did not work well when the soil was near saturation. Further recommendations included avoiding cable splices and long lead wires. Overall, it was reported that the strain gauges and pressure cells performed satisfactorily.

The automated data acquisition system at Mn/ROAD retrieves and processes the data and then sends the information to the Mn/DOT Materials Research Engineering Laboratory

where it is checked and stored on an Oracle database (Alvarez and Thompson, 1998). In this way, the data collection and processing is completely automated. No further information could be found regarding how strain values were estimated from the actual dynamic traces.

Virginia's Smart Road

Virginia's Smart Road is a 1.7 mile test track that will eventually be part of a 5.7 mile limited-access highway that will connect Blacksburg, Virginia to I-81 (Figure 2.8). It is a multi-use research facility in addition to an important transportation corridor for the public. The facility is designed to accommodate a variety of research efforts including bridge design, Intelligent Transportation Systems (ITS) development, safety and human factor research, pavement design, and vehicle dynamic research. Most of the research is a cooperative effort between the Virginia Department of Transportation (VDOT), FHWA and Virginia Polytechnic Institute and State University's Transportation Institute ("Virginia's Smart Road Project," 2005).

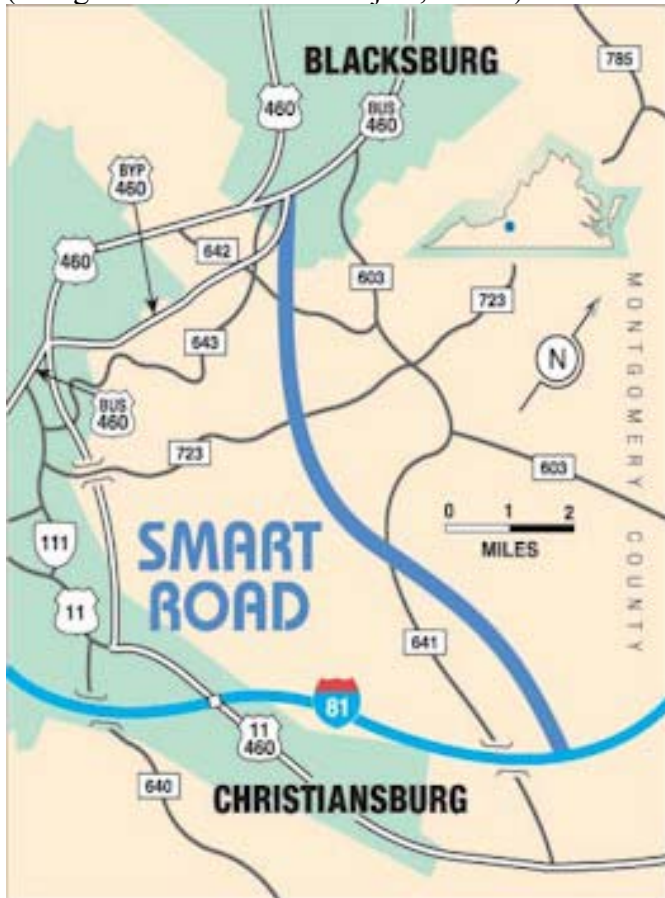


Figure 2.8 Map of Virginia's Smart Road ("Virginia's Smart," 2005).

The flexible pavement testing at the Smart Road consists of 12 sections, each approximately 350 ft long, consisting of different materials and all include embedded response and condition gauges. Again, the important aspect of the project in respect to

this report is the embedded instrumentation and subsequent collection and processing procedures.

Like Mn/ROAD, the Smart Road instrumentation array consisted of asphalt strain gauges, pressure cells, TDRs and thermocouples. The data acquisition scheme at Smart Road consisted of two units; one, to collect the static or condition data, and the other to collect dynamic data. Both systems were manufactured by IOtech Inc. and required signal conditioning cards for each gauge (Al-Qadi et al., 2004). The dual acquisition scheme was also used at NCAT, and will be discussed in Chapter 3.

Three software programs were developed at the Virginia Tech to collect, organize, and process the dynamic data (Al-Qadi et al., 2004). SmartAcq was developed to collect the condition data at specified intervals and the dynamic data during the presence of a vehicle. The dynamic gauges were sampled at 500 Hz per channel, the temperature probes are collected every 15 minutes and the TDRs were sampled hourly. The program allowed the user to control the data acquisition systems through a Windows environment. The collected data were then separated into distinct files by gauge, test section and date using Smart Organizer software.

The final software program, SmartWave, was developed to display and process the dynamic strain and pressure data. Al-Qadi et al. (2004) noted that the dynamic traces were originally viewed individually in a spreadsheet program, but the process was inefficient due to the large amount of traces and data points per trace. Therefore, researchers at Virginia Tech developed the SmartWave program which allowed for easier viewing and processing of the dynamic traces (Al-Qadi et al., 2004). The program allowed the user to see the trace and customize the data processing commands. The processing consisted of cleaning the signal and collecting the important values from the trace. After cleaning the signal of electronic noise, the program automatically collected the extremum [sic] value for each axle of the 6-axle test vehicle. The peak value per axle could be either compression or tension for the asphalt strain gauges and compression for the pressure cells. From this process, the collected strain magnitude was the absolute value from the baseline of the trace to the peak point determined from the SmartWave algorithm.

After processing, the dynamic response data were stored in an Access database along with the environmental (condition) data. The data were stored in such a way to allow for easy retrieval among the two databases. Further, queries were developed to allow extraction of just maximum response values of replicate tests (Al-Qadi et al., 2004).

The data acquisition scheme implemented at the Test Track was similar to the scheme at Virginia's Smart Road. As explained in the next chapter, proprietary programs and developed algorithms were used to collect and process the data in a Windows environment. Also similar to Smart Road, both processes involved some human interaction.

CHAPTER 3 - TEST FACILITY

NCAT TEST TRACK

The NCAT Test Track is a 1.7 mile full-scale asphalt testing facility located in Opelika, Alabama (Figure 3.1). The NCAT Test Track was created in 2000 as a cooperative between state DOTs and Federal Highway Administration (FHWA) to investigate, at a full-scale level, the needs of the transportation system and asphalt industry. The first test cycle, completed in 2002, investigated different materials in regards to rutting and surface distress. The second test cycle, which began in October 2003, included sections continuing traffic from the 2000 cycle as well as sections that were milled and inlaid to test new surface materials. Additionally, eight test sections were devoted to the Structural Study and are the focus of this research.

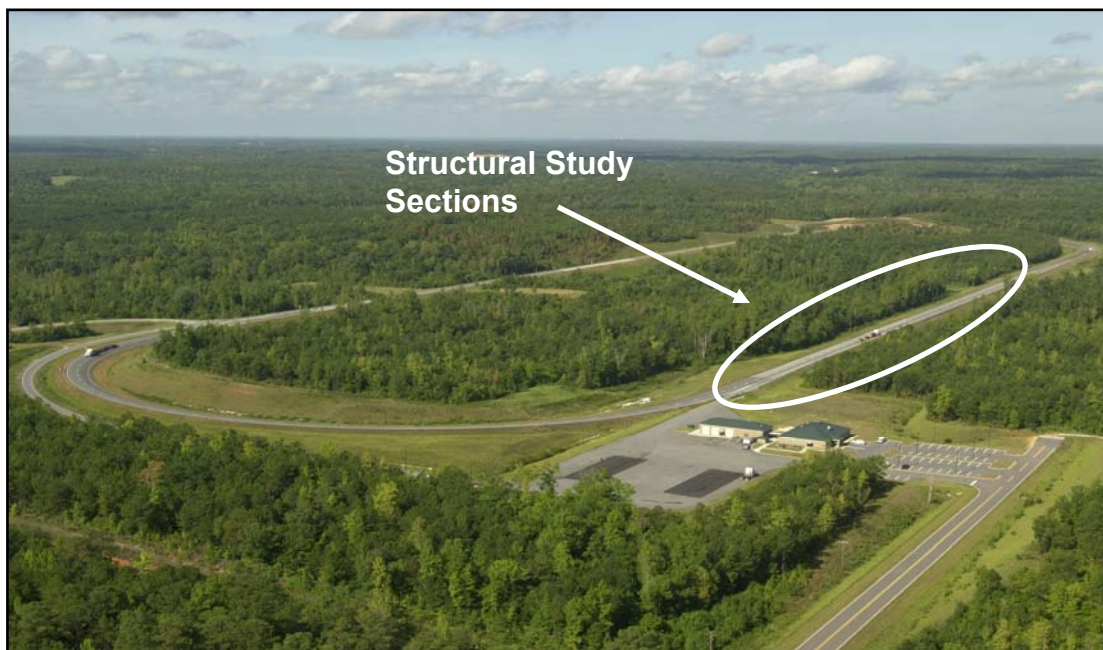


Figure 3.1 Aerial Photo of the NCAT Test Track.

The trucking fleet, consisted of five triple-trailer trucks and a standard FHWA class 9 18-wheeler truck, that applied over 1,000,000 passes (approximately 10 million ESALs) during the two-year testing cycle. In other words, the NCAT Test Track was loaded with roughly ten years of traffic volume in two years. In this manner, the testing is somewhat accelerated, but in all other aspects, the testing is as close to an open-access highway as possible. Further, the trucks were operated at 45 miles per hour and are driven by human drivers. This testing scheme is both safe and more closely replicates highway traffic.

NCAT STRUCTURAL STUDY

The Structural Study, sponsored by ALDOT, Indiana DOT (InDOT) and FHWA, consisted of eight test sections with three different HMA thicknesses and two different binder types (PG 67-22 and an SBS modified PG 76-22). All eight sections had an underlying 6 in. crushed granite granular base over fill material which was constructed

over the existing embankment. Figure 3.2 shows the cross sections of the structural study sections, N1-N8. Notice that the sections were a full factorial experiment with N7 serving as a duplicate to N6 with an SMA surface, and N8 is a duplicate of N7 with an asphalt-rich bottom layer.

The sections were designed structurally using the 1993 AASHTO Design Guide (AASHTO, 1993), and mix designs were performed according to ALDOT specifications. The sections were designed to show a variety of distresses over the life of the experiment, and it was intended that at least the 5 and 7 in. sections would exhibit fairly extensive structural distress in order to correlate performance to field-measured pavement responses. The thin sections (N1 and N2) were designed for about 1.1 million ESAL, the medium sections (N5-N8) for 2.9 million ESAL and the thick sections (N3 and N4) for 7.8 million ESAL.

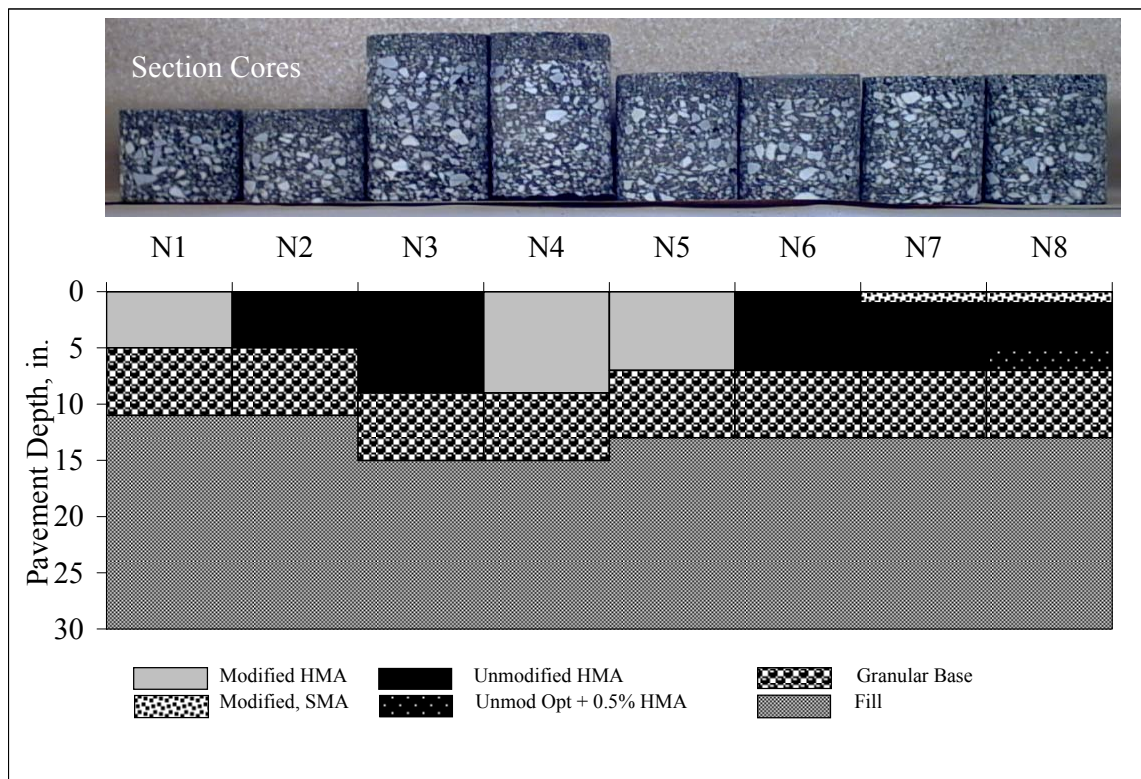


Figure 3.2 Structural Study Test Section Layout.

The main objectives of the 2003 NCAT Structural Study were to develop transfer functions for both fatigue and rutting and to investigate the effects of polymer modified asphalt. Further objectives included validating mechanistic models and correlating performance to heavy vehicle simulators. The design, construction and experimental plan can be found elsewhere (Timm et al., 2004).

INSTRUMENTATION

The test sections of the NCAT Structural Study were instrumented to measure the in situ conditions (i.e., temperature, moisture) of the pavement as well as the dynamic pavement

response under traffic (i.e., stress, strain). The schematic of the instrumentation, including both the condition and response gauges, at each test section is shown in Figure 3.3. A complete description of the gauges, data acquisition system, installation and construction can also be found elsewhere (Timm et al., 2004), but some brief descriptions are given here to provide adequate background to this research.

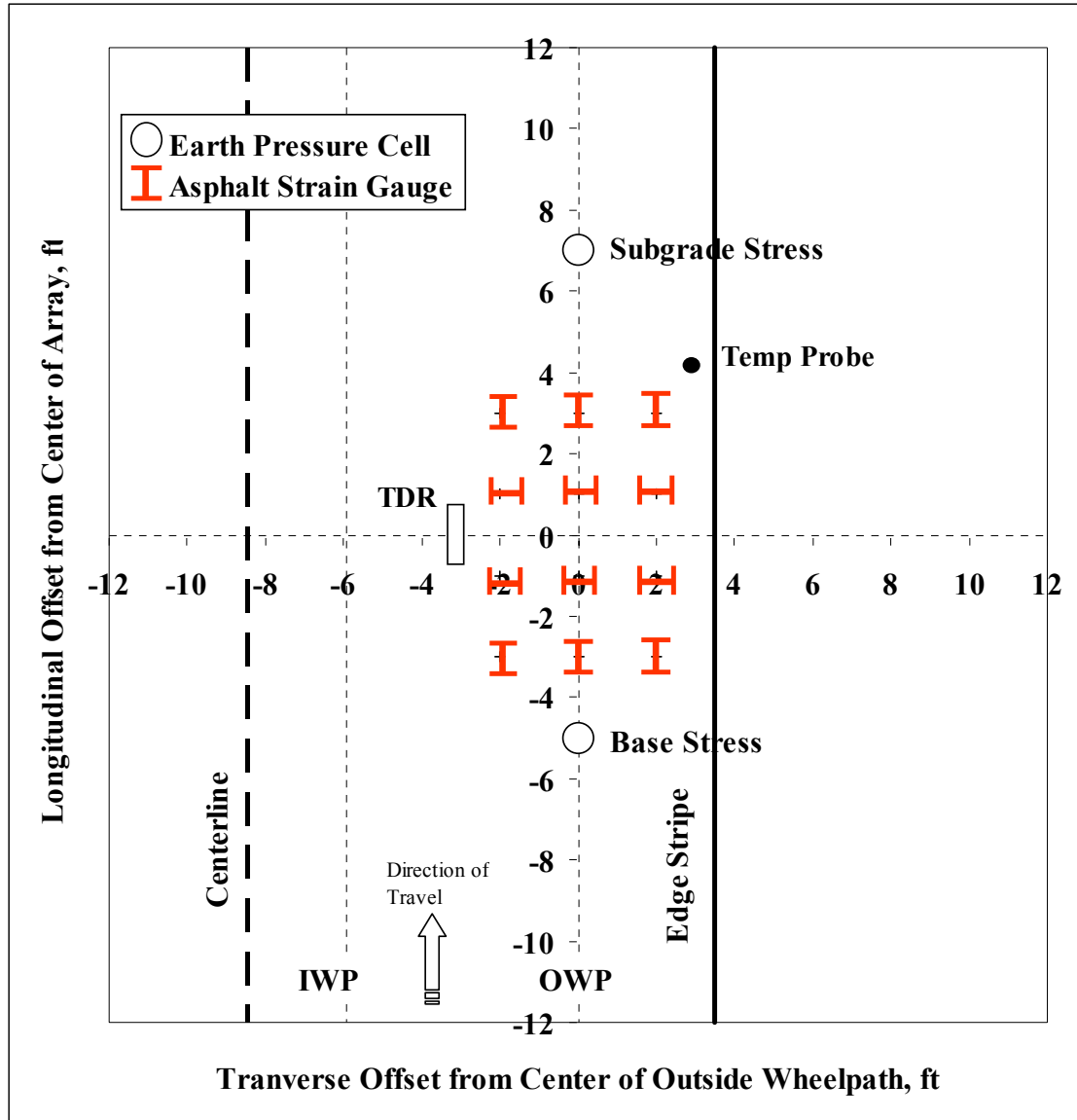


Figure 3.3 Schematic of Instrumentation (Timm et al., 2004).

In situ Conditions

To measure the condition of the pavement structure, thermistors and time domain reflectometry (TDR) probes (Figure 3.4) were installed to measure the pavement temperature profile and the subgrade moisture content, respectively. The thermistor bundle measured the pavement temperature at three depths: near the surface, 2, 4 and 10 in. deep. The TDR probes were installed 3 in. deep into the fill layer and measured gravimetric and volumetric moisture contents of the soil. As suggested by the

manufacturer specific calibration functions were developed for the TDRs using the on-site subgrade soil.

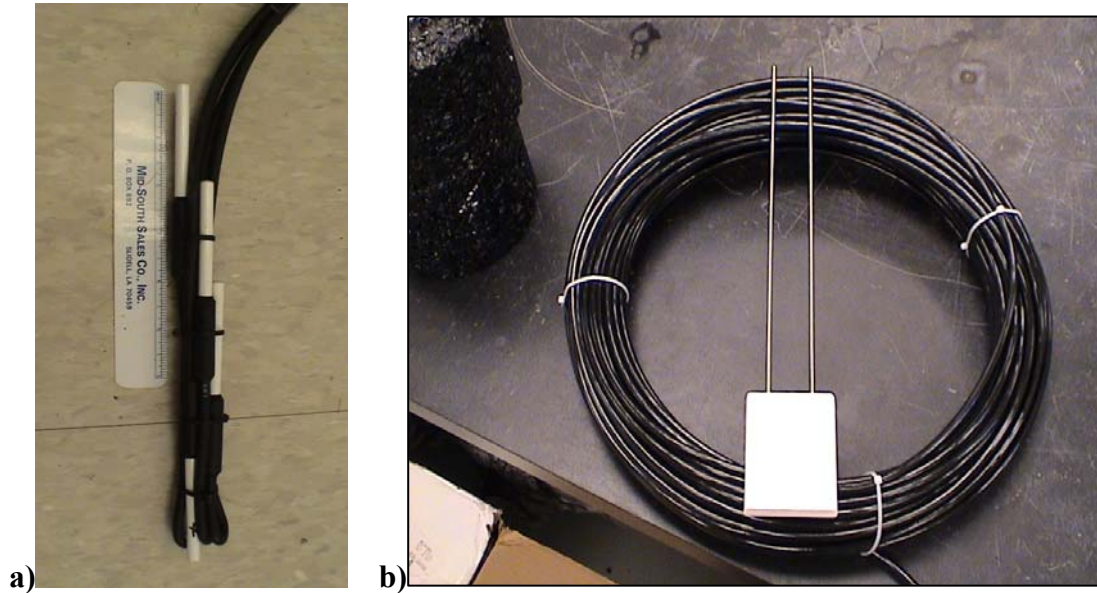


Figure 3.4 In Situ Instruments a) Thermistor Bundle b) TDR.

The temperature and TDR probes were sampled using a Campbell Scientific CR10X datalogger located at each test section in the roadside box. The roadside box and datalogger are shown in Figure 3.5. The datalogger sampled the gauges every minute and recorded the hourly average, maximum and minimum readings. Hourly readings were transmitted through the radio modem to the data storage computer throughout the two-year testing cycle to continuously monitor the pavement environmental condition.

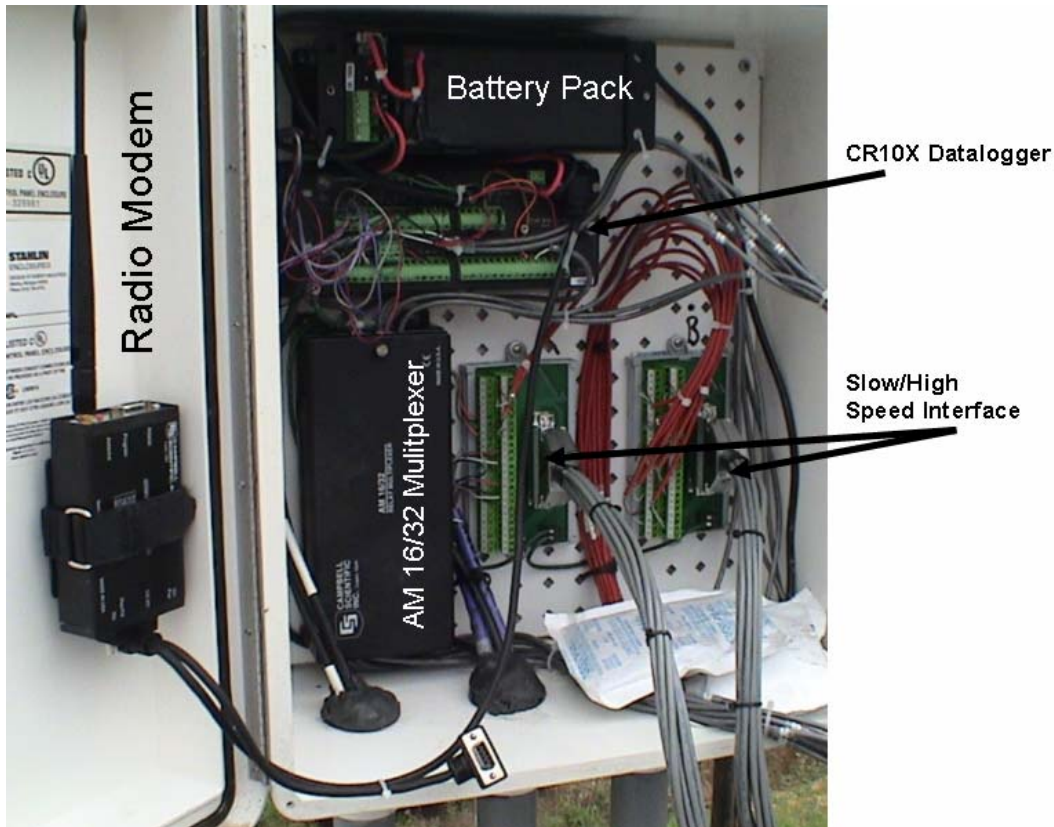


Figure 3.5 Roadside Box and Datalogger (Timm et al., 2004).

Dynamic Pavement Response

Two critical pavement responses were measured with instrumentation at the Test Track. The first was the vertical pressure, which was measured using Geokon earth pressure cells, shown in Figure 3.6a. The second critical response was the horizontal strain at the bottom of the HMA layer, which was measured with CTL asphalt strain gauges (Figure 3.6b).

The CTL asphalt strain gauge is a full-bridge Wheatstone strain gauge mounted on an epoxy bar with flanges to secure the device in the HMA layer. The H-shaped gauges are similar to those used at both Mn/ROAD and Smart Road. The gauges were installed at the bottom of the HMA layer, and they were orientated in both the longitudinal (parallel to traffic) and transverse (perpendicular to traffic) directions. Additionally, the gauges were installed at three different lateral offsets in the wheelpath to help ensure a direct hit of the truck tire over a gauge. One gauge was installed directly in the center of the outside wheelpath and one on either side of that gauge at a 2 ft offset. Also notice from Figure 3.3 that the strain gauge array is repeated. The redundancy is included to account for the inevitable loss of gauges during construction and subsequent trafficking, as advised by Mn/ROAD researchers and others (Beer et al., 1996). Further, if redundant gauges survived, then they provided duplicate data in the analysis.

As mentioned, two Geokon earth pressure cells were installed in each section to measure the critical vertical stresses involved in rutting analyses. One pressure cell was installed at the top of the base layer, and the other at the top of the fill layer. Each gauge was installed in the wheelpath, and no redundant or offset pressure cells were installed due to their robust design and cost.

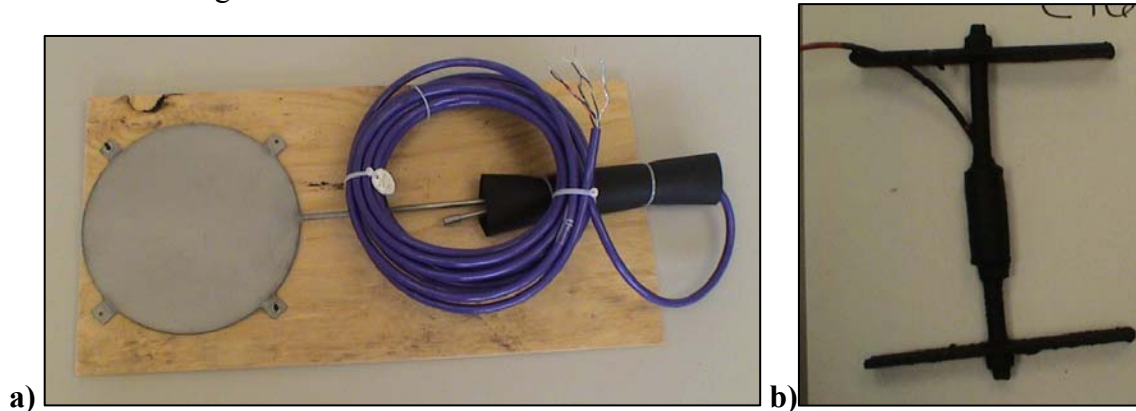


Figure 3.6 Dynamic Gauges a) Asphalt Strain Gauge b) Earth Pressure Cell.

The dynamic pavement response gauges required a much higher sampling frequency than did the in situ condition gauges; therefore, a separate data acquisition scheme was developed. A portable DATAQ highspeed dynamic data acquisition system was used to connect to the roadside box through the slow/highspeed interface (Figure 3.5) and collect dynamic data. The testing setup is shown in Figure 3.7 including the roadside box and portable DATAQ system. The signal conditioning cards within the acquisition system were gauge-specific, supplied the needed excitation voltage to the gauge and performed needed amplification to the signal. The data were then streamed, real time, to the acquisition software on a laptop computer. Because the system was portable, only one data acquisition system was needed to sample all eight test sections. The highspeed data acquisition scheme used at the NCAT Test Track was both user-friendly due to its Windows software environment and economical due to its portable nature.

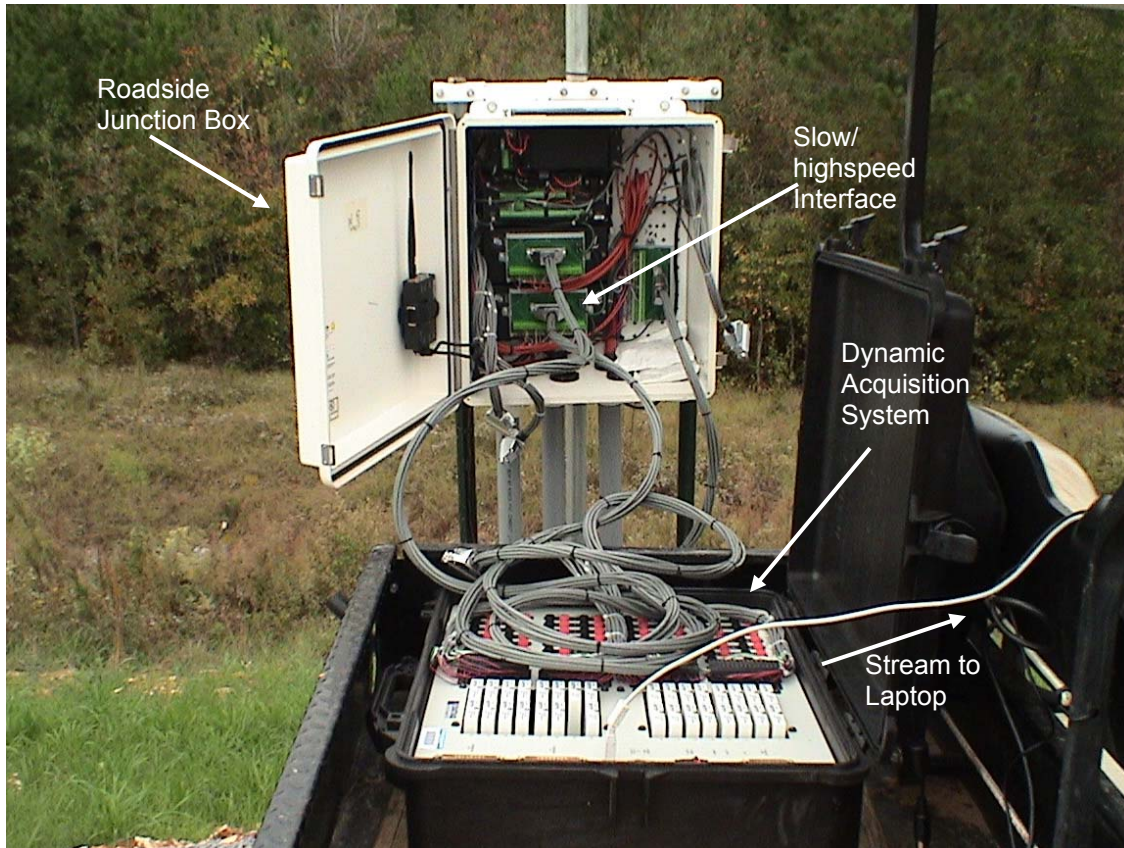


Figure 3.7 Dynamic Data Acquisition Scheme (Timm et al., 2004).

DATA COLLECTION EFFORTS

During the 2003 test cycle, there were many routine data collection efforts. The main efforts relevant to this project were the dynamic, environmental, falling-weight deflectometry (FWD) and performance data collection. Each are described briefly below.

Dynamic Data Collection

During a typical dynamic data collection day, the portable acquisition system was taken to each section, starting at N8 and progressing to N1, and three passes of each truck were collected. A small sensitivity study was conducted, and it was determined that three truck passes captured the full variability of the data. This investigation will be explored further in Chapter 5. It should be noted that initially, dynamic response data were collected monthly, but once fatigue distresses were noticed in April 2004, the effort was increased to weekly. It took two hours to collect data from all eight sections, and the gauges were sampled at a rate of 2,000 Hz per channel in order to capture the full response of the pavement under truck traffic. To serve as reference, this was the same sampling frequency as used at Mn/ROAD for dynamic data collection (Mateos and Snyder, 2002).

Due to the steady traffic at the Test Track and the enormous amount of data that comprises one truck pass, it was not practical nor necessary to collect dynamic data

continuously. As described later in the Chapter 5, relationships between pavement temperature and induced strain were developed to quantify the response for each truck pass of the two-year test cycle.

Environmental Data Collection

The environmental data, including the in situ condition gauges and an on-site weather station, were sampled continuously throughout the test cycle. As mentioned prior, the in situ gauges were sampled every minute and hourly summaries were reported and stored on the data acquisition computer in the laboratory. The data were transmitted wirelessly from the roadside box to the computer in the on-site lab building, and the wireless modem can be seen attached to the door of the roadside box in Figure 3.5.

FWD Testing

On a monthly basis, ALDOT performed FWD testing on all the test sections at the Test Track. FWD testing was conducted at three predetermined locations per test section in both the inside and outside wheelpaths, and each testing location was thumped twice. At the beginning of the testing cycle, three random locations were determined for each of the eight test sections. FWD testing, transverse profiles and density measurements were taken at these three locations for the extent of the two-year test cycle. The Dynatest 8000 FWD device was used at the Test Track and is shown in Figure 3.8.

The deflection data were then used in a backcalculation procedure to determine the stiffnesses of the pavement layers. This was critical to the Structural Study because the monthly deflection data provided in situ material properties for the pavement layers at a variety of seasons and temperatures. The FWD testing and backcalculation protocol are documented in detail in an NCAT report (Timm and Priest “Material Properties,” 2006).



Figure 3.8 FWD Testing and Data Collection.

Performance Data Collection

Performance data were collected weekly to record the cracking and rutting development over the testing cycle. Every Monday, truck traffic was paused to facilitate performance testing and any needed track and truck maintenance.

Cracking was monitored using a unique crack mapping method developed at the NCAT Test Track. First, the pavement surface was very carefully inspected, and the cracks were marked, including individual cracks and cracked areas. Figure 3.9 shows the pavement being carefully inspected and marked. Then a video record was taken of the marked pavement using a camera attached to a boom on a skid-steer tractor (Figure 3.10). The video was then digitized, and the coordinates of the cracking were determined from the digital record. From the coordinates, crack maps were produced, as shown in Figure 3.11. The dark lines indicate individual cracks and areas of cracking, and the dashed lines show the location of the wheelpaths. This procedure kept a very careful record of the amount of cracking and crack development in each test section.

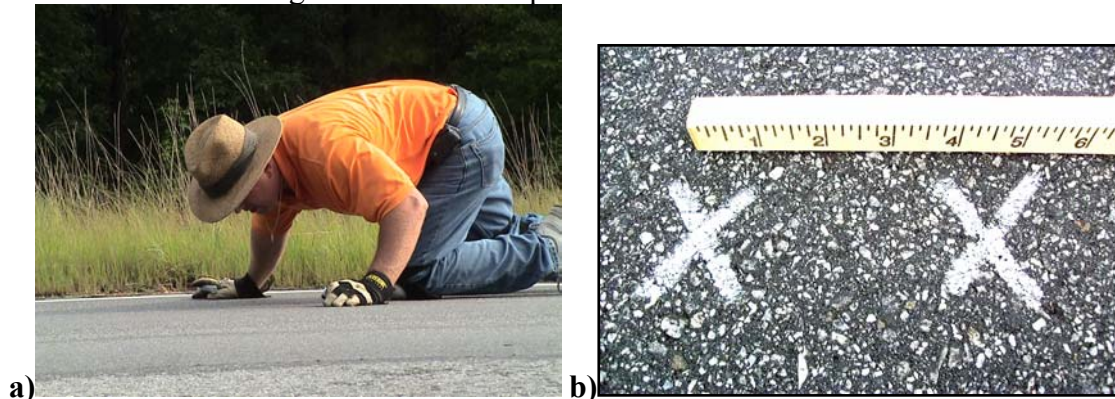


Figure 3.9 a) Pavement Inspection and b) Crack Marking.



Figure 3.10 Camera Apparatus for Crack Record.

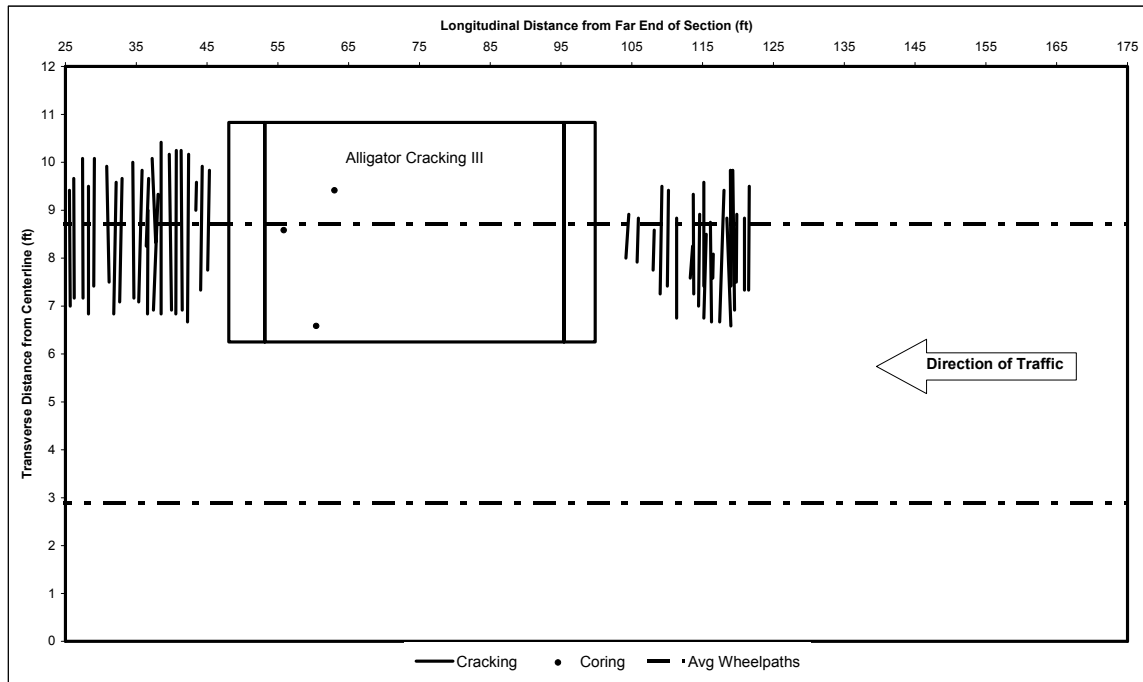


Figure 3.11 Crack Map Example.

Along with crack mapping, the rut depths were measured weekly with a transverse profile dipstick and an automated pavement survey vehicle, both shown in Figure 3.12. Transverse profiles were measured using a dipstick at the three established random locations and at the center of the instrumentation array in each test section. The automated survey vehicle used an array of lasers to compute the maximum rut depths along the length of the experiment.



Figure 3.12 Rut Depth Measurements a) Dipstick b) Automated Pavement Survey Vehicle.

CONCLUDING REMARKS ON TEST FACILITY

The NCAT Test Track is a state-of-the-art, full-scale test facility with the capability of conducting a variety of asphalt testing. Additionally, it has the support of the NCAT laboratory located in Auburn, Alabama.

In regards to studying structural distresses and developing transfer functions, the facility had many advantages. These included full-scale pavement sections, actual tractor-trailer test vehicles, human drivers, pavement instrumentation, environmental monitoring and the ability to conduct a wide range of performance and material characterization testing. All of these elements are essential to a successful M-E analysis procedure. As alluded to prior, the Test Track has all the characteristics of an open-access highway with the control and monitoring capabilities of a research facility.

CHAPTER 4 - DYNAMIC STRAIN DATA

INTRODUCTION

As mentioned in the literature review, the instrumentation at the NCAT Test Track and the dynamic data generated from the instrumentation was an important and central aspect of this research. The embedded strain gauges and pressure plates allowed for direct measurement of the pavement response; thus, there was no reliance on mechanical models. This situation was beneficial because all models are based on a set of assumptions that simplifies real world conditions to some degree. By measuring the responses directly, the assumptions and simplifications were not of concern. Further, the collected dynamic data could also serve to evaluate mechanical models, if needed.

With the benefits of dynamic response data, came unique challenges. The raw dynamic strain traces, the focus of this chapter, were highly variable and often unpredictable. The variability was largely attributed to the vehicle dynamic effects and trailer alignment along with electrical noise and drift in the signals themselves. Once the data were collected, the signals had to be cleaned, processed and stored in an efficient and streamlined manner. With the variety of traces, along with noise in the signal and signal drift, the task was not simple. Although literature regarding Virginia's Smart Road indicated that these issues were encountered and addressed, there was little documentation on how exactly the dynamic strain data were handled and processed. Further, beyond the Smart Road, there was little guidance to follow.

The method that was developed at the NCAT Test Track to handle and process the dynamic data was automated yet required some engineering judgment and interaction. The process pertains to both pressure and strain data, but the strain data are the focus here.

After the strain traces were processed, a procedure was developed to determine the strain magnitude for a given test section and day of data collection. Recall that there were twelve strain gauges, five trucks and three passes of each truck for each test section. All these data were incorporated into one strain value, and the procedure is discussed below in detail. It is important to document how the strain values were computed for context to this research and for guidance to further research.

STRAIN TRACE INVESTIGATION

As mentioned above, the dynamic strain data from live trucks were highly variable. Figures 4.1-4.5 are a small sampling of the different strain traces presented here to serve as examples. All five traces were collected on April 27, 2004 from test section N8, and all the traces are from a triple-trailer truck. Figures 4.1 and 4.2 are from the same longitudinal gauge located in the center of the wheelpath, and Figures 4.3 and 4.4 are from the same center-of-wheelpath transverse gauge. Figure 4.5 is from a transverse gauge located to the right of the center gauges.

From the figures, a few features should be pointed out. In all the figures, the steer, tandem, and five trailing single axles are visible. For clarification, the axles are marked in Figure 4.1. Notice for the longitudinal gauges (Figures 4.1 and 4.2), there is a compression wave (compression is negative) as the tire approaches the gauge prior to the tensile peak. Also notice that there is a full strain reversal between every axle, even within the tandem axle configuration. In Figure 4.2, the single axles show a diminishing strain response, even though all five axles weighed approximately the same. After further investigation, it was determined that the strain changes were in fact due to the mechanical alignment of the trailers (Timm and Priest “Wheel Wander,” 2005). In other words, the axles on that particular truck are aligned in such a way that the individual trailers tend to track toward the center of the lane. In view of that observation, it is important to note that the gauges were very sensitive to the lateral placement of the tire or the relative distance between the tire and the gauge.

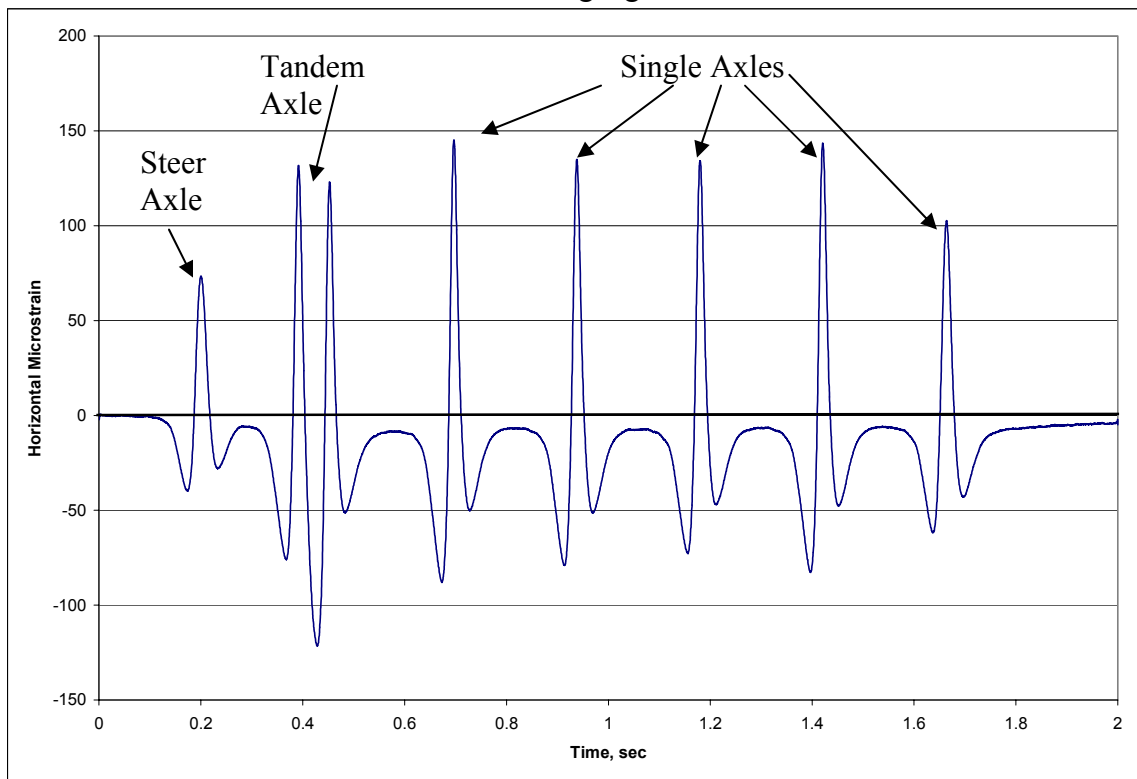


Figure 4.1 Longitudinal Strain Trace – Example 1.

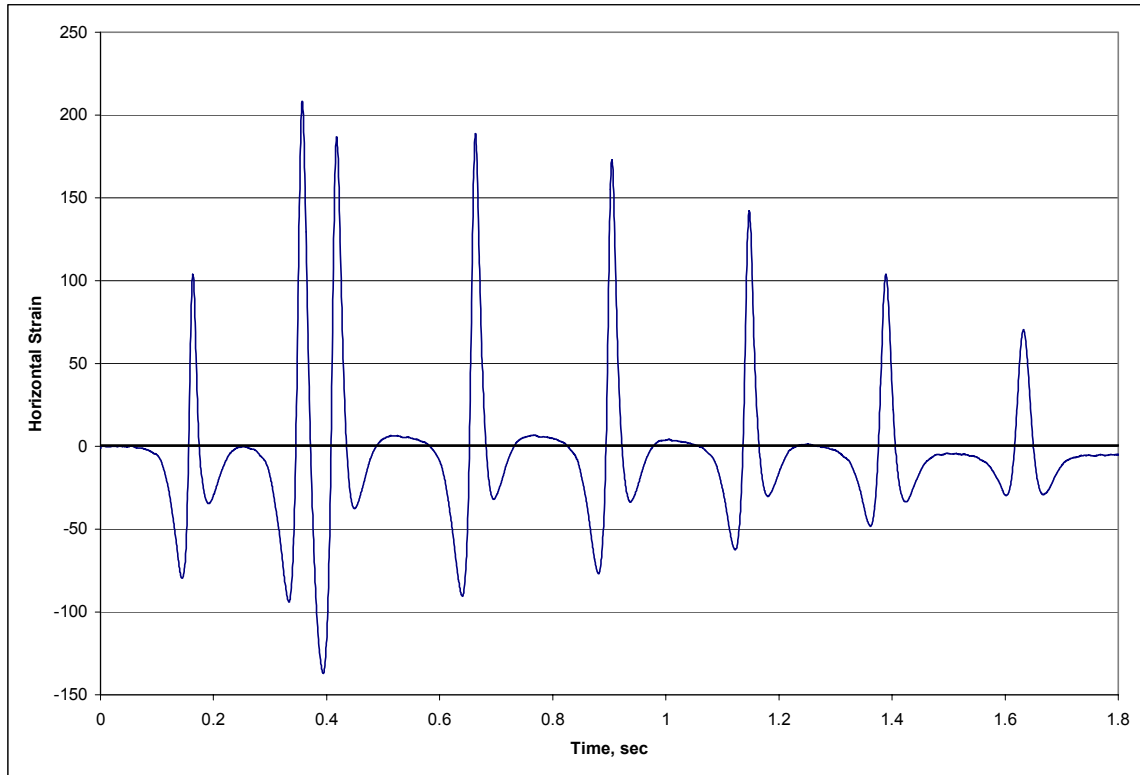


Figure 4.2 Longitudinal Strain Trace – Example 2.

As expected, the transverse gauges (Figures 4.3-4.5) did not have the preceding wave as the truck tire approached due to its perpendicular alignment. Figure 4.3 is an example of a trace where the tire was slightly off the gauge (to the left or right of it), pushing it in a compressive response. Figure 4.4 is an example of signal drift within a single strain trace. Some signals drifted more than others, and the drift complicated processing because there was not a steady baseline between each axle. The last strain trace (Figure 4.5) is an example of some of the strange and nearly unexplainable responses that often show up within a truck pass. Notice the compressive spike preceding the steer axle and last single axles. Also notice the double hits at the top of the tandem and first single axles, highlighted by the circles in the figure. The data were collected from an uncracked test section under what can be assumed as normal conditions. Therefore, the rather unexplainable characteristics of the given trace are considered simply byproducts of the sensitive instrumentation and acquisition process.

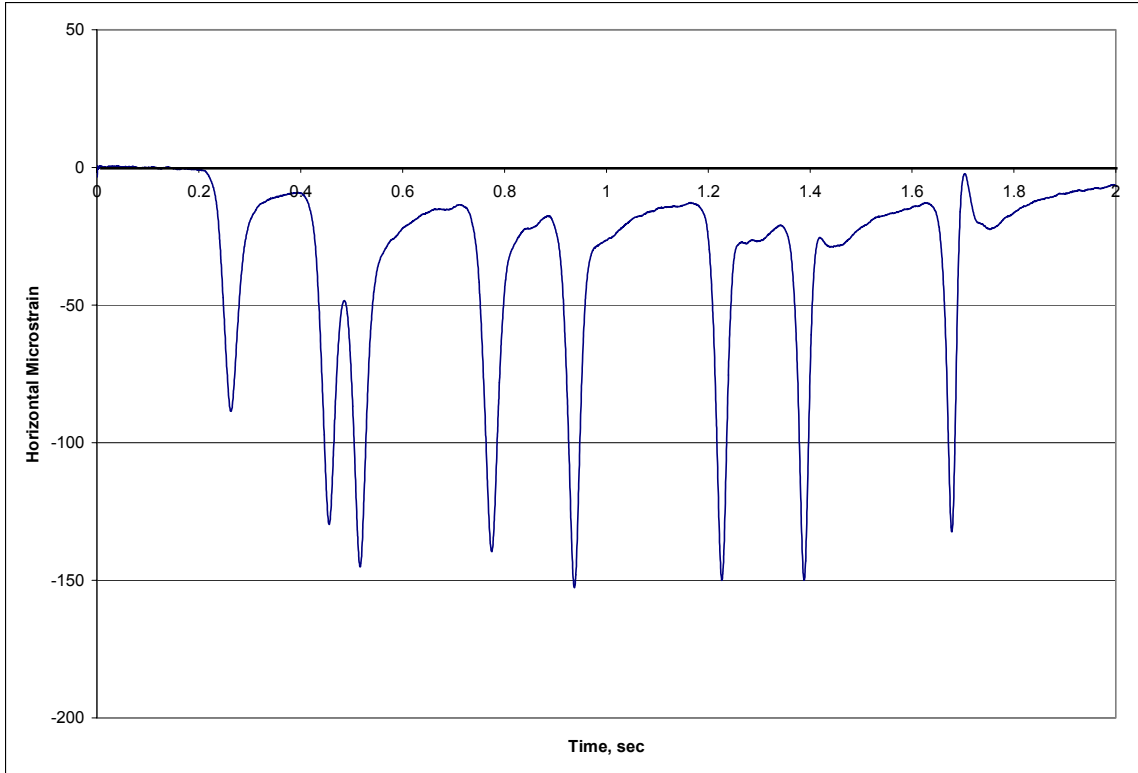


Figure 4.3 Transverse Strain Trace – Example 1.

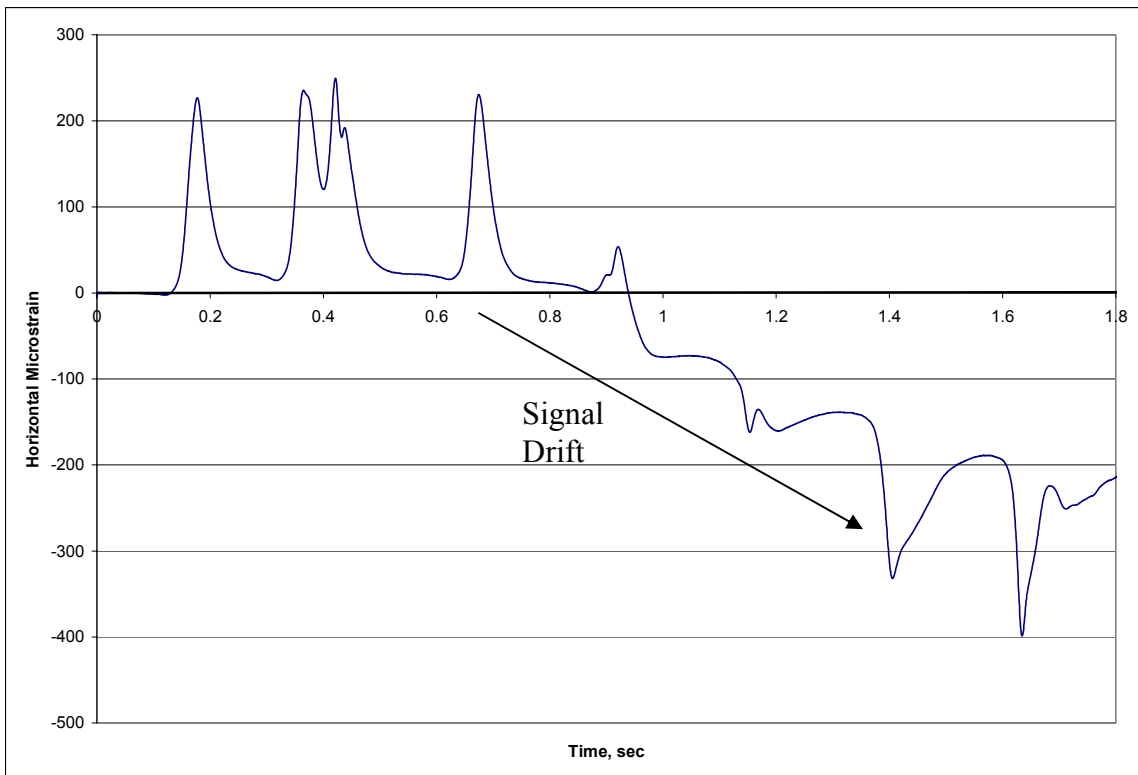


Figure 4.4 Transverse Strain Trace – Example 2.

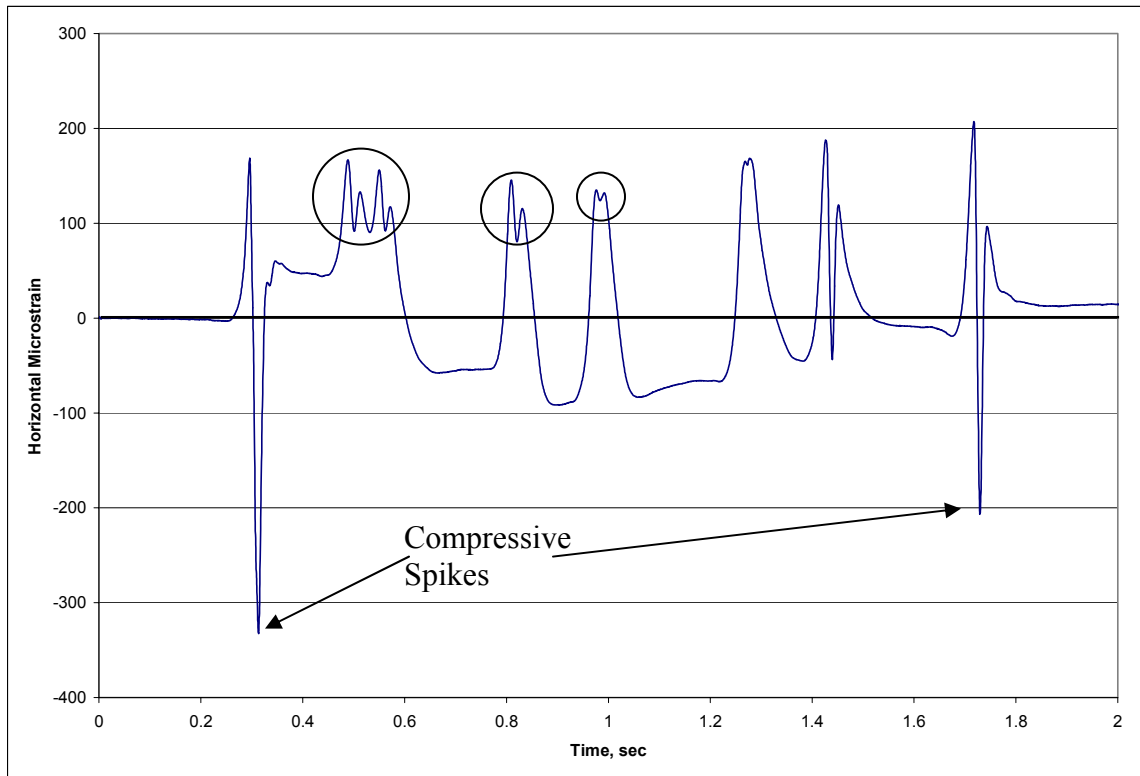


Figure 4.5 Transverse Strain Trace – Example 3.

Figures 4.1-4.5 are just a few examples of the different strain traces that were collected from live truck data. As with this example, every test section at any testing date had a wide range of different responses of which these are only a small sampling.

STRAIN TRACE PROCESSING

As mentioned above, the dynamic strain gauges were very sensitive to the exact lateral placement of the load were susceptible to noise and signal drift. Therefore, there were many challenges in determining how to best handle the data. In developing a processing scheme, there were a few components that were important to include and a few issues that needed to be addressed. Some of these are listed below:

- Clean the signal of electrical noise.
- Record the important data.
- Produce an accurate and relevant strain value.
- Robust enough to handle all varieties of strain traces (one scheme for all traces).
- Reproducible output (not overly dependant on processor judgment).
- Automated and efficient system.
- Easily sort and query data.

Many different ideas and schemes were explored, including measuring peak strains from an original baseline, calculating strain amplitudes per axle and even trying to calculate the area under the strain trace curve. But only one approach stood up to all the

requirements listed above. It should be noted that a graphical engineering software package DADiSP was used to develop the processing algorithms and procedures. The steps below are contained in one window worksheet within DADiSP that allowed for a simplified and organized processing procedure.

First, the signal was cleaned of electrical noise by taking a moving average of 20 points. The moving average smoothed the curve, as shown in Figure 4.6, without losing the important peaks and valleys. Then the inflection points of the signal were established and marked. The processor could adjust certain parameters, including the spread of points that the program scans and the minimum strain difference between consecutive inflection points, to manipulate the program in order to mark the relevant points. This step involved human judgment and interaction. In most cases, the parameters did not have to be adjusted, but in some cases it was necessary to have the option. For instance, some traces had erroneous inflection points within one axle hit or along the baseline which did not need to be marked. As an example, the small humps on the tandem and first and second single axle on the strain trace showed in Figure 4.5 (circled in the figure) should not be considered a strain cycle or an important event.

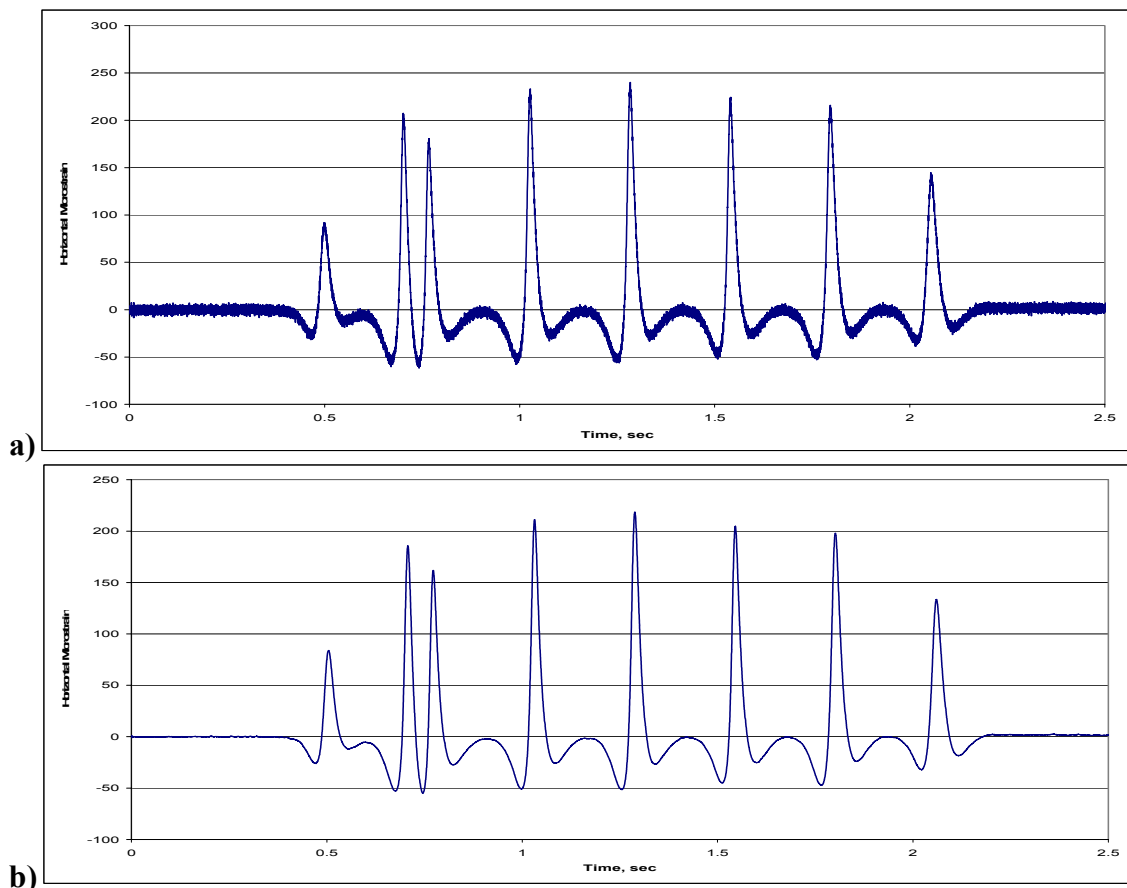


Figure 4.6 Longitudinal Strain Trace a) Before and b) After Moving Average.

After the processor was satisfied with the inflection points, an algorithm was run to compute an average strain amplitude of the truck pass. The amplitude took into account both the compressive and tensile responses into an overall amplitude. Also, the amplitude averaged the effect of different strain responses due to mechanical alignment. Figure 4.7 is an illustration of the strain amplitude that was computed for the strain trace in Figure 4.2. Notice that the inflection points are marked with dots, and the strain amplitude is between the top and bottom line. The figure does not show the scale in strain, but the value is not of importance in this discussion, merely how the inflection points were gathered and the strain magnitude was quantified.

The strain amplitude was determined by first calculating the average of all the inflection points. This is the middle line in Figure 4.7. Ordinarily, the average was at or near the signal's baseline. Then the inflection points above the mean line were averaged to produce the high line or maximum portion of the amplitude. Then the same was done with the inflection points below the mean line to produce the lower line. The strain amplitude and response for that truck pass was then the difference between the maximum and minimum average values.

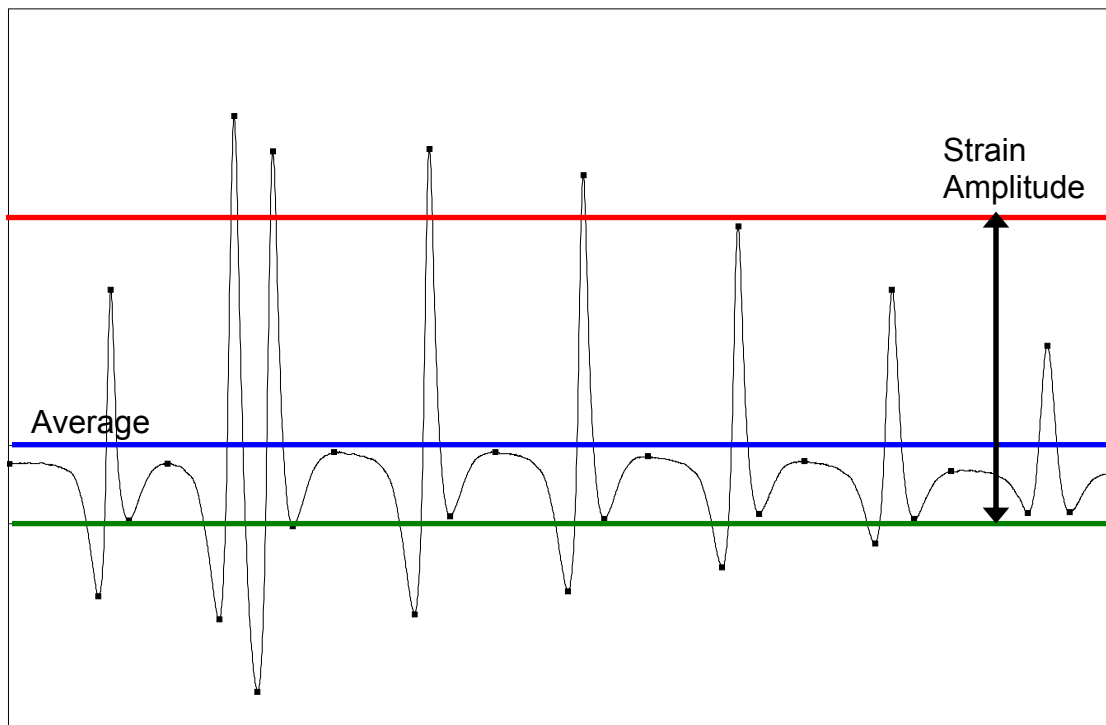


Figure 4.7 Strain Amplitude Illustration – Example 1.

Processing the axles individually was considered, but it was deemed impractical and unnecessary because the axles were similar in pounds per tire. Also, in instances where the signal drifted, it was difficult to determine a baseline and peak for each axle. Again, consider Figure 4.4 as an example. If the strain magnitude was calculated from the axle peak back to the original baseline, inaccurate strains would have been determined.

Further, it is difficult to determine a relative baseline and maximum for each axle of that signal. Figure 4.8 shows the processed strain trace from Figure 4.4 using the developed procedure. The average amplitude gives an overall measure of the induced strain response of that truck over eight strain cycles (one for the steer, two for the tandem and one for each of the singles). As intended, the amplitudes shown in Figures 4.7 and 4.8 are essentially an average of the amplitude of all eight of the individual axles, considering both the compression and tension response. Further, Figure 4.9 shows the processed strain trace and subsequent strain amplitude for the rather irregular strain trace shown in Figure 4.5. From the figure, the processing algorithm does an adequate job of recording the relevant values and calculating an average strain amplitude for the truck pass.

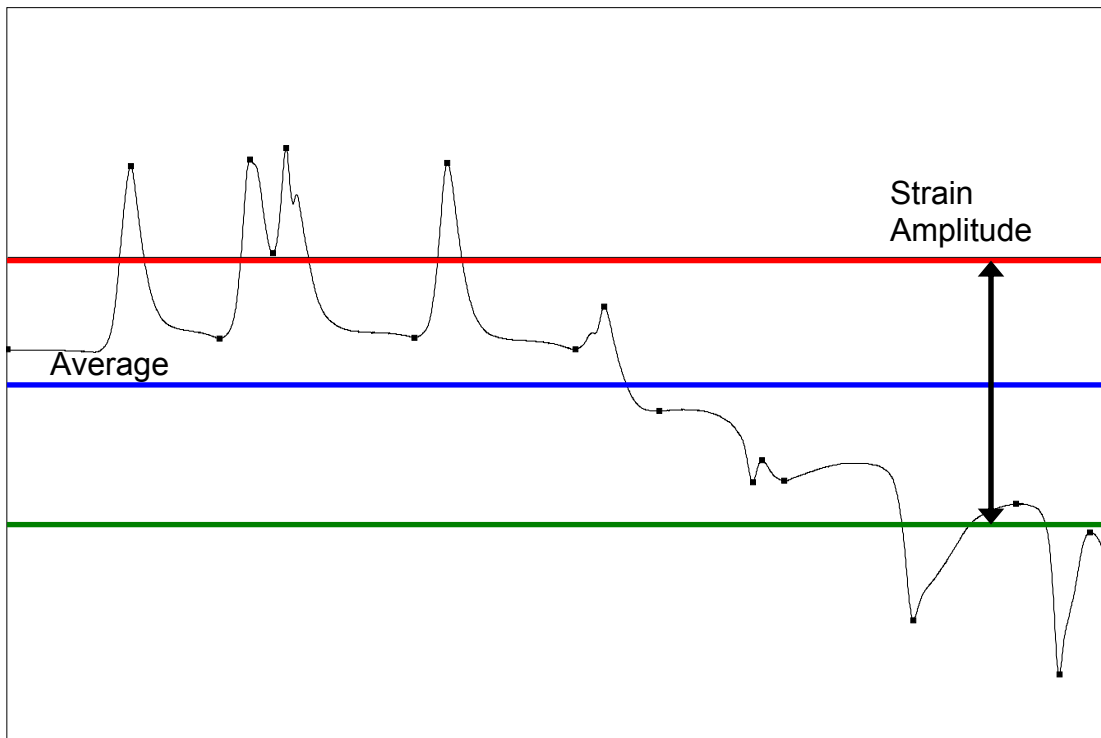


Figure 4.8 Strain Amplitude Illustration – Example 2.

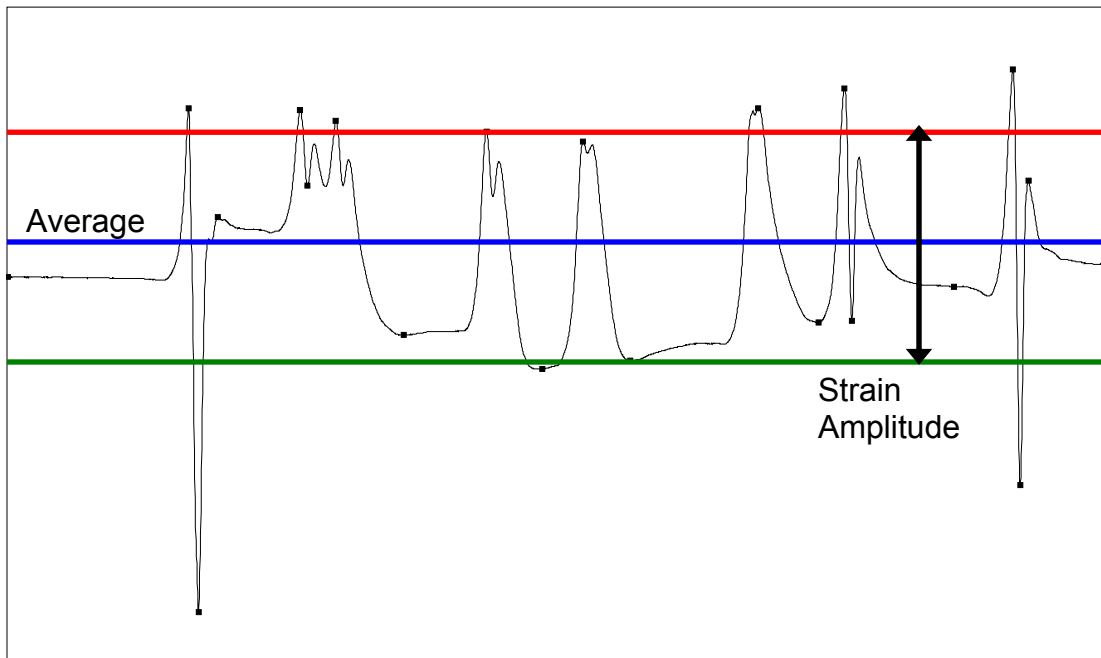


Figure 4.9 Strain Amplitude Illustration – Example 3.

In the processing window (Figure 4.10), there was a graphical view of the original trace in the top left and the processed signal in the top right. From the visual information in the processed window, the processor could then make needed adjustments to the parameters to mark the significant inflection points in order to produce the most accurate strain amplitude for the given signal. As mentioned, the adjustments to the algorithm included the number of points scanned to calculate an inflection point and the minimum difference between consecutive inflection points.

Once the signal was satisfactory, the processor “recorded” the truck pass. The program at this point asked for the gauge identification, truck identification and the pass number to keep the information organized. The recorded data are shown in the bottom right window which includes the gauge factor (which is unique to each strain gauge), truck, pass, maximum and minimum inflection point as well as the amplitude in microstrain.

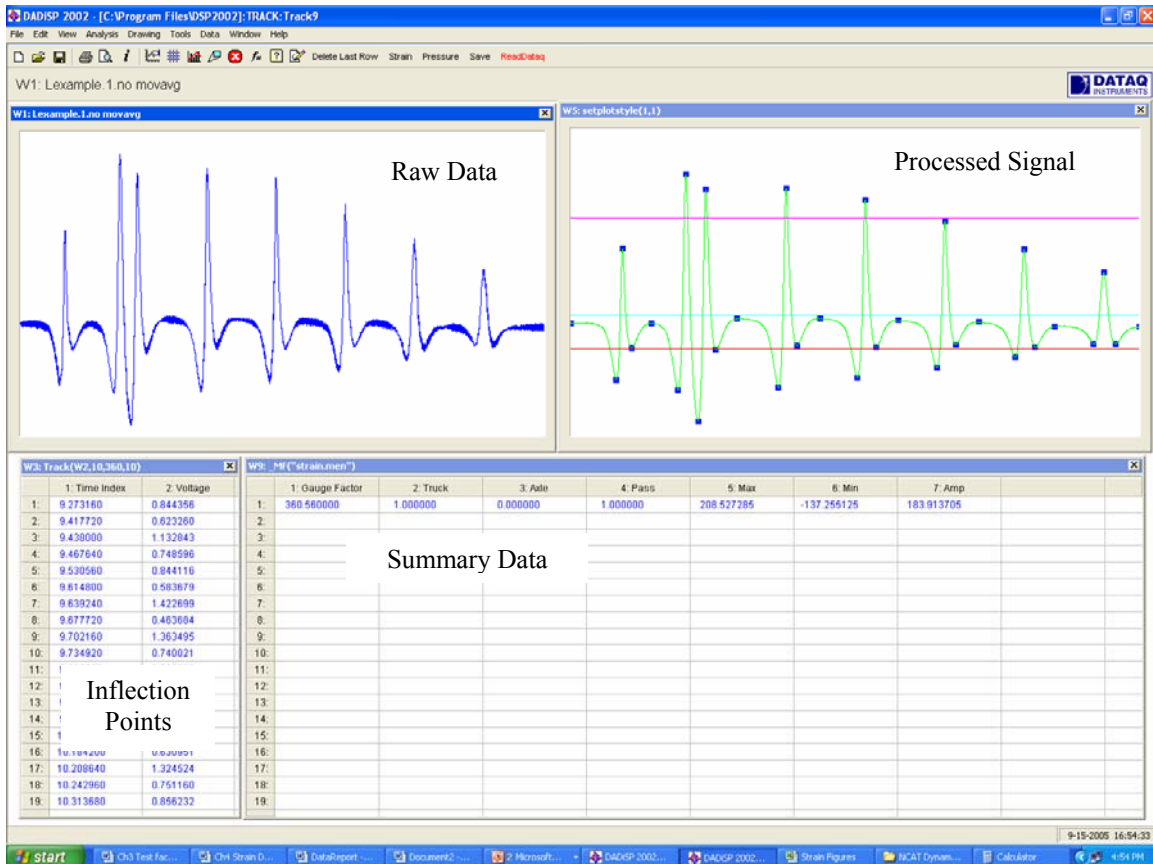


Figure 4.10 Strain Processing Window.

From the processing window, the strain traces were easily imported from the acquisition software, processed and recorded. For the most part, no adjustments to the algorithm were necessary, and the process was fairly efficient. All eight test sections, including 112 strain gauges, each with fifteen truck passes, took approximately ten hours of processing. Therefore, a week’s worth of dynamic data was collected and processed before the next data collection effort.

STRAIN CHARACTERIZATION

All of the truck passes for each strain gauge were collected, processed and stored. But recall that there were twelve strain gauges per test section; therefore, one truck pass produced, at most, twelve different strain readings. More precisely, there were six gauges at each orientation, so each truck pass had at most six readings in both the longitudinal and transverse orientation.

Depending on where the truck tires actually passed through the gauge array, the strain values varied. For example, Figure 4.11 shows three longitudinal strain traces from the same truck pass, one at each lateral offset. From the figure, the truck tire was closest to the right gauge because it registered the highest strain value, and the left gauge registered the lowest. It could be argued that the right strain gauge registered the “best hit” for this

particular truck pass. The next truck may have been closer to the center gauge, causing it to register the highest.

Because the strain reading that most accurately measured the response of the truck was of interest, the maximum reading of each orientation (transverse and longitudinal) was considered the strain response for each corresponding truck and pass. In the case of Figure 4.11, it was the right longitudinal gauge, and for other passes, it may have been the center or left gauge. If an average was taken of all the longitudinal amplitudes, then the strain value would be incorrectly reduced. Remember that the reasoning for an array of gauges, rather than just gauges located directly in the wheelpath, was to capture the lateral placement of the trucks. With this scheme, it was more likely that one of the three offsets very closely registered a direct hit of the tire over the gauge, thus producing the maximum strain value.

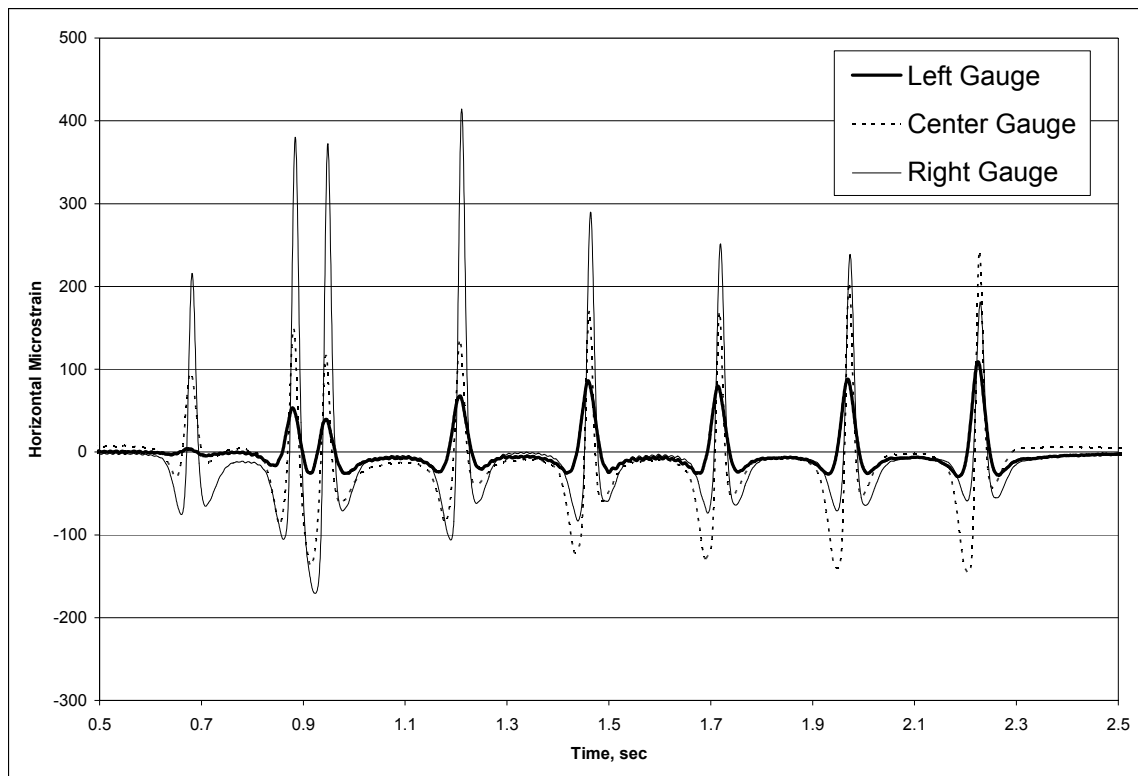


Figure 4.11 Effect of Lateral Offset.

DATA STORAGE

The processed strain data, along with the other collected data from the project, was stored in a Microsoft Access database. Each strain reading was stored by date, section, orientation and location which allowed for easy retrieval and investigation. The maximum and minimum inflection points along with the strain amplitude were stored. Queries were created to determine the maximum strain amplitude reading per truck pass in the manner described above. The Access database was also critical in combining and

relating all the data from the project including field performance, material properties, environmental condition and trucking data.

CONCLUDING REMARKS ON DYNAMIC DATA

Processing dynamic pavement response data under live truck traffic is quite a challenge considering the volume of data collected and the variability in the data. The quirks of the sensitive instrumentation adds one level of complexity, and the live truck traffic adds another. These challenges have been noted by other researchers dealing with dynamic data and truck loading (e.g., Al-Qadi et al., 2004).

The processing procedure developed at the NCAT Test Track slowly evolved as the test cycle progressed. It began in a spreadsheet program retrieving inflection points manually and evolved to a more robust and efficient process. As the understanding of the traces grew, new ways to automate the process were incorporated. The final procedure still involved a level of human interaction which is both important and necessary. There are times when judgment is necessary regarding the validity of the gathered data or basic engineering judgment is needed to determine the relevant characteristics of each dynamic trace.

It should be noted that the method is not infallible, but it does produce repeatable and accurate strain values for the vast majority of signals. The results are repeatable in the sense that the same numbers are generated regardless of the processor. It must be further noted that the processing personnel did receive extensive training and a quality assurance system was in place to catch any mistakes in the processing procedure. As mentioned, many improvements to the process have been made throughout this test cycle, and it is expected that even more will be added in the subsequent testing cycles to make the process more efficient and flexible to the variety of traces.

CHAPTER 5 – METHODOLOGY AND PARAMETER CHARACTERIZATION

INTRODUCTION

The fatigue transfer functions developed from the 2003 NCAT Test Track were derived strictly from field data without laboratory testing or theoretical models. Therefore, the process was fairly unique and required a massive amount of data collection and synthesis. From Figure 1.1, the inputs (material properties, environment, traffic and the pavement structure) for M-E analysis were measured and quantified, in situ, at the Test Track. The material properties were determined using FWD testing; the environmental data were collected continuously via temperature probes, TDRs and the weather station; the traffic was monitored by weight and mileage data; and the layer thicknesses were directly measured during construction. Further, the pavement response was measured from field instrumentation (strain gauges and pressure plates) rather than calculated using a theoretical model. And finally, the pavement performance was monitored and recorded in the field.

From the above field data collection efforts, the fatigue transfer functions were developed or calibrated by working Figure 1.1 in both the forward and backward direction, as shown in Figure 5.1. Simply stated, the transfer functions were calibrated to most closely relate the pavement response to performance through a transfer function. The methodology section will further describe how exactly the damage was calculated and accumulated, and the parameter characterization will describe in more detail how all the components in Figure 5.1 were quantified.

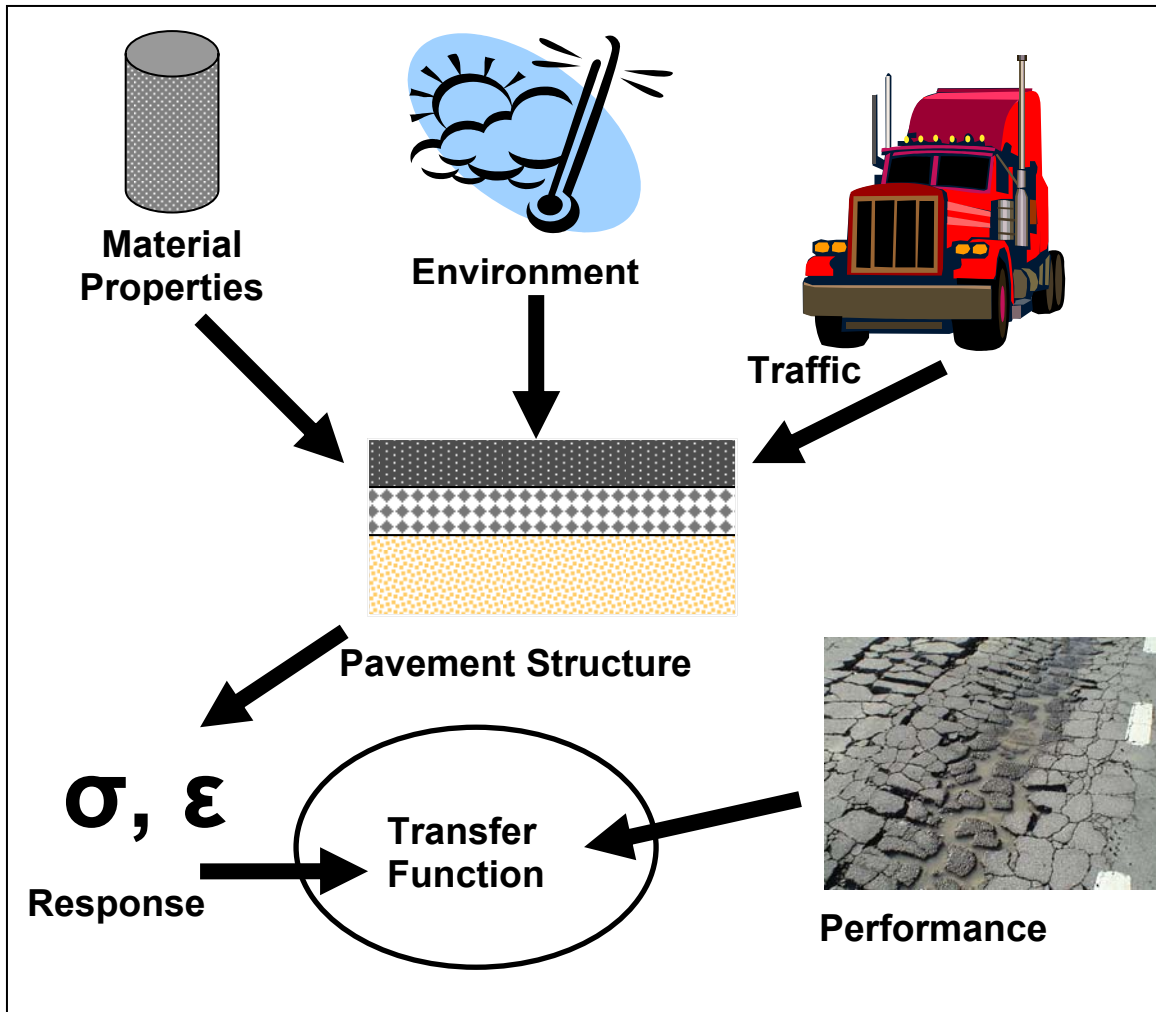


Figure 5.1 Illustration of Transfer Function Development.

METHODOLOGY

As a very general explanation, the fatigue transfer functions were developed by first summing or accumulating the damage, according to Miner's hypothesis, due to the applied truck loads and then calibrating the functions so that the damage equaled unity at the time of observed failure. As mentioned in Chapter 2, failure can be defined in many ways and will be explored in more detail later. The damage was calculated hourly to account for changes in strain magnitude and HMA stiffness due to daily temperature fluctuations. The induced strain is dependant on temperature somewhat indirectly though the stiffness of the HMA layer, which is a function of the temperature of the material.

Recall from Miner's hypothesis (Equation 1.1) the two variables: the allowable cycles until failure, N_f , and the applied loads, n . In order to successfully develop transfer functions, these two parameters had to be calculated over the testing time to accurately accumulate the damage. A record of the traffic data, or applied cycles, and temperature data were kept continuously over the test cycle, but the strain data and FWD data were collected only periodically. As mentioned prior, it was not practical to collect continuous

dynamic or stiffness data for every truck pass or every hour. As a result, relationships were developed to accurately estimate the stiffness and strain data at a given condition (temperature). The stiffness – temperature and strain – temperature relationships, as well as the respective procedures to develop the relationships, are presented later in this chapter.

In summary, the procedure employed to calibrate fatigue transfer functions in this study followed these steps:

1. Determine the number of truck passes for the given hour (triple-trailer trucks and box trailer).
2. Determine the mid-depth temperature of the HMA layer for the given hour from temperature probe data.
3. Use the strain – temperature relationship to estimate the induced strain due to the given truck at the given temperature.
4. Use the stiffness – temperature relationship to estimate the HMA stiffness at the given temperature.
5. Determine the time of fatigue failure.
6. Calculate the cycles to failure (N_f) for the given condition.
7. Calculate the incremental damage (D_i) for the given traffic cycles (n) and cycles to failure (N_f).
8. Repeat for each hour and accumulate the damage over the test cycle until the failure criterion is met.
9. Calculate the regression constants (calibrate the model) so that the total damage (D) equals 1 at time of failure.

The remaining topics of this chapter will discuss in more detail how the data were generated and how the relationships were quantified in the steps above. In other words, each element in Figure 5.1 will be further discussed.

TRAFFIC CHARACTERIZATION

Weight Data

The triple-trailer trucks used at the NCAT Test Track were loaded to accelerate the testing without venturing too far from U.S. legal axle weights (20-kip single axle, 34-kip tandem axle) The generic load distribution is shown in Figure 5.2, but the exact loads were monitored and varied slightly from truck to truck. Exact axle weight data are given in Table 5.1 for the five triple-trailers and the box trailer. Notice that the box trailer was not loaded as heavily as the triples because it served as the conventional highway vehicle comparison, in both configuration and load, for trucking and fuel studies. From the weight data and subsequent discussion, the triple-trailers were considered equal and duplicates of the same testing vehicle, while the box trailer was considered a separate vehicle for the analysis.

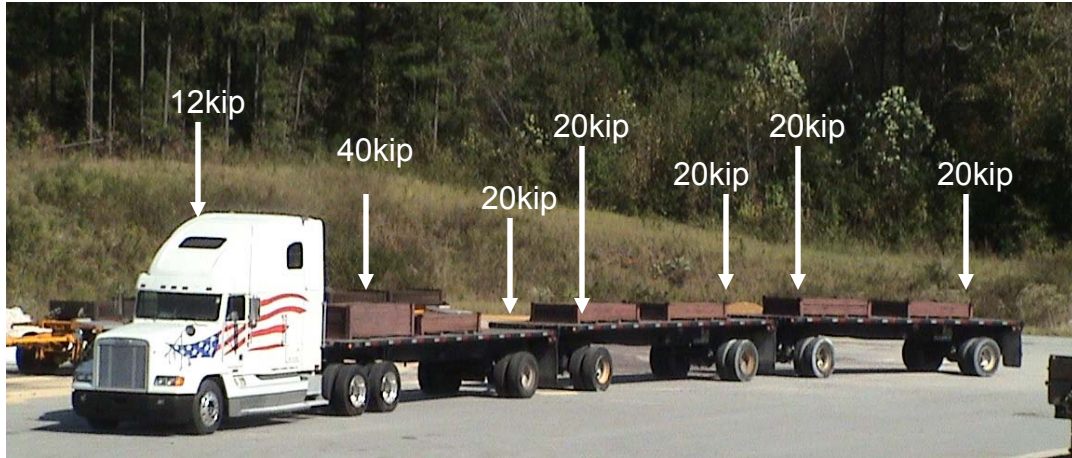


Figure 5.2 Triple-Trailer Weight Distribution.

Table 5.1 Axle Weight Data by Truck

	Steer	Drive Tandem, lb		Single Axle, lb				
Truck ID	lb	1	2	1	2	3	4	5
1-Triple	10150	19200	18550	21650	20300	21850	20100	19966
2-Triple	11000	20950	20400	20950	21200	21000	20900	20900
3-Triple	10550	20550	21050	21000	21150	21150	21350	20850
4-Triple	10500	21050	20700	21100	21050	21050	20900	21050
6-Triple	11200	19850	20750	20350	20100	21500	19500	20300
Average	10680	20320	20290	21010	20760	21310	20550	20613
COV	3.9%	3.9%	4.9%	2.2%	2.5%	1.7%	3.6%	2.2%
	Steer	Drive Tandem Axle		Rear Tandem Axle				
5-Box	11550	16850	17000	16800	16100			

Lateral Distribution of Traffic Loads

The lateral distribution of the axle loads, or wheel wander, was measured and investigated at the NCAT Test Track for two main reasons: to determine if the wheel wander was comparable to other open-access highways and to better understand the dynamic strain data. The lateral position of the outside tire was measured using axle-sensing strips installed in a pattern such that the lateral offset of the tire could be calculated. Further information regarding the installation, calibration, data processing and results of the lateral positioning system used at the Test Track can be found elsewhere (Timm and Priest “Wheel Wander”, 2005).

Figure 5.3 is a summary of 3,400 axle passes separated into the two shifts, AM and PM. From this figure, the distribution was observed to be normal and have a comparable standard deviation, although at the low end, to other open-access highways (Timm and Priest “Wheel Wander,” 2005). The distribution of loads greatly affects field performance, so verifying that the Test Track traffic was similar to open-access roadways allowed for the direct application of results from the Test Track to open facilities. Some other full-scale testing schemes, including loaded wheel apparatuses, travel the same path and do not include representative wheel wander. Therefore, their results are even further

accelerated but do not replicate field performance. This accelerated damage occurred at the WESTRACK experiment, a full-scale testing facility in Nevada, where robotically-driven trucks with little or no wheel wander were used to traffic the test sections (Epps et al., 2002).

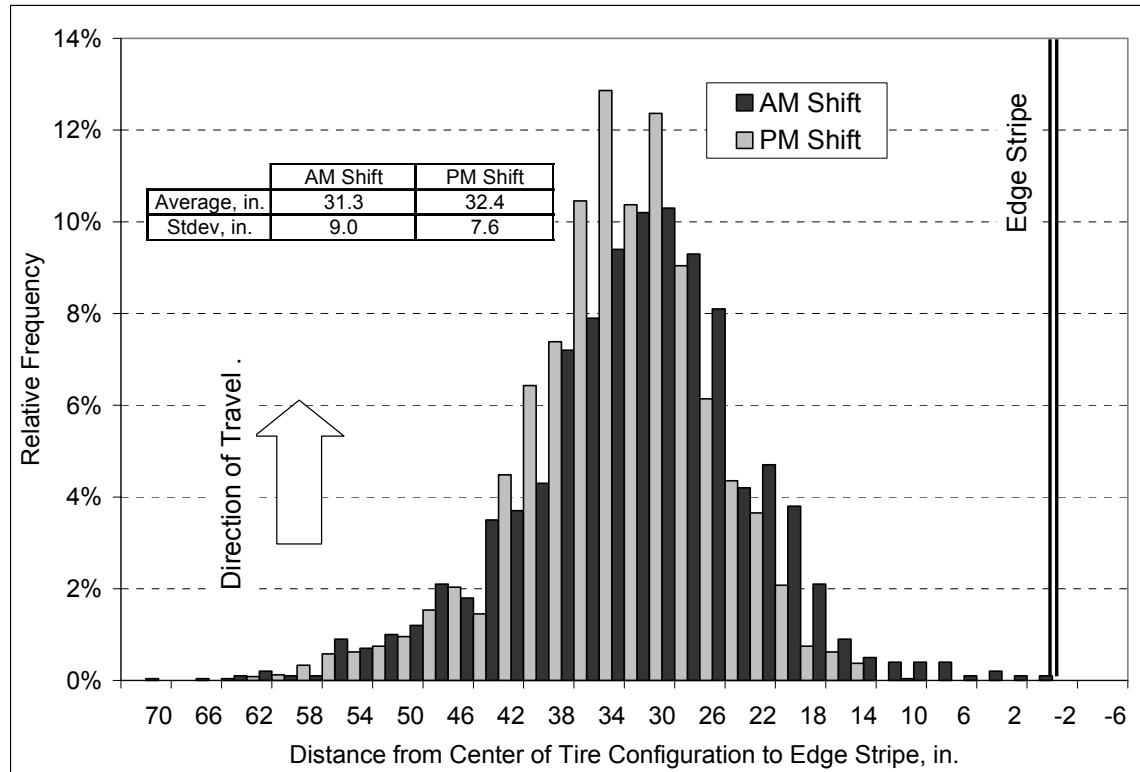


Figure 5.3 Statistical Summary of Wheel Wander Data (Timm and Priest “Wheel Wander,” 2005).

The wheel wander data were then broken down to investigate the lateral offset of each individual truck and driver, which is presented in Figures 5.4 and 5.5. The figures show the average offset and spread of the data for each vehicle and shift as well as the three strain gauge offsets. From these figures, one can see that each truck’s trailers are aligned a little differently as was discussed in regards to the strain data in Chapter 4. For example, Truck 3 trailed fairly extensively towards the center of the lane. The figures also show that the drivers were fairly consistent in regards to where the steer axle was placed. Considering all the drivers, the steer axle was typically placed between 19 and 29 in. from the outside lane stripe. From the figures, representative wheel wander, in regards to both the strain data and replicating highway traffic, is only achieved when all the trucks were included together. It is important to note that Truck 6 was added to the fleet following this investigation, which is why it is not included in Figures 5.4 and 5.5.

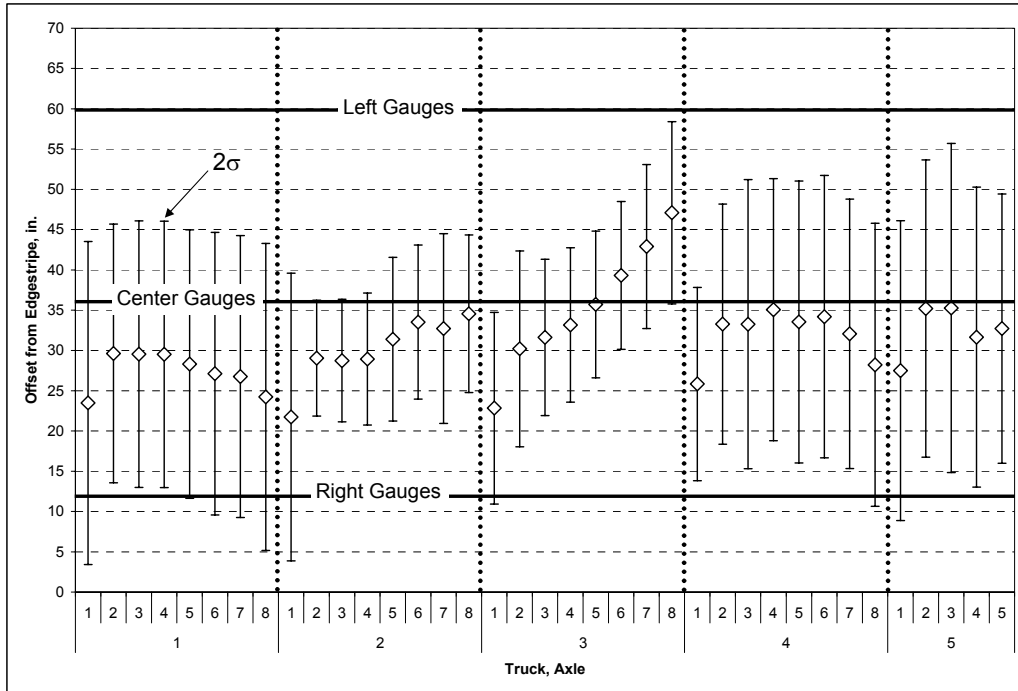


Figure 5.4 Wheel Wander Data – AM (Timm and Priest “Wheel Wander,” 2005).

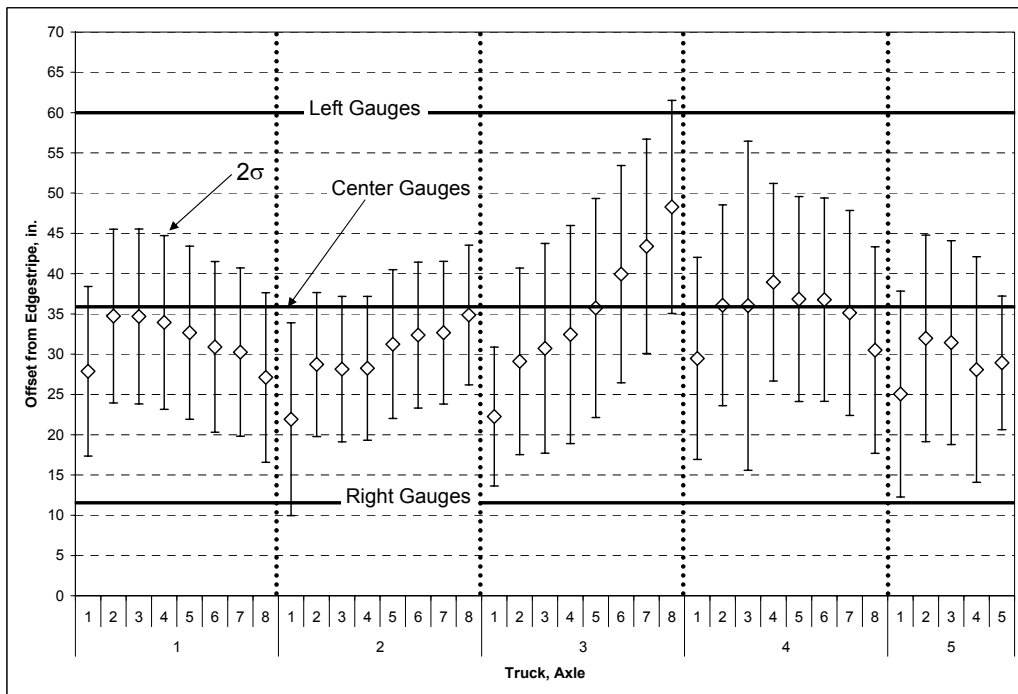


Figure 5.5 Wheel Wander Data – PM (Timm and Priest “Wheel Wander,” 2005).

To further investigate the effect of lateral placement on the collected strain data, ten consecutive passes of each triple-trailer were collected and analyzed. The strain data, shown in Figure 5.6, agreed with what was concluded from the wheel wander data. The individual trucks were fairly consistent by pass, and the range of variability was captured in about three passes. The figure shows the average strain magnitude over the number of passes shown on the x-axis. From the figure, no additional information was gathered with ten passes versus three passes. Additionally, the only way to gather the full range of strain response from the various sensors in the array was to gather data from all of the trucks, and thus capture the full lateral wander. Therefore, the testing scheme consisted of collecting and processing, in the manner described in Chapter 4, three passes of all the trucks. Then, the maximum strain response for each pass, considering all the triple-trailers, was determined and averaged together to quantify the strain response for that test section. Basically, the five different trucks provided the full range of registered strain response per pass, and then three passes were averaged to account for random variation in the data.

A similar observation was made regarding the effect of lateral position on the recorded strain values at Virginia’s Smart Road. Al-Qadi et al. (2004) reports that when collecting dynamic data, multiple truck passes are collected and processed in attempt to collect a direct hit of the tire over the gauge. From the multiple passes, the maximum strain value was considered the direct hit and was stored.

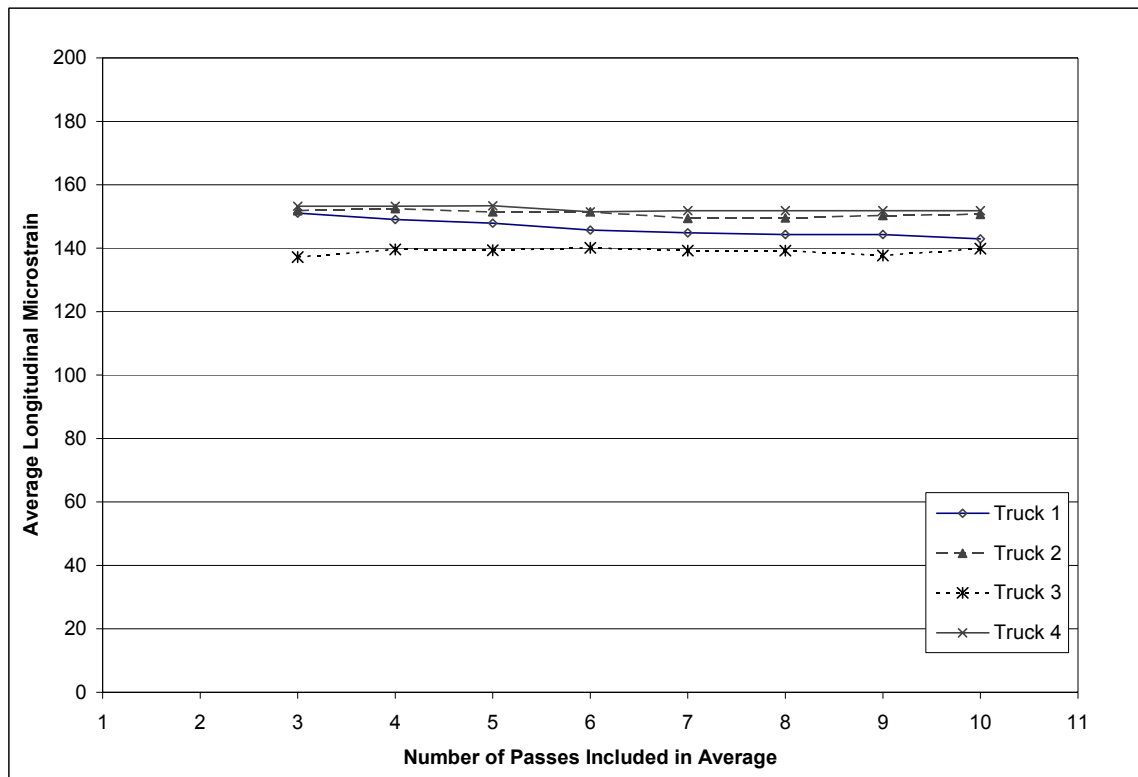


Figure 5.6 Average Strain by Truck and Pass.

Traffic Volume

The trucking operation at the NCAT Test Track consisted of two 7.5 hour shifts, five days a week. The traffic volume data were recorded based on the mileage per shift and then converted to laps per hour based on the shift schedule and track length (1.7 mile/lap). Typically, each truck completed 28 laps in an hour. From above, the triple-trailer laps were combined and considered together, while the box trailer was considered separately.

Concluding Remarks on Traffic Characterization

The traffic at the NCAT Test Track was highly controlled, and thus the characterization was fairly straightforward. There were only two vehicle types, and the only difficulty came in conjunction with the embedded instrumentation. For M-E design of open-access facilities, the traffic characterization will be more complicated with a variety of different vehicles over a range of loads. Load spectra, which incorporates the range of axle type and loads, is most suited for M-E design and is one of the main benefits of the M-E design process. Traffic data adds another layer of conditions, along with environmental, to the M-E design procedure flow chart shown in Figure 2.1.

The investigation into the lateral distribution of the traffic was critical in understanding the collected strain data and accurately quantifying the strain response under traffic. It was also important to verify that the wheel wander, and thus the performance, at the Test Track was comparable to open-access facilities.

HMA STIFFNESS CHARACTERIZATION

Backcalculated Stiffness Data

As described in Chapter 3, FWD testing was conducted monthly at three random locations per test section. The pavement layer stiffnesses were then backcalculated from the FWD deflection data using EVERCALC 5.0. For backcalculation, the pavement structure was divided into three distinct layers as shown in Figure 5.7. A few different cross sections were investigated, and the cross section shown produced the lowest error and most repeatable results. As supplemental information, the Structural Study sections were in a fill area of the original Test Track construction, and the eight sections were built up from the deeper cross section of the 2000 testing cycle. Therefore, the backfilled material had a different stiffness than the existing soil, which was also technically a fill. Additionally, when the crushed granite granular base was considered separately, the backcalculated moduli were extremely low and highly variable. Further information regarding the FWD testing plan and backcalculation procedure can be found elsewhere (Timm and Priest “Material Properties,” 2006).

The HMA stiffness was of most interest to this research; therefore, any reference to stiffness from here on refers to the HMA stiffness. Further, the stiffness data presented are averages of the stiffness values from the outside wheelpath at the three random locations within each test section. The average stiffness value along with the average section thickness used to calculate the mid-depth temperature, gave the best correlation

between HMA stiffness and temperature, which was the ultimate goal of the material characterization portion of this research.

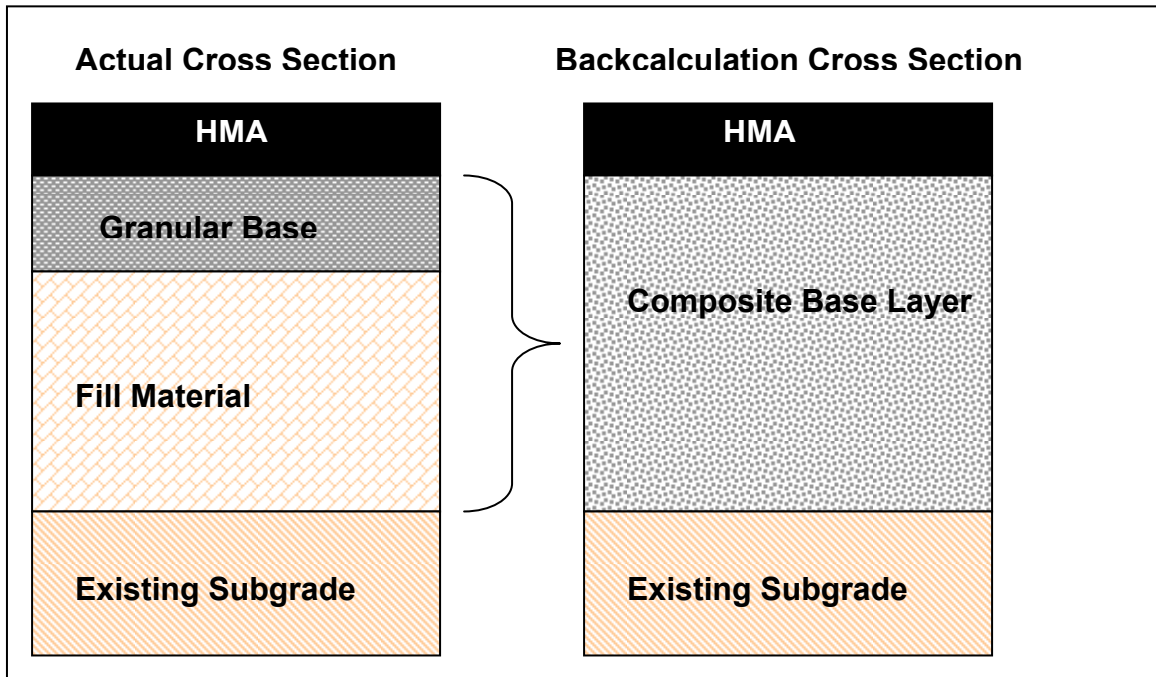


Figure 5.7 Actual and Backcalculation Cross Section.

Seasonal Trends

As noted prior, the HMA stiffness is highly dependant on temperature, which can be seen in Figure 5.8. The figure shows the seasonal trend in the stiffness data for all eight test sections. Note that the data have not been corrected to a reference temperature in order to explore the effect of temperature. As expected, when the temperature increased in the summer, the pavement softened. Also notice after the summer, sections N1 and N2 deviated from the general trend of the other test sections. The deviation in stiffness was due to the extent of cracking in those two sections at that time. The remaining material analysis disregards any stiffness data after initial cracking was observed because traditional M-E design does not account for cracking in the pavement models (“Thickness Design,” 1982; Eres, 2004). Further, the presence of cracks can cause erroneous deflection data from the FWD.

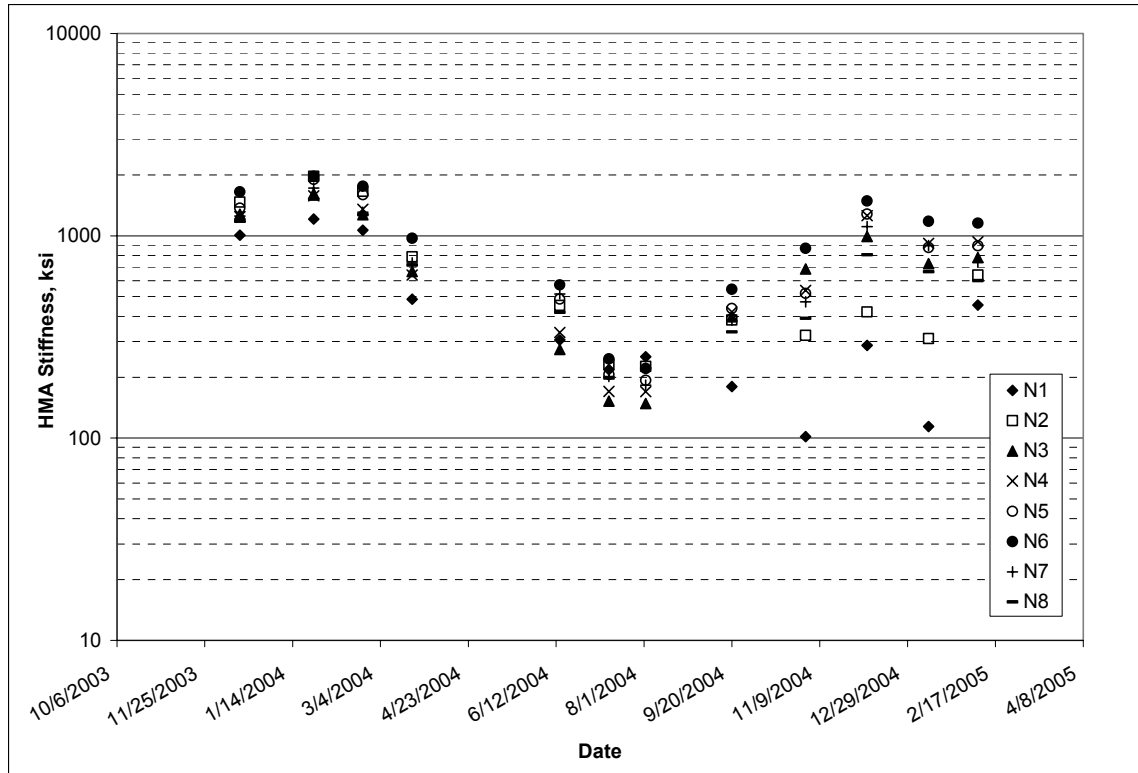


Figure 5.8 Seasonal Trend in HMA Stiffness.

Stiffness Prediction Models

The effect of temperature on stiffness can be better explored by plotting the stiffness as a function of temperature rather than date. Figure 5.9 shows the average stiffness as a function of the mid-depth temperature of the HMA layer. The mid-depth temperature was calculated from temperature probe data collected during FWD testing, assuming a linear temperature profile. The mid-depth temperature is often correlated to stiffness and proved to be the best predictor of stiffness for this study.

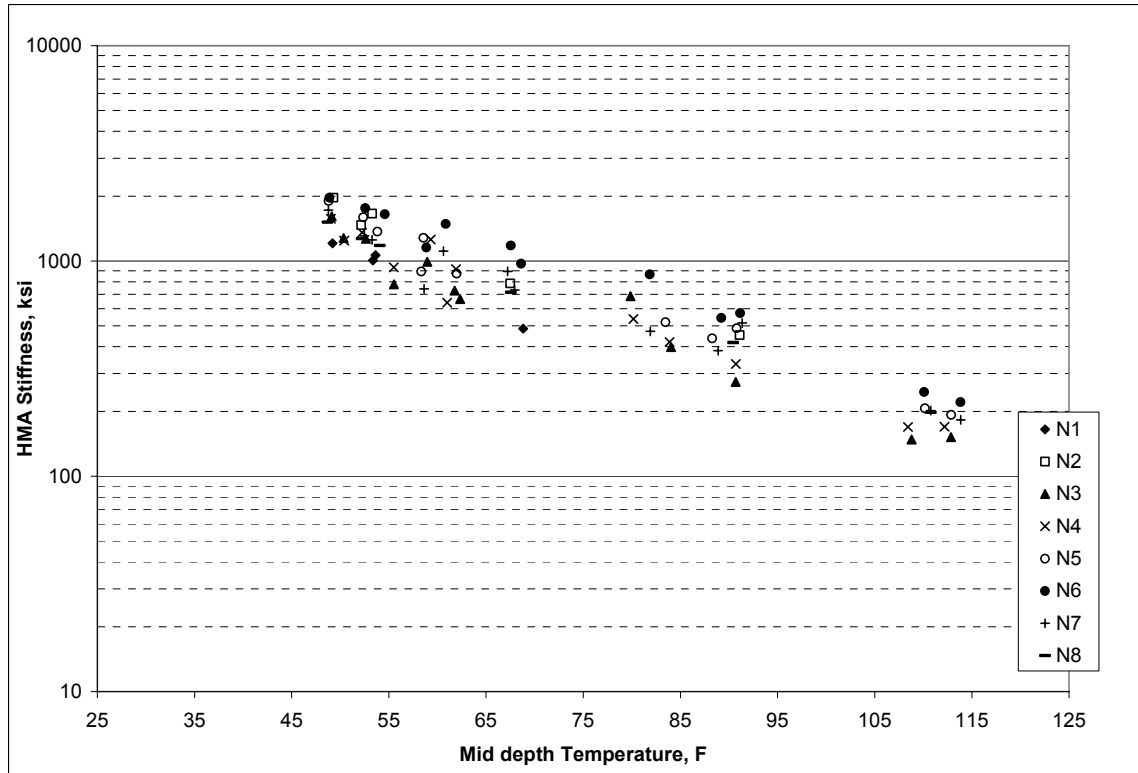


Figure 5.9 HMA Stiffness vs. Mid-depth Temperature.

According to Jameson, Sharp and Vertessy (1992), a similar procedure for investigating fatigue performance was employed at the Australian Accelerated Loading Facility (ALF). They too determined the in situ HMA stiffness – temperature relationship using backcalculated FWD deflection data over a variety of temperatures. During the testing cycle, the stiffness was estimated from the established relationships. Additionally, the researchers at the Australian ALF used the mid-depth HMA temperature and commented that the mid-depth temperature was better correlated to stiffness than the temperature at other depths.

The stiffness – temperature relationship was defined using the following model:

$$E = \alpha_1 e^{\alpha_2 * T} \tag{5.1}$$

where: E = HMA stiffness, psi

T = Mid-depth HMA temperature, °F

α_1, α_2 = Regression constants

A regression analysis was performed for all eight sections, individually, to create accurate models to predict the in situ stiffness given the temperature, which was collected every hour. The relationships were established for each section to account for any differences due to cross section, binder type or construction variability.

The regression constants and R² value for the eight test sections, as well as a general equation considering all the data, are given in Table 5.2 following the form of Equation 5.1. The general model is a good predictor of stiffness, and including other factors like

the HMA thickness and binder type (PG 67-22 unmodified vs. PG 76-22 modified) did not increase the model accuracy. It should be noted that another investigation of the same data determined that there was no significant evidence that the two binders produced consistently different mixtures stiffnesses (Timm and Priest “Material Properties,” 2006). It is also important to point out that there was limited pre-cracking backcalculated stiffness data for sections N1 and N2 because the first FWD testing date was December 2003, and the sections showed signs of cracking in April and June of 2004, respectively. The limited data can also be seen in Figure 5.9 where the data for N1 and N2 covered a small temperature range. Yet extrapolation was warranted because the trend was similar to the other sections.

Table 5.2 Regression Analysis for HMA Stiffness – Temperature Relationship.

Section	α_1	α_2	R^2
N1*	11,696,542	-0.0457	0.985
N2*	14,308,573	-0.0414	0.952
N3	8,809,046	-0.0378	0.904
N4	8,030,572	-0.0351	0.915
N5	11,415,436	-0.0386	0.940
N6	8,482,965	-0.0302	0.962
N7	8,067,465	-0.0342	0.917
N8	6,918,499	-0.0321	0.989
All	8,187,876	-0.0340	0.850
Alvarez and Thompson	4,841,000	-0.048	

* Limited FWD Data

Research using data from Mn/ROAD found a similar correlation between HMA temperature and in situ stiffness which followed the model of Equation 5.1. The regression constants determined by Alvarez and Thompson (1998) are also shown in Table 5.2 and serve as a check of reasonableness. Although the relationship developed by Alvarez and Thompson (1998) used the temperature at 1/3 depth, the relationship follows the same trend and is similar to the relationships developed at the NCAT Test Track. It is also interesting to note that the binder used at Mn/ROAD was a much softer binder than that used at the Test Track. A softer 120/150 penetration (roughly PG 52-34) binder was used, and notice that the intercept value for the temperature – stiffness relationship was much lower than the equations derived at the NCAT Test Track. The relationship developed by Alvarez and Thompson (1998) simply serves as a check and provides confidence in the data.

Concluding Remarks on HMA Characterization

From the above analysis, a relationship between mid-depth HMA temperature and in situ stiffness was developed for each test section. Therefore, the hourly temperature readings were used as predictors of stiffness over the entire testing cycle. This provided a much more accurate stiffness number than a seasonal or monthly average. Additionally, the

analysis quantified the effect of temperature on HMA stiffness, which can be used in other design and research efforts. The study also determined that there was not a significant difference in the in situ stiffness amongst the two binders, which was not necessarily expected (Timm and Priest “Material Properties,” 2006).

STRAIN RESPONSE CHARACTERIZATION

General Trends

As with the HMA stiffness data, seasonal trends and damage were observed with the strain data over time (Figure 5.10). The induced strain is a function of the stiffness of the mix, which is in turn a function of temperature. As a result, the strain response is strongly correlated with the temperature of the HMA layer. From Figure 5.10, the strain values increased during the warmer months and returned to lower values as the fall set in. Recall from prior discussion that the strain values presented are the average over three passes of the maximum reading (best hit) for the five triple-trailer trucks. Additionally, the values presented in Figure 5.10 are from the longitudinal-orientated strain gauges, exclusively.

Unlike the stiffness data, the strain data are also a function of the thickness of the HMA layer. The load bearing capacity of the HMA increases with thickness; thus, the induced strains at the bottom of the layer are reduced with thicker HMA sections. The thickness effect is the central concept behind M-E design: determine the needed layer thicknesses to control the critical responses, such as horizontal strain at the bottom of the HMA layer, given the traffic and seasonal conditions. The thickness effect is especially evident for the two 5 in. sections, N1 and N2, which have much higher strain levels than the other sections. It is more difficult to distinguish the other sections from Figure 5.10, but they will be explored in more detail later.

Another important observation from Figure 5.10 was that the strain values for N8 did not trend back down as the other sections did during the second fall season. This was a result of cracking that was progressing through section N8 beginning in July 2004. By the following fall, the pavement was fairly damaged and no longer intact; therefore, the recorded strain values were higher. Also notice that the strain values for N1 and N2 were especially high after the first spring, when the sections began to show fatigue cracking. Strain data collected after visible cracking were not included in the fatigue models for the same reasons as the stiffness data. One, the readings are especially variable and erratic, and two, it is common practice that fatigue models or transfer functions assume an intact pavement structure.

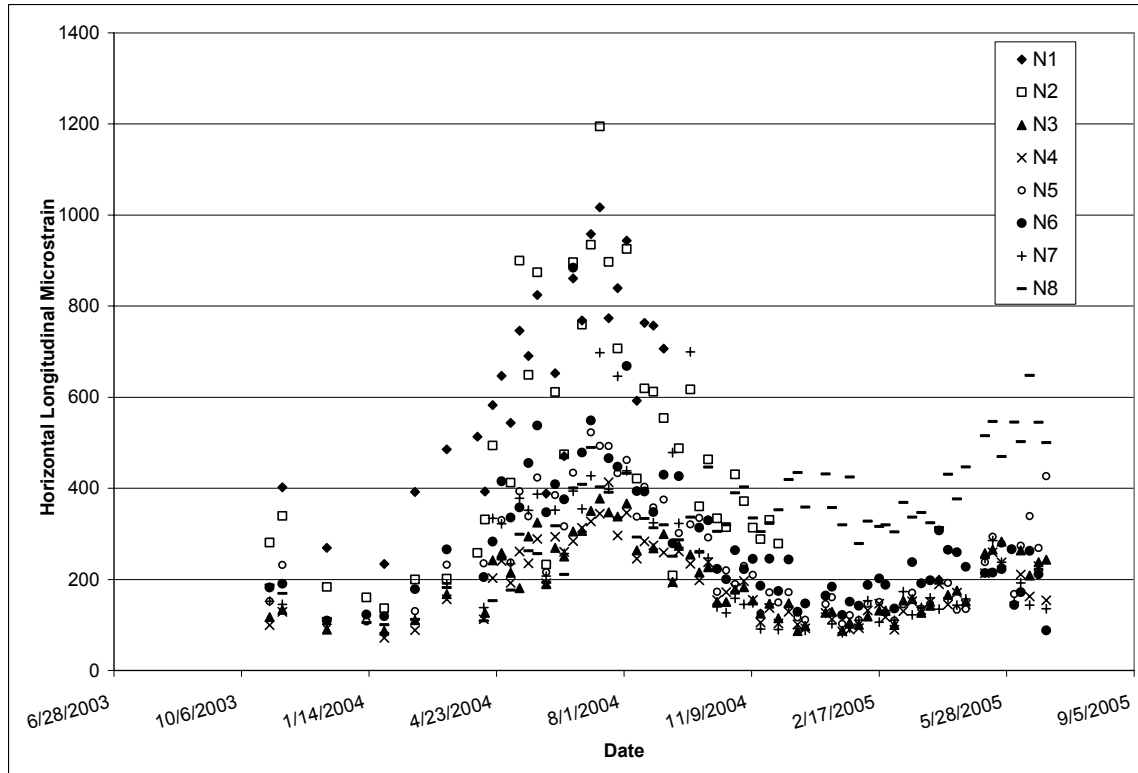


Figure 5.10 Seasonal Trends in Longitudinal Strain Data.

As mentioned, the data presented in Figure 5.10 are from the longitudinal strain gauges, but a similar analysis can be performed considering the transverse gauges. Further, the two orientations were investigated to determine which, or both, should be used in the fatigue prediction models. To compare the two responses, the maximum transverse reading was plotted against the maximum longitudinal reading for each pass, shown in Figure 5.11. In other words, all three passes of many collection dates are presented in Figure 5.11 without averaging. Further, the data shown in Figure 5.11 are from all eight test sections including only pre-cracking dates. There is quite a bit of scatter in the data because it was pooled over a wide range of conditions, but generally speaking, the strain was higher in the longitudinal rather than the transverse direction. From the linear regression line, the longitudinal strain was about 36 percent higher than the transverse strain.

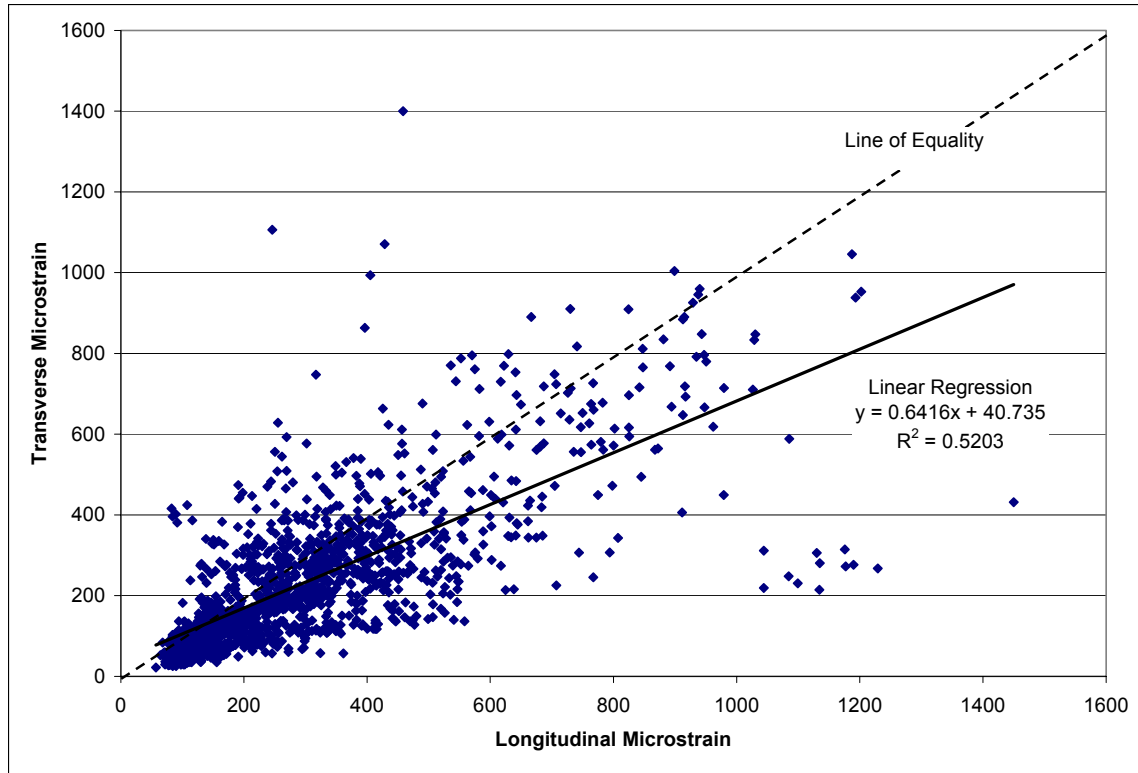


Figure 5.11 Transverse vs. Longitudinal Strain.

Figure 5.12 is another presentation of the same data in Figure 5.11 using a cumulative distribution curve of the ratio of longitudinal strain to transverse strain. From the figure, the longitudinal strain is greater (ratio greater than 1) for approximately 80 percent of the data. Figure 5.12 better portrays the cluster of data at the lower strain levels in Figure 5.11. Al-Qadi et al. (2004) also observed that the longitudinal strain was higher than the complimentary transverse strain. If the two were considered together, an average would have falsely reduced the strain value. It was decided that the most severe response should be used in the analysis, and it was important to stay consistent throughout the procedure. As a result, only the longitudinal strain was considered in the development of the fatigue transfer functions.

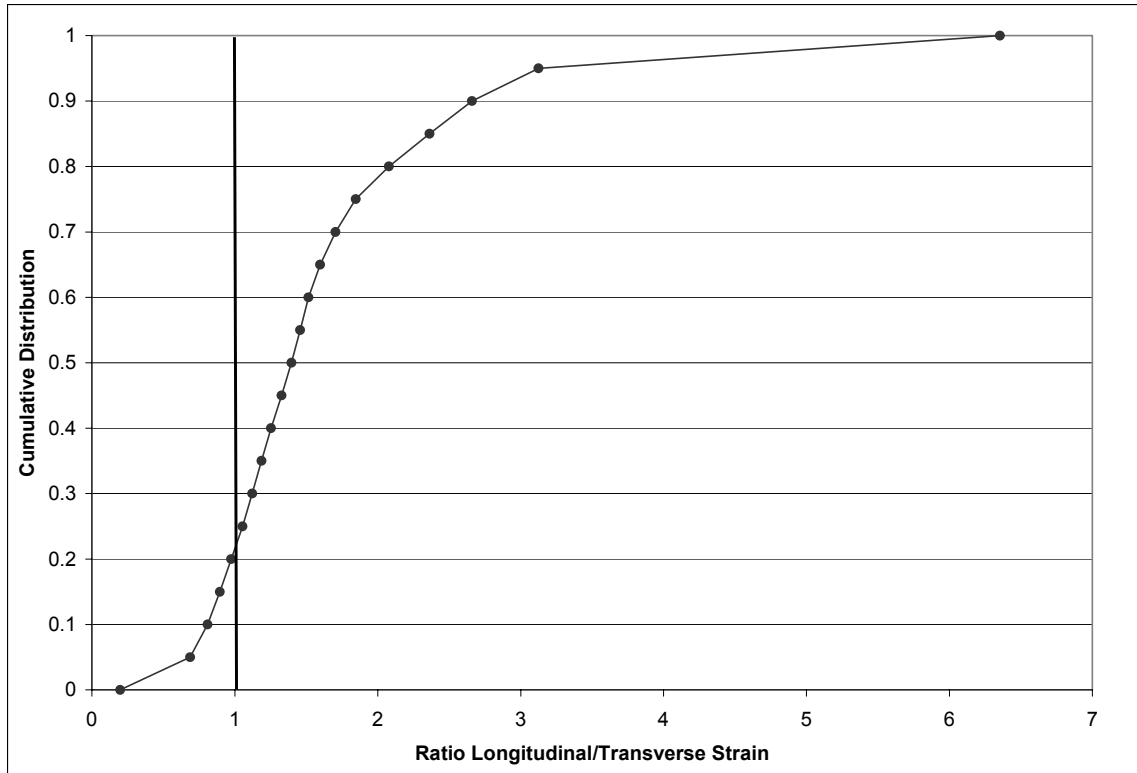


Figure 5.12 Cumulative Distribution of Strain Ratio.

Comparison Between Sections

One of the main objectives of the NCAT Structural Study was to evaluate the two different binders, neat PG 67-22 and SBS modified PG 76-22, and quantify any difference in response and performance. One portion of the investigation included the strain response data. Figure 5.13 shows a summary of the strain data collected from the eight test sections. The data presented are pre-cracking longitudinal strain response under the triple-trailers, and the data were corrected to a reference temperature of 68 °F, according to:

$$\varepsilon^* = \varepsilon * M_T \tag{5.2}$$

where: ε^* = Corrected strain to 68 °F
 ε = Measured strain at temperature, T

$$M_T = \frac{\varepsilon'_{68}}{\varepsilon'_T} \tag{5.3}$$

ε'_{68} = Predicted strain at 68 °F
 ε'_T = Predicted strain at temperature, T

The figure shows the average temperature-corrected strain value along with the standard deviation. Notice that the variability in the strain data ranged from 20 to 60 microstrain, with N3 being the least variable. It follows reason that N3 is less variable than the others because only a few gauges survived construction and the first months of traffic.

Therefore, most of the readings came from the same gauge and the same truck, unlike the other sections where the maximum reading came from different gauges and trucks.

Another observation from Figure 5.13 is that the three thicknesses are fairly obvious in the strain data. On average, the thinnest sections (N1, N2) register the highest strains, while the thickest (N3, N4) show the lowest. Yet, if inspected closely, N2 and N6 along with N3 and N8 have fairly similar values. Section N8 strain values were more on the order of the 9 in. sections, yet it showed cracking first among the 7 in. sections. It is not immediately clear why the strain in section N8 is lower than the other 7 in. sections. Harvey et al. (1995) investigated the concept of rich bottom asphalt pavement structures in the laboratory and determined that the stiffness of a mixture with 0.5 percent higher asphalt content and lower air voids was estimated to increase by 1.15 due to densification. Perhaps, the rich bottom layer in section N8 was also more dense and thus more stiff than the other base HMA mixtures. Slippage at the HMA/rich-bottom interface was also investigated and shown to have occurred (Willis and Timm, 2006) which contributed to lower strain values at the bottom of the rich-bottom lift where the strain gauges were located. Also, N2 shows lower strains than N1, mostly due to the fact that N2 is significantly stiffer than N1 (Timm and Priest "Material Properties," 2006). Further, there may be some data in the N1 set that included cracking. This is because the cracking in section N1 was not first observed until it was an area of interconnected alligator cracking. Therefore, there may have been cracking in the dates before, thus raising the strain values, but there was no way to estimate that date.

Like the thickness effect, it is not easy to make any sweeping conclusions on the effect of binder type on strain data from Figure 5.13. The modified section N1 seemed to have significantly higher strain than its counterpart, while there is less difference for the 7 in. sections, and the thick modified section (N4) conversely showed a slightly lower average strain value. As mentioned above, the high values measured in section N1 may be due to the subsequent inclusion of dates where cracking was present, but this is the best data available.

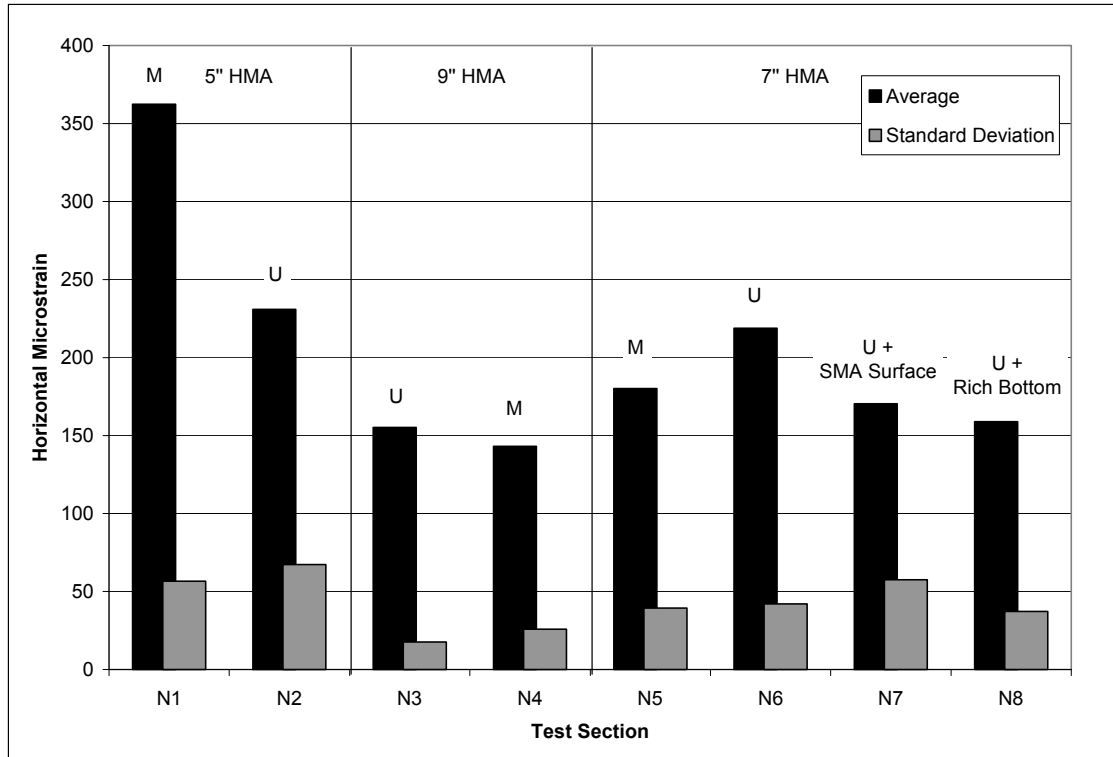


Figure 5.13 Temperature-corrected Strain Data by Test Section.

To better quantify the effect of binder type, a statistical analysis was performed using the data presented in Figure 5.13. A two sample t-test was conducted to determine if sections N1 and N2 were statistically different considering the strain data. From the analysis, section N1 had statistically higher strain response than N2 at a 95 percent confidence level (two-sided p-value = 0.003). Further, the thick sections, N3 and N4, were also statistically different from each other (two-sided p-value = 0.002). Although N3 and N4 were found to be statistically different, the estimated difference was much greater for N1-N2 than N3-N4. The estimated difference of means showed that N1 was greater than N2 by 57%, which is fairly significant, while N3 was higher than N4 by only 8%. The difference between N3 and N4 might be statistically different, but it is not practically different. Due to the nature of the statistical procedure, the large sample size of N3 and N4 ($n = 65$) along with the relatively low standard deviation may tend to skew the analysis.

To compare the four 7 in. sections together, an analysis of variance, ANOVA, was conducted at the same confidence level. From the analysis, there was a difference between the four sections (p-value = 0.000). Further, from a Tukey comparison, it was determined that section N6 was statistically higher than the other 7 in. test sections. When the two 7 in. counterpart sections, N5 (modified) and N6 (unmodified), were compared, it was found that unmodified section N6 strain values were statistically higher than N5 (two-sided p-value = 0.000). Like N3-N4, this observation is a little counterintuitive. One might expect the mixes with a stiffer binder (PG 76-22) would in turn be stiffer, thus showing lower strain values for the same loading and thickness.

From the analysis, no sweeping conclusions can be made with regards to the effect of binder grade and modification on strain response. The modified 5 in. section had higher strain values than the unmodified section, the thickest sections were practically the same, and the modified 7 in. section had lower strain values than its modified partner. The above observations in strain data were probably due to construction and spatial variability rather than an effect of binder type.

On the other hand, the effect of HMA layer thickness is conclusive. An ANOVA analysis was conducted by pooling the test sections, considering only the three different HMA thicknesses, and it was determined that all three were statistically different (p-value < 0.000).

Strain Prediction Models

In a similar manner as the stiffness data, it was not practical to collect dynamic data continuously (extremely costly in equipment and time). In addition, Figure 5.6 showed that no new information is gained after approximately three passes. Therefore, it was important to develop an accurate model to predict the strain magnitude over the entire two-year testing cycle on a per hour basis. The strain magnitude was a function of the mid-depth HMA temperature as well as the thickness of the asphalt layer, so individual regression models were determined for each test section. The individual models accounted for thickness and other individual peculiarities, and a generic model was developed from all the test sections which included a thickness term. Additionally, the strain magnitude was a function of the testing vehicle. The box trailer had to be considered separately because it was loaded differently, and the box trailer had five axles or strain cycles rather than eight. The models presented below allowed for calculations of strain due to each vehicle from the hourly temperature readings collected in each test section.

The effect of temperature on strain is shown in Figures 5.14 and 5.15 for the triple-trailers and the box trailer, respectively. The regression followed a power relationship:

$$\varepsilon_t = \beta_1 T^{\beta_2} \quad (5.4)$$

where: ε_t = Horizontal tensile strain

β_1, β_2 = Regression constants

The regression constants and R^2 value are presented in Tables 5.3 and 5.4 for the triple-trailers and box trailer, respectively. A few details should be noted from the two tables and figures. First, there were only five dynamic data collection dates before cracking appeared on April 8, 2004 in section N1; therefore, the data were rather limited for the triple-trailers. Second, there was also insufficient data for the box trailer prior to cracking in N1 because the vehicle was not acquired until January 2004 and was collected only once before cracking. As a result, the generic model (Equation 5.6) was used to estimate the strain value for the box trailer in section N1. In future studies, more data, including dynamic response and FWD testing, should be collected at the beginning of the project in order to limit these issues. From the R^2 values, the mid-depth HMA temperature was a reasonable predictor of the induced strain from each respective vehicle.

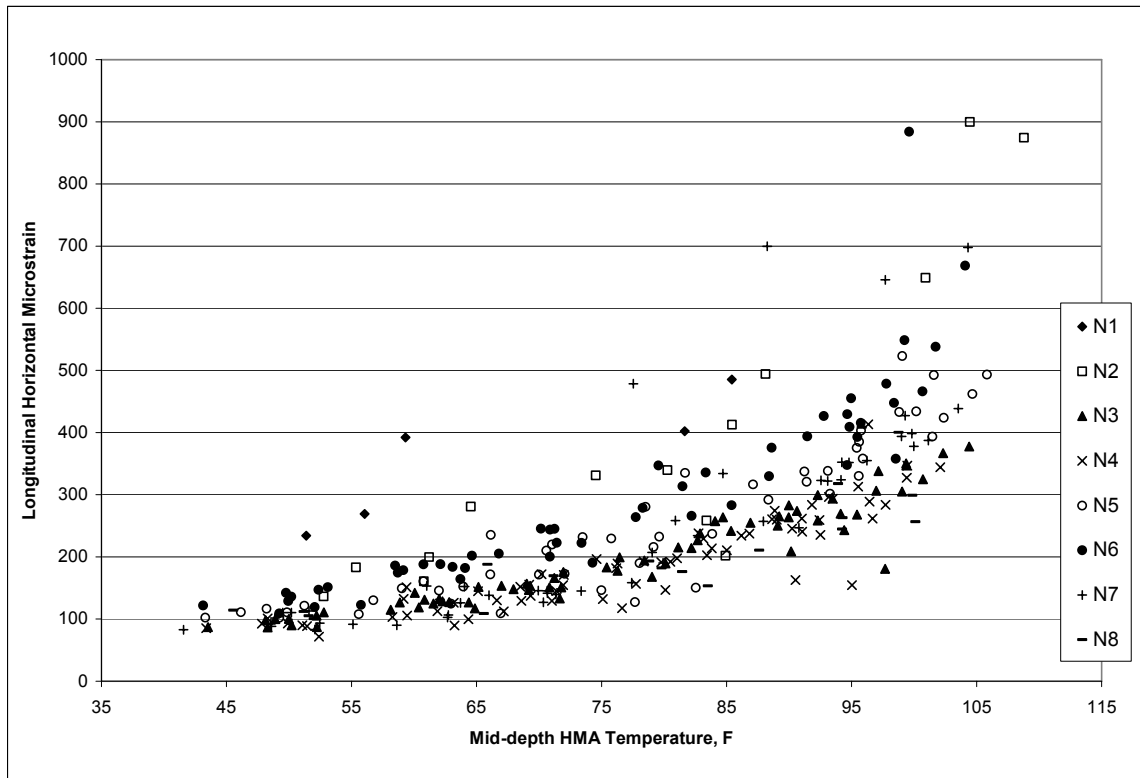


Figure 5.14 Triple-Trailer Strain – Temperature Relationship.

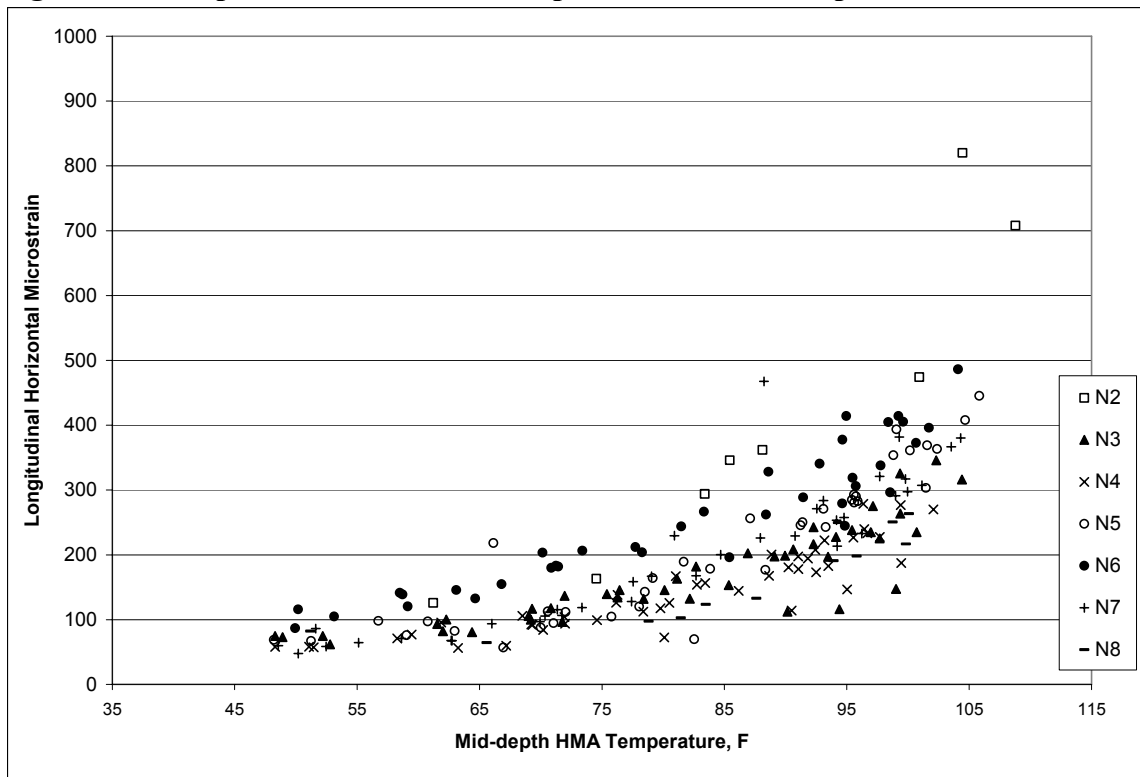


Figure 5.15 Box Trailer Strain – Temperature Relationship.

Table 5.3 Triple-Trailer Regression Analysis for Strain – Temperature Relationship.

Section	β_1	β_2	R^2
N1*	4.0439	1.066	0.763
N2	0.0005	3.081	0.877
N3	0.0508	1.899	0.909
N4	0.0211	2.086	0.822
N5	0.0109	2.291	0.881
N6	0.0132	2.293	0.810
N7	0.0022	2.652	0.705
N8	0.0532	1.887	0.730

* Limited data available

Table 5.4 Box Trailer Regression Analysis for Strain – Temperature Relationship.

Section	β_1	β_2	R^2
N1**			
N2	3.922E-05	3.579	0.871
N3	5.501E-03	2.332	0.773
N4	1.304E-03	2.632	0.773
N5	1.440E-04	3.185	0.887
N6	1.852E-02	2.155	0.881
N7	8.310E-04	2.796	0.821
N8	1.170E-04	3.157	0.850

** Not enough data to perform regression

The generic relationships including thickness are given in Equations 5.5 and 5.6 below for the triple and box trailer, respectively.

$$\epsilon_t = 5.557T^{1.0258} - 30.730t \quad (R^2 = 0.70) \quad (5.5)$$

$$\epsilon_t = 2.1228T^{1.190} - 26.448t \quad (R^2 = 0.71) \quad (5.6)$$

where: t = HMA thickness, in.

The thickness value used in the regression was the as-built, surveyed HMA layer thickness directly over the instrumentation array. It should also be noted that including the binder type in the regression did not significantly improve the model; therefore it was not included for simplicity.

Strain Distributions and Endurance Limit

Of importance in recent years has been the field characterization of a strain endurance limit below which fatigue cracking will not occur. While this structural study was not

designed to determine an endurance limit, an examination of field-measured strains relative to the amount of observed fatigue cracking may begin to establish such a limit.

Figure 5.16 compares the strain distributions obtained from each test section over the two year research cycle. The graph was derived from the strain-temperature relationships quantified above in Tables 5.3 and 5.4 with the measured temperature data obtained from in situ thermocouples. The result was two years of strain data from which distributions could be determined and plotted. Data from section N8 were not included since slippage was believed to have occurred between layers thus skewing the strain measurements.

As will be described in great detail below, sections N1, N2 and N6 showed the greatest amount of cracking over the two-year period. These are also the sections with the highest average (50th percentile) strain levels. The remainder of the test sections show an average strain level of less than 200 $\mu\epsilon$ with the thickest sections (N3 and N4) in the 150 to 170 $\mu\epsilon$ range. It is interesting to note the divergence around the 30th percentile where sections N3 and N4 have distinguishably lower strain levels than any of the others and these sections have yet to show any cracking. This corresponds to approximately 110 to 125 $\mu\epsilon$. Though it is too early to determine if this is a true fatigue limit, and more trafficking and observation is needed to determine if the other sections begin to crack, it appears that the data could support a field-determined threshold of at least 100 $\mu\epsilon$.

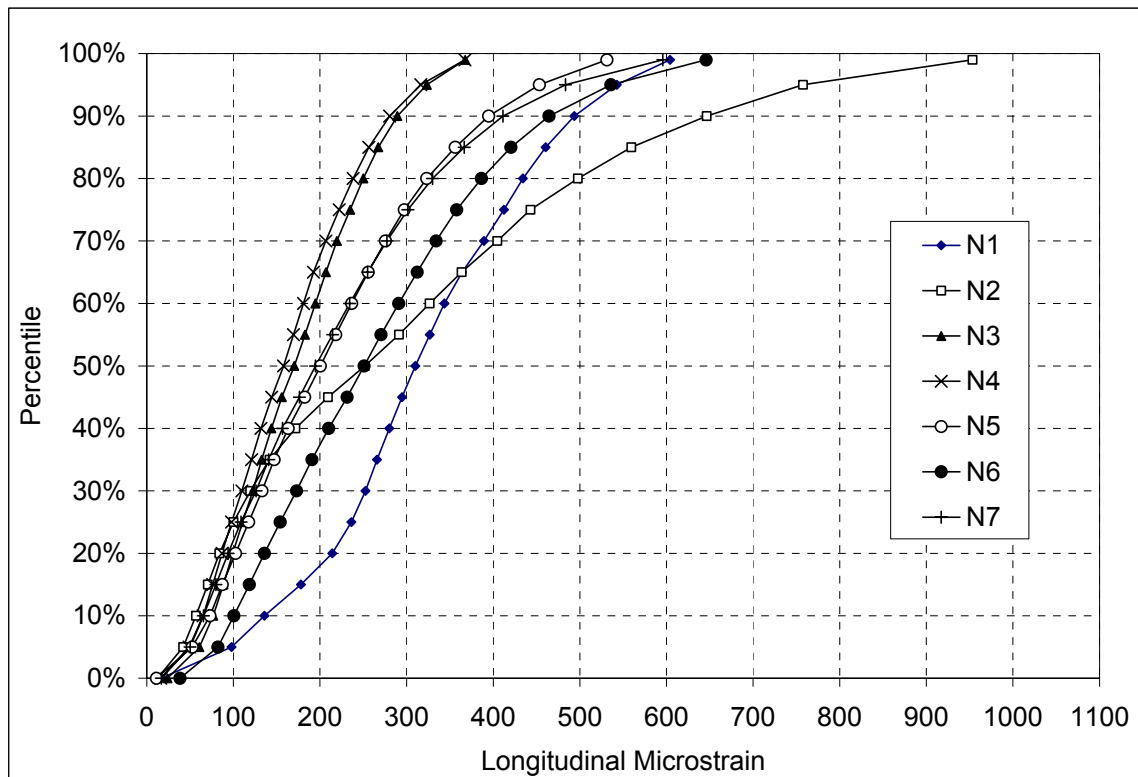


Figure 5.16 Strain Distributions.

Concluding Remarks on Strain Characterization

As with the stiffness data, the above analysis was crucial to developing fatigue transfer functions at the NCAT Test Track. The relationships between strain and temperature allowed for an accurate calculation of the in situ strain magnitude for each hour of the testing cycle. In this way, the calculated damage and subsequent fatigue models were based on field measurements. Additionally, the generic functions developed, as well as the binder grade and thickness investigation, can aid in future design and analysis projects for similar HMA mixtures.

FATIGUE PERFORMANCE CHARACTERIZATION

Observed Fatigue Distress

As discussed in Chapter 3, the performance of the test sections was monitored on a weekly basis including crack mapping and rut depth measurement. Because this report focuses on fatigue transfer functions, the cracking data were of most importance.

At the date of this report, sections N1, N2 and N8 had shown excessive fatigue failure, and the distress of all three sections progressed in a similar fashion. First, small transverse cracks appeared in the wheelpath, as shown in Figure 5.17. This observation was consistent with finding the measured longitudinal strains greater than those in the transverse direction (i.e., greater longitudinal strain lead to transverse cracks). After the initial transverse cracking, the cracks progressed to the end of the wheelpath and often arched in the direction of traffic (Figure 5.18). Later, the individual transverse cracks became interconnected into the classical alligator pattern fatigue cracking, also shown in Figure 5.18. Pumping of the fines from the unbound aggregate base through the cracks was also observed in the individual transverse cracks as well as the alligator cracked areas. The pumping proved that the cracks propagated all the way through the HMA layer. Cores were also taken in the cracking area to verify that the cracks were in fact bottom-up cracking.



Figure 5.17 Transverse Cracking in Wheelpath - Section N8.

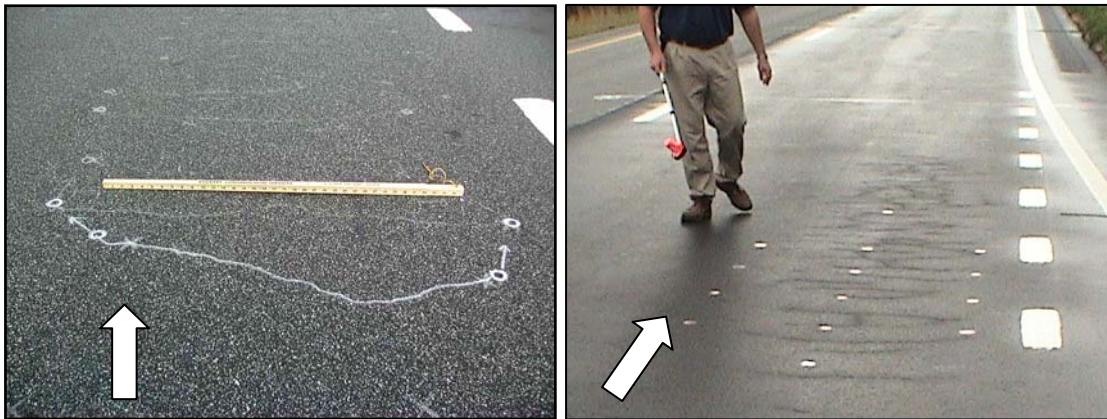


Figure 5.18 Progressed Fatigue Cracking.

Once the first cracks appeared, the progression of failure was fairly rapid, especially after pumping began. The granular base was easily pumped as water infiltrated through the cracks and into the structure, and the base support was lost. This led to further deterioration and rutting. In Figure 5.19, the rut depth in section N8 is easily noticed from the ponding of rain water. Additionally, Figure 5.20 shows the extensive deterioration of sections N1 and N2 including massive cracking, gaps and standing water. It is important to note that in some of the figures above, the cracks in the photograph were marked with a silver pen for easier visibility and for the video record, and the arrows indicate the direction of travel.



Figure 5.19 Water Ponding Due to Rutting– Section N8.

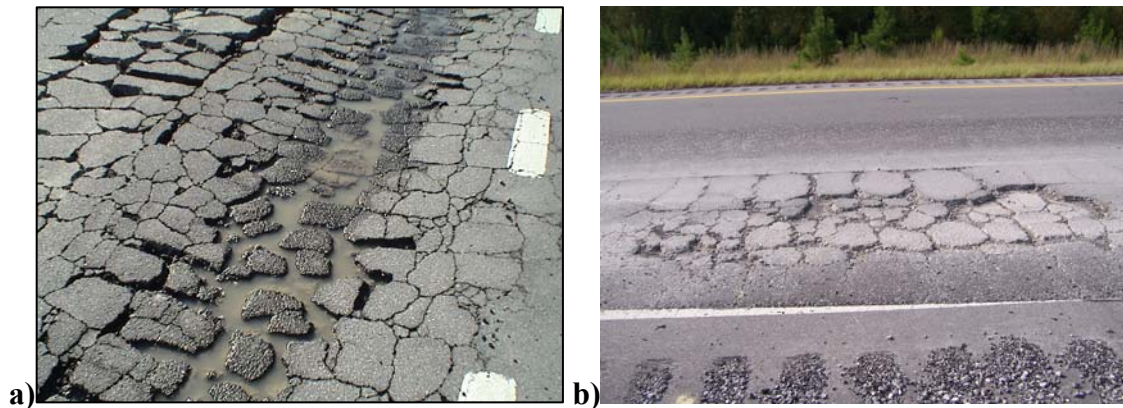


Figure 5.20 Extensive Fatigue Cracking in Section a) N1 b) N2.

The fatigue cracking of sections N1, N2 and N8 originated in the outside wheelpath near the gauge array area. Because the sections did not fail prematurely, it was not likely that the gauges were the cause of the cracking. The sections were fatigued and reaching the end of life, and the gauge array was an area of discontinuity. It is probably a more accurate description to conclude that cracking was going to occur in the section due to fatigue and first appeared in the gauge array because the presence of the gauges caused

an area of weakness within the section. As the distress progressed, the cracking expanded past the gauge array and also developed in the inside wheelpath.

Crack Mapping

The cracking coordinates determined from the procedure described in Chapter 3 were used to make graphical crack maps in order to keep a visual record of the cracking. The crack maps were often more useful than even photographs because the format was consistent. The crack maps provided valuable insight into how the cracks progressed and at what rate. To serve as an example of the crack maps and the observed fatigue cracking development at the NCAT Test Track, a series of four crack maps from section N2 are shown in Figures 5.21-5.24. To explain the maps further, the horizontal dot-dashed lines are the center of the wheelpaths, the grey outline is the gauge array area and the solid black lines are individual transverse cracks or areas of interconnected fatigue cracking.

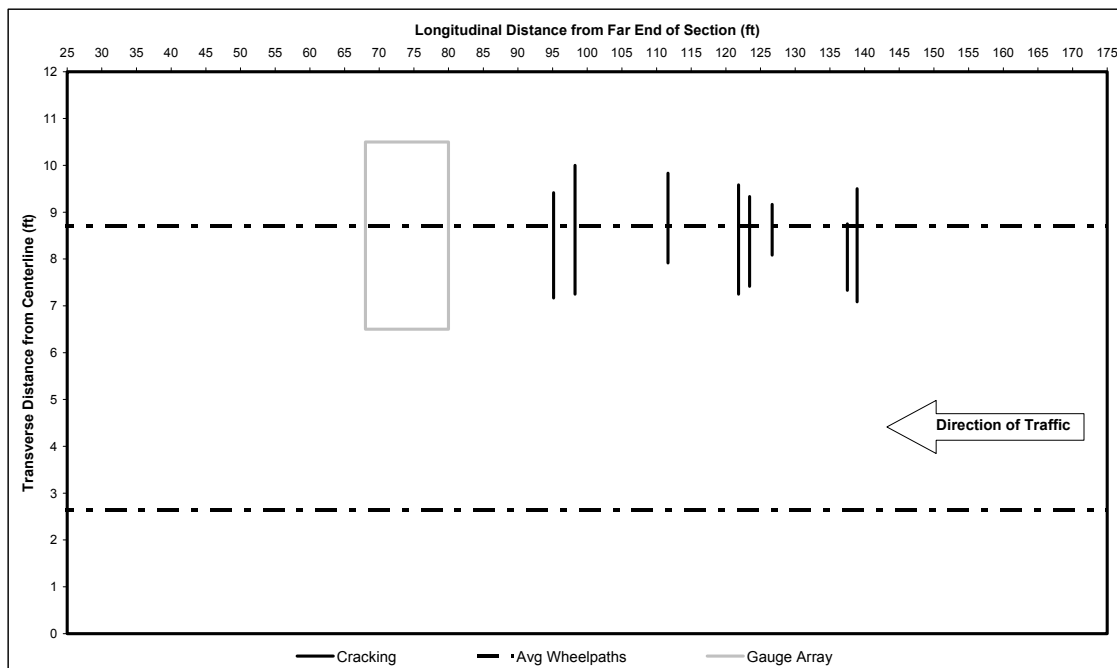


Figure 5.21 N2 Crack Map 6/21/2004.

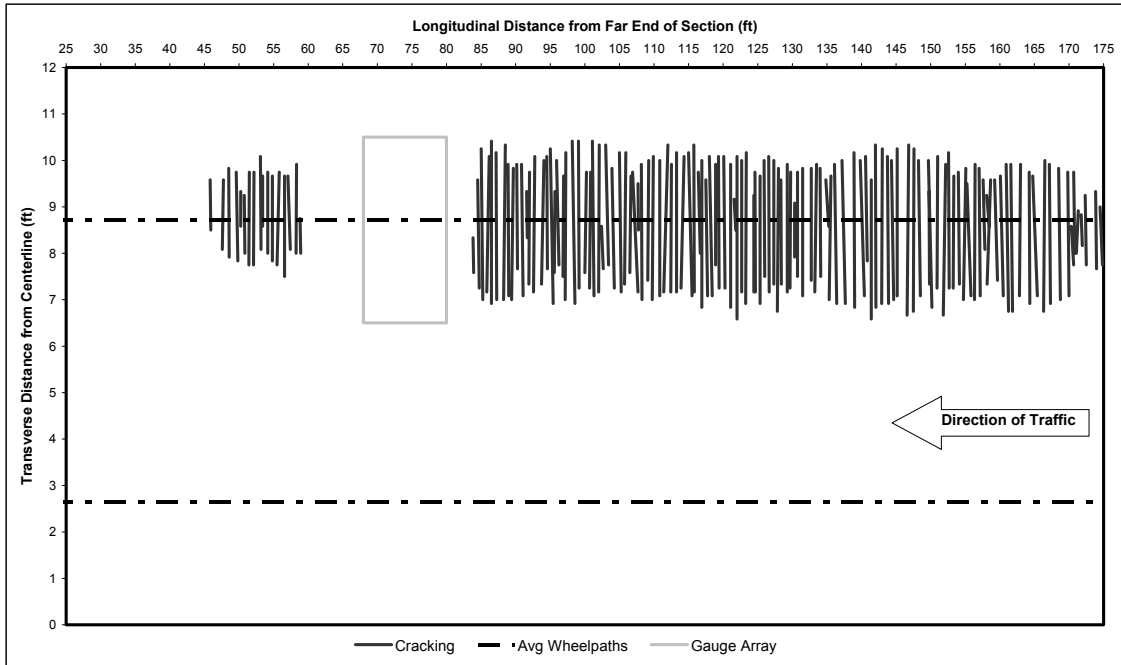


Figure 5.22 N2 Crack Map 6/28/2004.

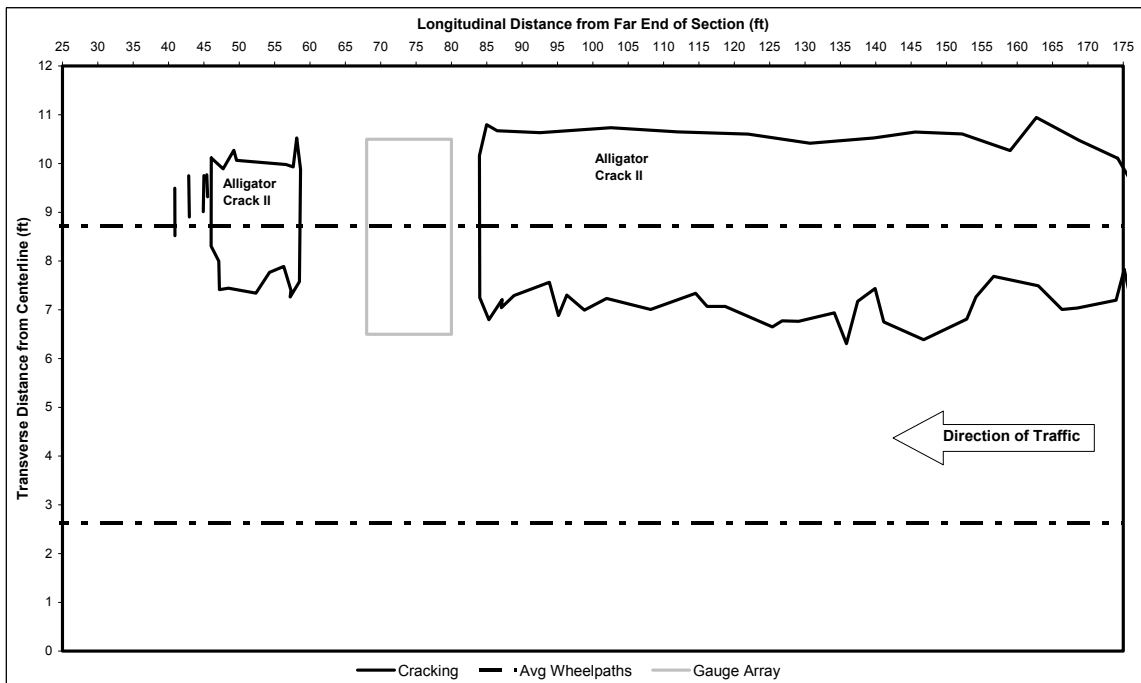


Figure 5.23 N2 Crack Map 8/02/2004.

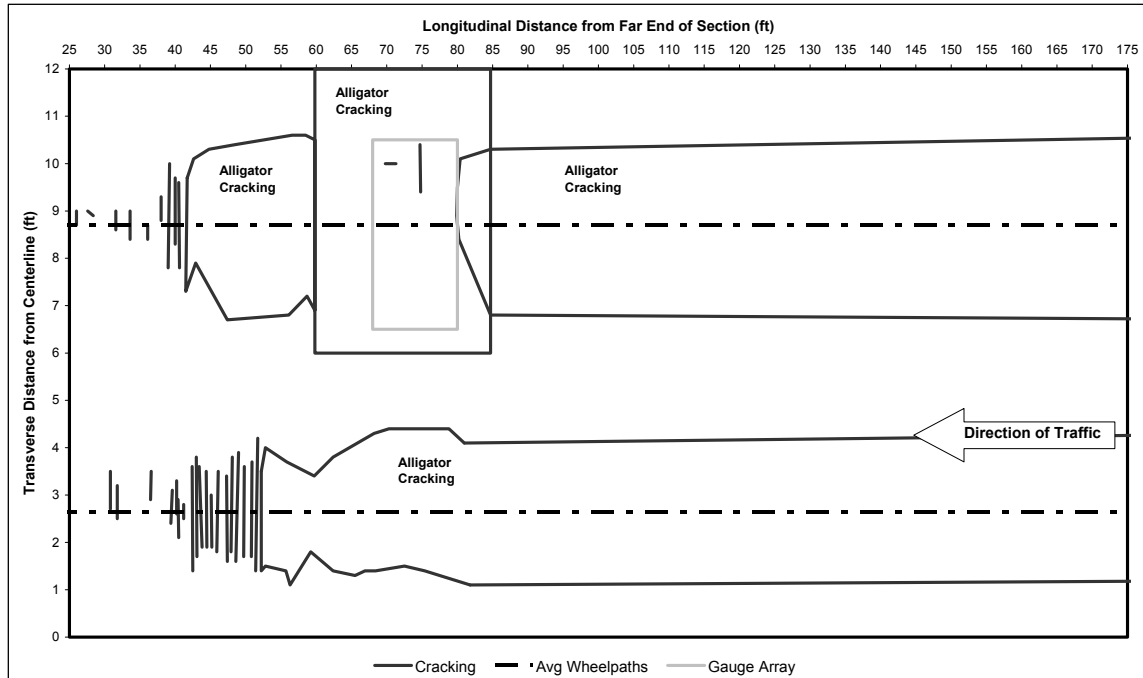


Figure 5.24 N2 Crack Map 10/18/2004.

As explained above, once the first cracks appeared after approximately 2.6 million ESAL, the fatigue distress progressed rapidly. From Figures 5.21 and 5.22, one can see that eight individual cracks progressed to cracking covering nearly the whole outside wheelpath in one week (or approximately 100,000 ESAL). After a month (Figure 5.23) the individual cracks became interconnected, and within four months (Figure 5.24), both wheelpaths had full fatigue cracking with pumping.

The figures above are just examples of a few select dates of one test section. Similar maps were generated from the cracking data for the other test sections to monitor and record the performance in an easy format.

Data Processing and Characterization

Although the crack maps provided a good graphical representation of the fatigue distress, there was a need to quantify the amount of cracking with a numerical value in order to plot the distress data and determine a definitive failure criteria. Recall from Chapter 3 that the cracking video records were digitized and coordinates were obtained from the video record. The coordinates were used to create the crack maps shown in the section above and were also used to quantify the amount of cracking in each test section.

The coordinates were processed using a formatted spreadsheet and customized algorithms. The crack coordinates were imported into the spreadsheet, and the crack map was displayed. The type of cracking was identified, and then a specific algorithm was run to measure the amount of cracking given the coordinates. Five categories of cracking were used to classify the cracks observed at the NCAT Test Track:

1. Transverse cracking – wheelpath

2. Transverse cracking – non-wheelpath
3. Longitudinal cracking – wheelpath
4. Longitudinal cracking – non-wheelpath
5. Interconnected fatigue cracking (alligator cracking)

The longitudinal cracking and non-wheelpath transverse cracking observed at the Test Track were mainly top-down surface cracking rather than fatigue cracking, and they were found primarily in the other test sections (not part of the Structural Study). Therefore, they will not be discussed in detail here. The fatigue distresses, wheelpath transverse and alligator cracking, were quantified as an area following the guidelines of prior work including the LTPP Distress Manual, AI MS-1 and M-E PDG. It is important to mention that the LTPP Distress Manual identifies the first stages of fatigue cracking as longitudinal cracking in the wheelpath, but at the Test Track, the initial stages of fatigue cracking were transverse cracks. Therefore, they are included as fatigue cracking in this study.

Individual transverse cracks, like those in Figure 5.21 and 5.22, were measured by their length, in feet, and then assigned a width of 1 ft to get an area measurement. The LTPP Distress Manual measures fatigue cracks in affected area, but does not offer precise recommendations on how to determine an area of an individual crack. Often, there were many closely-spaced individual cracks, and considering each having a 1 ft width would have over exaggerated the approximation. Therefore, if two consecutive transverse cracks were less than 5 ft away from each other, they were considered together, and a trapezoidal area was calculated from the four coordinates of the two cracks. Basically, the algorithm went from crack to crack, determined the distance from the current crack to the prior crack, and if the distance was less than 5 ft an area was calculated. If not, the length was determined and assigned a 1 ft width. The total area of transverse cracking was then determined by adding the individual areas.

For the areas of alligator cracking (e.g., Figures 5.23 and 5.24), the method of coordinates was used to find that traverse area. The method of coordinates, found in most introductory surveying textbooks (e.g., Wolf and Brinker, 1994), utilizes the following equation to find the area of an irregular geometric shape:

$$A = \frac{1}{2} \left(\sum_{i=1}^n y_i (x_{i-1} - x_{i+1}) \right) \quad (5.7)$$

where: A = area of closed traverse

i = point of traverse

n = number of points in traverse

x = x-coordinate

y = y-coordinate

For this analysis, all fatigue cracking, regardless of type or level of severity, was considered together; therefore the grand total area of fatigue cracking included the transverse wheelpath and alligator cracking. A similar procedure was used for the

calibration of the M-E PDG using performance data from LTPP sections (El-Basyouny and Witzczak “Calibration,” 2005).

Once the total area of fatigue cracking was determined from the above procedure, the percentages of cracked area were calculated. The percent of cracking considering the whole lane (12 ft X 150 ft) was calculated, and the crack progression is shown in Figure 5.25. Another common way to quantify fatigue distress is by percent cracking of the wheelpath. This was done to more easily compare between studies that may have a variety of different lane widths. Therefore, the percent of cracking in the wheelpath was also calculated and shown on the secondary axis in Figure 5.25. The wheelpath width was determined using the wheel wander data presented earlier in this chapter. Considering all the data presented in Figure 5.3, the standard deviation of the lateral distribution of axles was 8.3 in., and the wheelpath was considered to be three standard deviations wide or 25 in. This number was also reasonable considering the axle configuration; the outside edge of the outer tire to the inside edge of the inside tire is approximately 22 in.

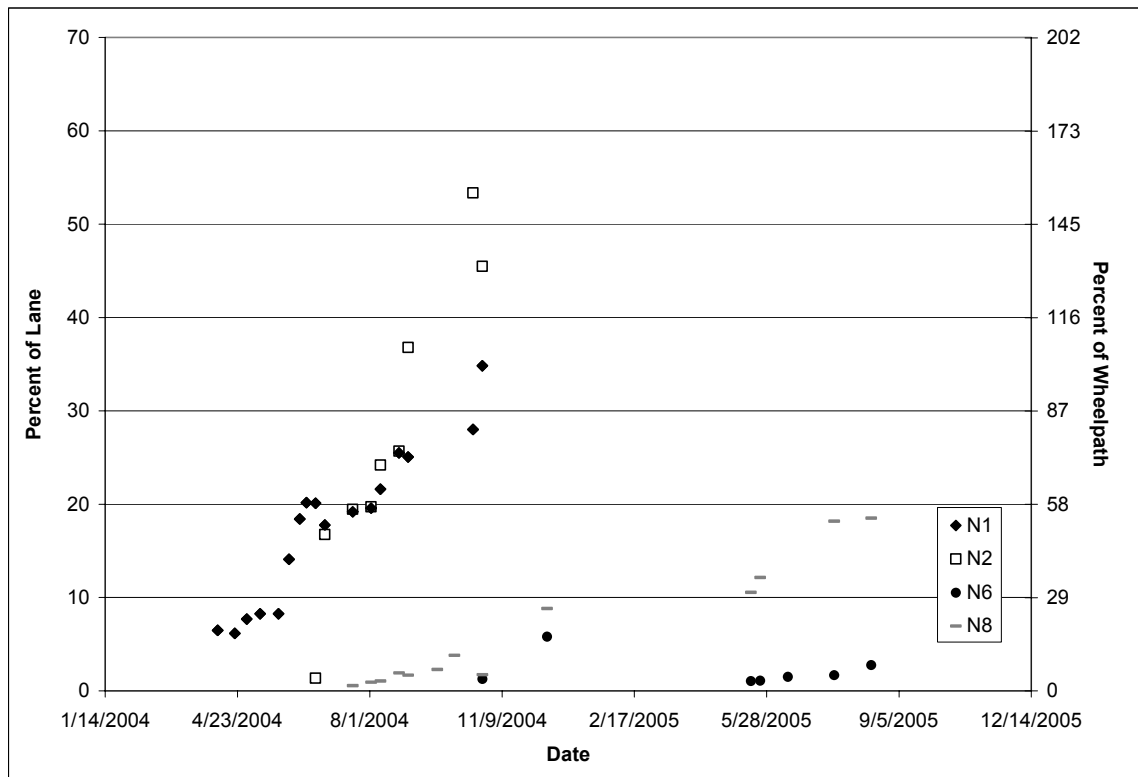


Figure 5.25 Percent Fatigue Cracking by Date.

Failure Criteria

In order to calibrate fatigue transfer functions, the distress level considered failure, where damage reaches unity, must be determined. Recall from Chapter 2 that it is common practice to consider fatigue cracking of 45-50 percent of the wheelpath or 20 percent of the total lane area as failure, and many widely accepted models have been calibrated in

this manner. Using the criteria of 20 percent of the lane area and Figure 5.25 as a guide, failure was reached in three test sections at the writing of this report, and the dates and crack levels are shown in Table 5.5.

Table 5.5 Section Failure Data.

Section	Failure Date	Cracking of Lane, %	Cracking of WP, %
N1	6/14/2004	20.2	58.3
N2	7/19/2004	19.5	56.2
N8	8/15/2005	18.5	53.5

CONCLUDING REMARKS ON METHODOLOGY AND CHARACTERIZATION

The procedure developed at the NCAT Test Track to develop fatigue transfer functions is both unique and relevant to other studies. The Test Track provided a great opportunity to develop performance models with both full-scale loading and the control of a research facility. The procedure developed relies strictly on data collected from the field, which follows that it should be directly applicable to design and analysis of public highways. Of course, the transfer functions developed here are somewhat specific to the materials and conditions under which they were developed; yet, they will be directly applicable to ALDOT and similar mixtures and comparable environmental conditions.

Further, the methodology as well as the data collection and synthesis procedures developed in this study should be applicable to other full-scale testing facilities and further experiments at the NCAT Test Track. The following chapter will show how all of the pieces described in this chapter come together to develop performance models. One important recommendation is to collect a fairly extensive amount of data at the beginning of the experiment before the sections are trafficked.

CHAPTER 6 – FATIGUE MODEL DEVELOPMENT

INTRODUCTION

At the time of this report, three test sections had reached the fatigue cracking failure criteria, as discussed in the prior chapter. Recall that cracking covering 20 percent of the total lane area was considered failure. Sections N1 and N2 reached failure in the summer of 2004, and section N8 reached failure in the summer of 2005. It should be noted that all three sections survived past their initial design life of 1.1 million ESAL for N1/N2 and 2.9 million ESAL for section N8.

Final fatigue transfer functions were developed using the data from the three failed test sections, and preliminary transfer functions were developed for the other sections based on the traffic and performance data, to date. Revisions will need to be conducted on these models after the sections deteriorate further.

METHODOLOGY

From Chapter 5, the hourly temperature data collected continuously throughout the two-year test cycle was the critical link between the traffic data and the HMA stiffness and strain data. For each hourly temperature, the in situ HMA stiffness and strain magnitude were calculated for each test section and vehicle type. Therefore, each lap of each truck was accounted for through the relationships established in Chapter 5.

The trucking database was organized by the number of laps that each truck traveled in a given hour. This was further simplified into the number of laps per hour that each type of truck, triple-trailer or box, traveled. The hourly traffic volume was then queried with the hourly temperature data. This information was the same for all test sections because they were each trafficked the same (the trucks must complete whole laps). The applied load cycles for each hour, n_i , was computed using these data. The number of load cycles equaled the number of truck laps times the number of strain cycles, or axles, for that vehicle. For example, the triple-trailer trucks had eight strain cycles, while the box trailer had five. Refer to the strain traces in Figure 6.1. The top signal is from a triple-trailer, and the bottom is from the box truck.

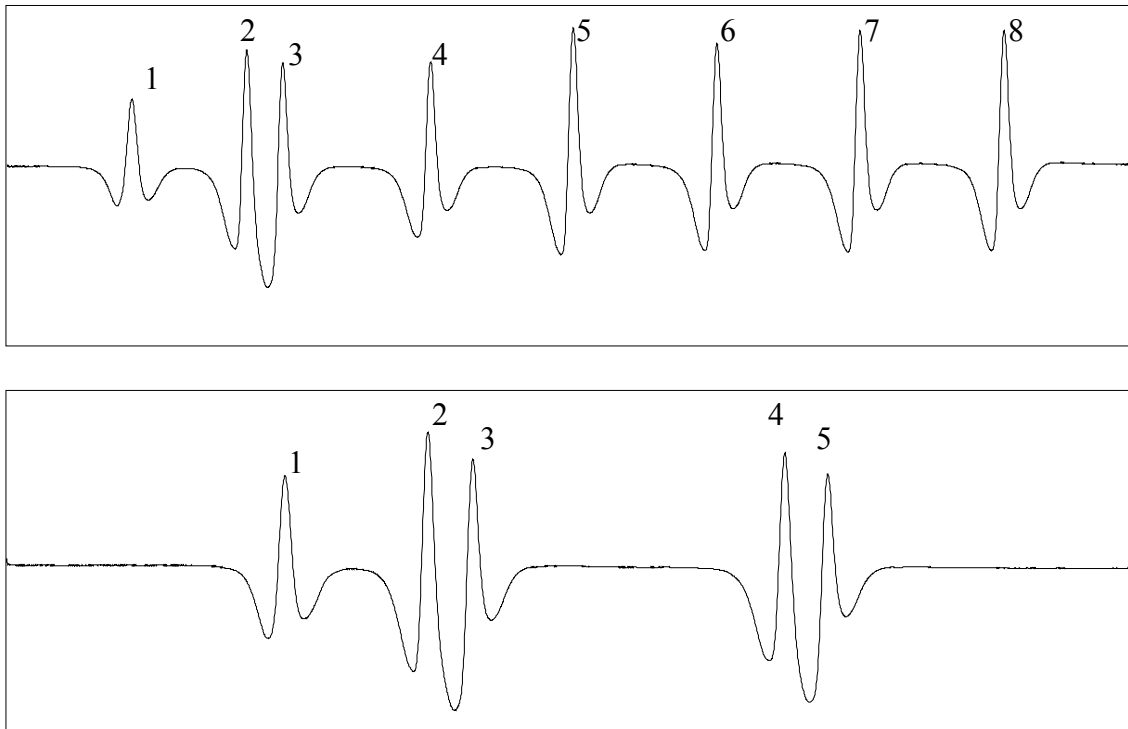


Figure 6.1 Strain Cycles for Triple-Trailer and Box Trailer Trucks.

Then the HMA stiffness and strain amplitude was calculated from the hourly temperature data, given the test section and vehicle type. With the applied loads, stiffness and strain values, the cycles to failure, N_{fi} , was calculated assuming a fatigue transfer function. From this, the incremental damage, D_i , was computed each hour using Miner's hypothesis first introduced in Chapter 1 and shown again here:

$$D_i = \frac{n_i}{N_{fi}} \quad (6.1)$$

where D_i = incremental damage for hour i

n_i = number of cycles for hour i

N_{fi} = number of cycles until failure under conditions of hour i

The total damage at any time was then the sum of the incremental damage, as shown in Equation 1.1.

Using the generated data described above, the fatigue models were then calibrated to fit the observed performance. The regression coefficients were determined such that the total damage, D , equaled unity at the determined date of failure. It is important to note that the effort of this research was to calibrate models previously developed (presented in Chapter 2) using full-scale field response, material and performance data. The exact models followed and the calibration results are discussed below.

FATIGUE MODEL

The current state of practice for fatigue transfer functions, including AI MS-1, Shell Oil Design Guide and the M-E PDG (MEPDG), is in the form of:

$$N_f = k_1 \left(\frac{1}{\varepsilon_t} \right)^{k_2} \left(\frac{1}{E} \right)^{k_3} \quad (6.2)$$

where: N_f = Number of load cycles until fatigue failure

ε_t = Applied horizontal tensile strain

E = HMA mixture stiffness

k_1, k_2, k_3 = Regression constants

and may contain a volumetric correction term including the VFB of the mix. As discussed in Chapter 2, these functions are often developed in the laboratory and then shifted or calibrated to field performance with correction factors. In the development of the AI MS-1 design guide, just the constant k_1 was adjusted to match field observation (Finn et al., 1977). In the development of the M-E PDG, all three regression constants were tweaked to better match LTPP performance data (El-Basyouny and Witzczak “Calibration,” 2005).

In a similar manner to the M-E PDG, all three regression constants were calibrated to fit the data collected at the Test Track for the models presented here. Also following the M-E PDG and accepted practice, the AI MS-1 equation was used as the base model and guide to the calibrated functions. The equation was presented in Chapter 2 and is shown here again for easy reference (“Thickness Design,” 1982):

$$N_f = 18.4 * C * (0.00432 * \varepsilon_t^{-3.29} * E^{*-0.854}) \quad (6.3)$$

where: $C = 10^M$

$$M = 4.84 * \left(\frac{V_B}{V_B + V_V} - 0.69 \right) \quad (6.4)$$

The volumetric term in the AI equation was not used for the models calibrated here. It was determined that there was not enough variation in the volumetrics of the test sections to make an impact (Timm and Priest “Material Properties,” 2006). All the test sections used a similar mix design; the only difference among sections (excluding N7 and N8) came from the binder grade. Further, notice in the above equation that the volumetric correction, C , is equal to 1 for mixes with air voids of 5 percent and binder volume of 11 percent. The mixes used at the Test Track were designed with targets very near these values. In fact, for sections N1 and N2, the average air void content was 6.5 percent, and the average binder volume was 11 percent. Therefore, the term was not considered, and the equation simplified to:

$$N_f = 0.0795 * \left(\frac{1}{\varepsilon_t} \right)^{3.29} * \left(\frac{1}{E} \right)^{0.854} \quad (6.5)$$

The above equation served as the base model that was then calibrated using the field data to create the final transfer functions.

The two 5 in. sections, N1 and N2, reached their terminal life within the span of the 2003 research cycle as well as one of the 7 in. sections, N8. Recall that section N8 included the rich bottom layer consisting of 2 in. of HMA with an additional 0.5 percent asphalt content. It was found that this section behaved differently in fatigue than did sections N1 and N2. Consequently, one fatigue function could not be developed that explained the performance of both the 5 in. sections and section N8. Upon further investigation, it was determined that section N8 performed differently than the other 7 in. and 9 in. test sections, also. Therefore, three transfer functions are presented here. One function for the 5 in. test sections was developed, termed the thin model. This model is separate because the data set is complete. Further, it is widely accepted (El-Basyouny and Witczak “Calibration”, 2005; Monismith et al., 1985; Tangella et al., 1990) that thin asphalt pavements are subjected to a different loading mechanism than are thicker pavements. Although sources do not agree with what is considered “thin”, the range is typically less than 2 in. to 5 in. The second transfer function developed was for section N8 and termed the rich bottom model. And finally, the third model presented, termed the thick model, was a first attempt at a calibrated model for the remaining test sections, N3-N7, based on data up to August 2, 2005. The three models are presented below followed by discussion of the calibration and section performance.

It should be noted that a full forensic investigation was conducted on Section N8 at the conclusion of the 2003 Test Track (Willis and Timm, 2006). While the details of this investigation are beyond the scope of this report, it was found that slippage had occurred between the rich-bottom and overlying HMA layer contributing to poor fatigue performance.

Thin Model

The response, material property and performance data from both sections N1 and N2 were considered to develop the fatigue transfer function given below in units of strain (in./in.) and psi:

$$N_f = 0.4875 * \left(\frac{1}{\varepsilon_t} \right)^{3.031} * \left(\frac{1}{E} \right)^{0.6529} \quad (6.6)$$

Both test sections failed in a very similar manner and within two months of each other. Section N1 failed prior to section N2, which was expected because the strain values of N1 were statistically higher, and N2 was slightly stiffer than N1. Both of these effects are quantified in the above equation.

Figure 6.2 shows the accumulation of damage over time for sections N1 and N2. From the figure, the damage at the terminal date does not exactly equal 1 for the test sections because it was not possible to develop an equation that will exactly match the performance of both test sections. Equation 6.6 minimizes the error for both sections and is acceptable to both. The error either under or over-predicts the failure by only a month.

Notice that the higher strains in section N1 cause the curve to increase steadily from the beginning of traffic. On the other hand, the accumulation of damage for section N2 does

not begin to rise until the spring months when the pavement warms up, the stiffness decreases and the strains increase.

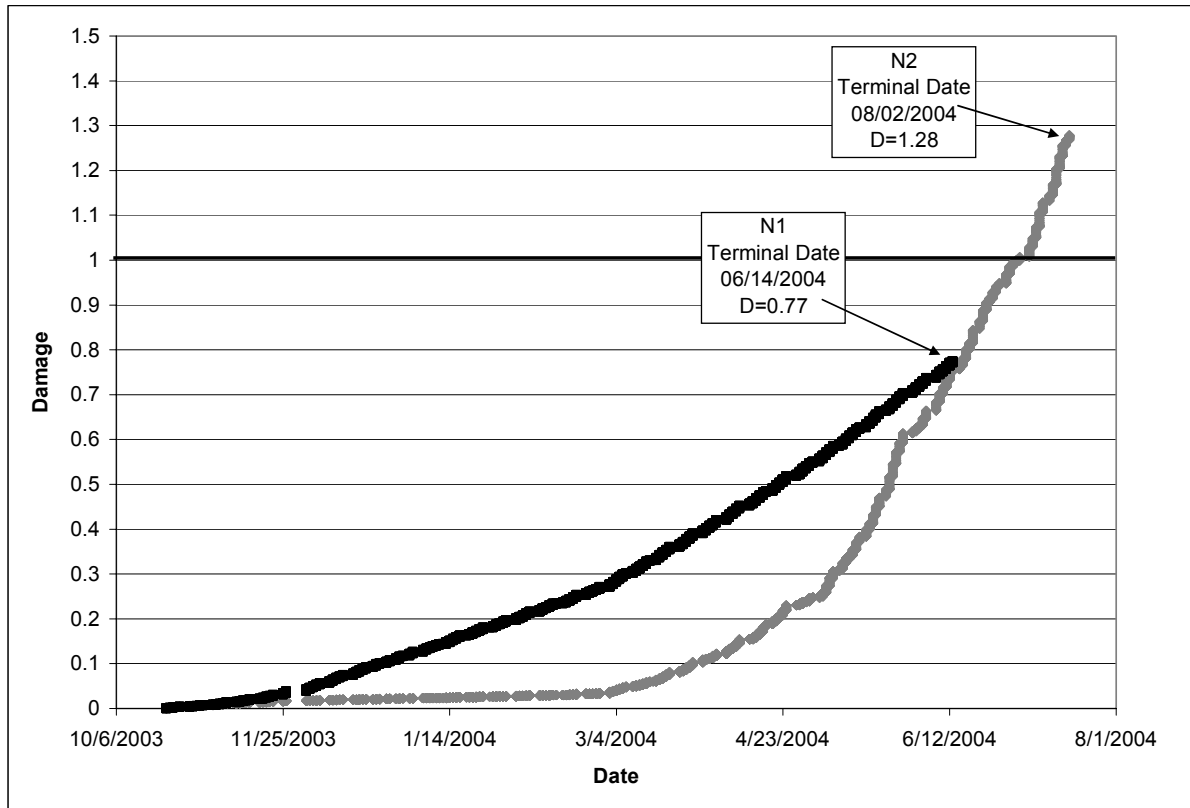


Figure 6.2 Damage Accumulation for Sections N1 and N2.

In order to verify the need for local calibration of fatigue transfer functions, two models presented in Chapter 2, the Monismith and Epps (1969) laboratory equation (Equation 2.3) and the field calibrated AI MS-1 (“Thickness Design,” 1982) design equation (Equation 2.5), were used in conjunction with data from sections N1 and N2. The results are shown in Figures 6.3 and 6.4, respectively. It should be noted that the volumetric terms required for the AI equation were determined from the as-built HMA properties found in Timm and Priest (“Material Properties,” 2006). From the figures, both models show similar patterns as Figure 6.2, but the magnitude of the calculated damage is off from the observed performance. For example, the laboratory equation predicted failure in the first few days of traffic (Figure 6.3). The AI MS-1 equation is an improvement from the laboratory equation, due to the field calibration, but the prediction was still overly conservative for the observed performance. At the time of fatigue failure, the calculated damage ratios using the AI design equation were above 20 for both sections. Imagine if these transfer functions were used for design; the resulting thicknesses would be far too conservative. Clearly, from Figure 6.3, field calibration is essential for accurate M-E design procedures. Further, from Figure 6.4, local field calibration is also necessary.

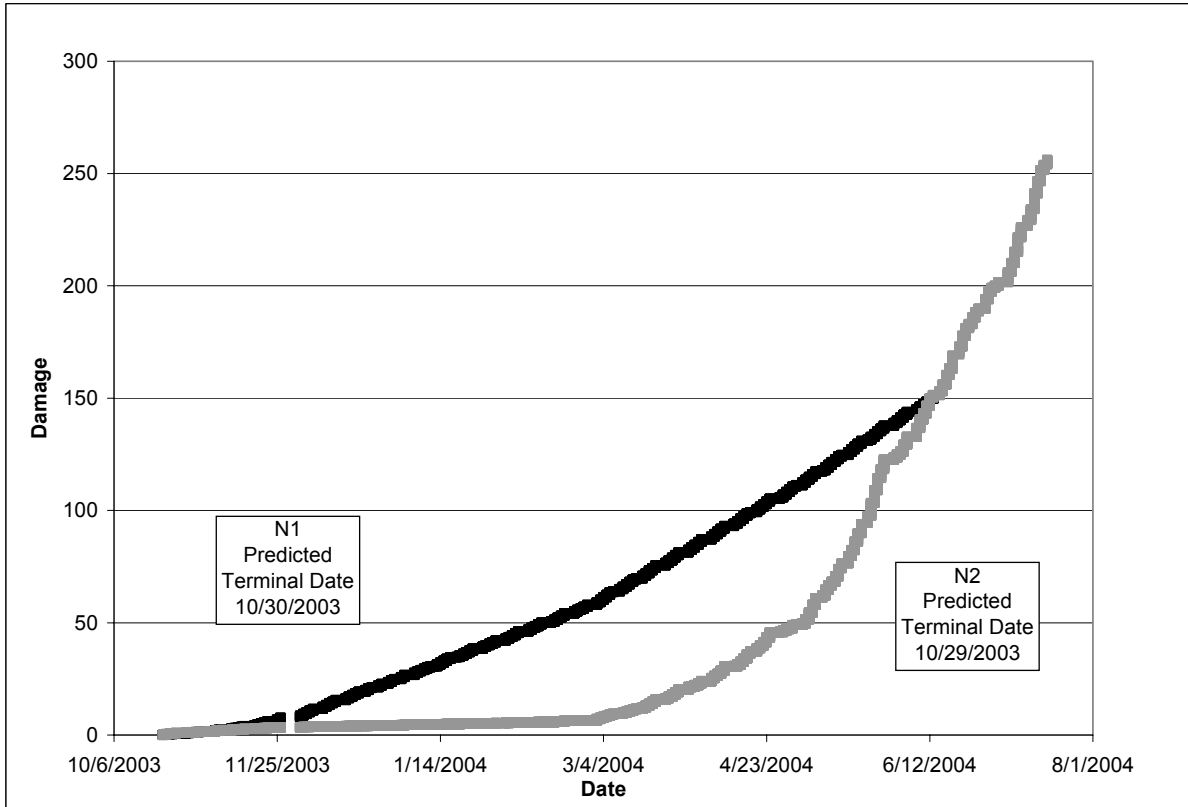


Figure 6.3 Monismith and Epps (1969) Laboratory Model Predictions for Sections N1 and N2.

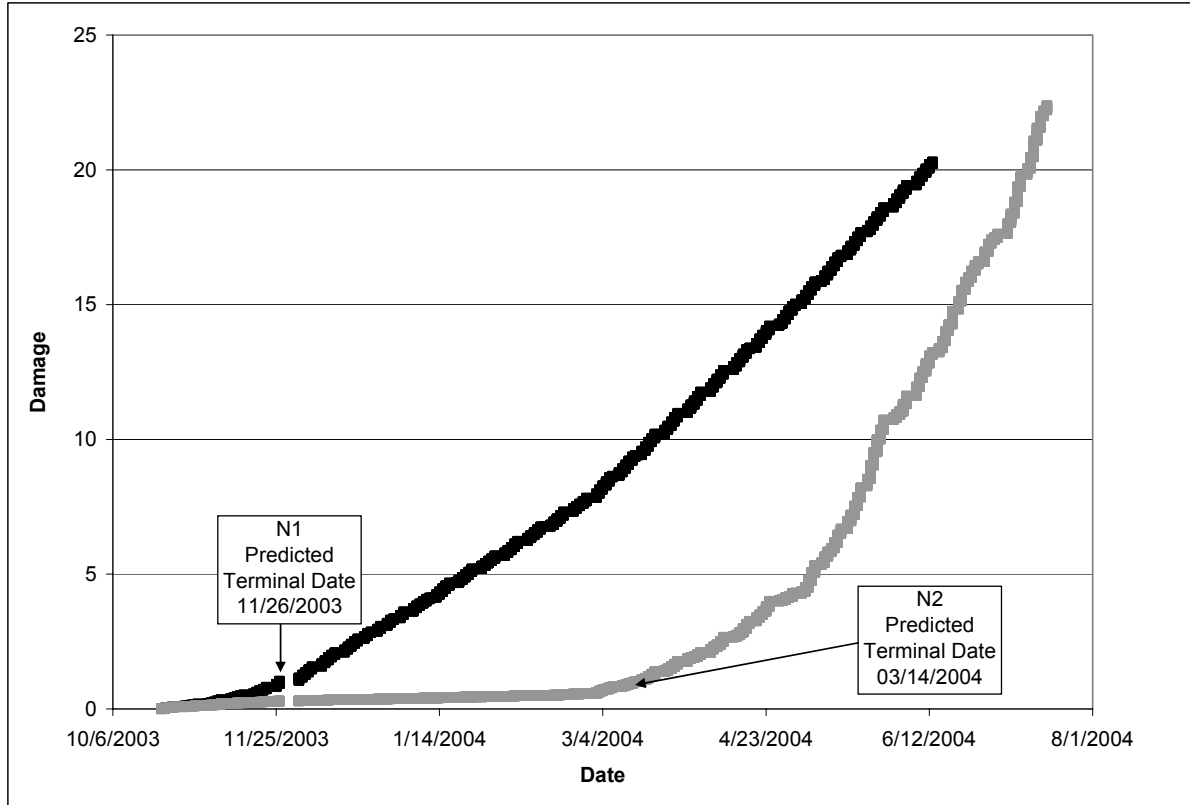


Figure 6.4 AI MS-1 Model Predictions for Sections N1 and N2.

Rich Bottom Model

Equation 6.5 was also calibrated according to the performance data of section N8, giving the following transfer function:

$$N_f = 0.4814 * \left(\frac{1}{\varepsilon_t} \right)^{3.007} * \left(\frac{1}{E} \right)^{0.6911} \quad (6.7)$$

Equation 6.7 may not look too different from Equation 6.6, yet if the thin model were applied to N8, the damage would be over 4.0 at the time of failure. The damage curve for section N8 is shown in Figure 6.5. As alluded to in the discussion of N2, most of the fatigue damage is accumulated in the warmer months. Because N8 lasted longer, the full seasonal effect is shown. Also notice from the figure that the damage is equal to 1 at the time of failure because this model was calibrated to only one set of data.

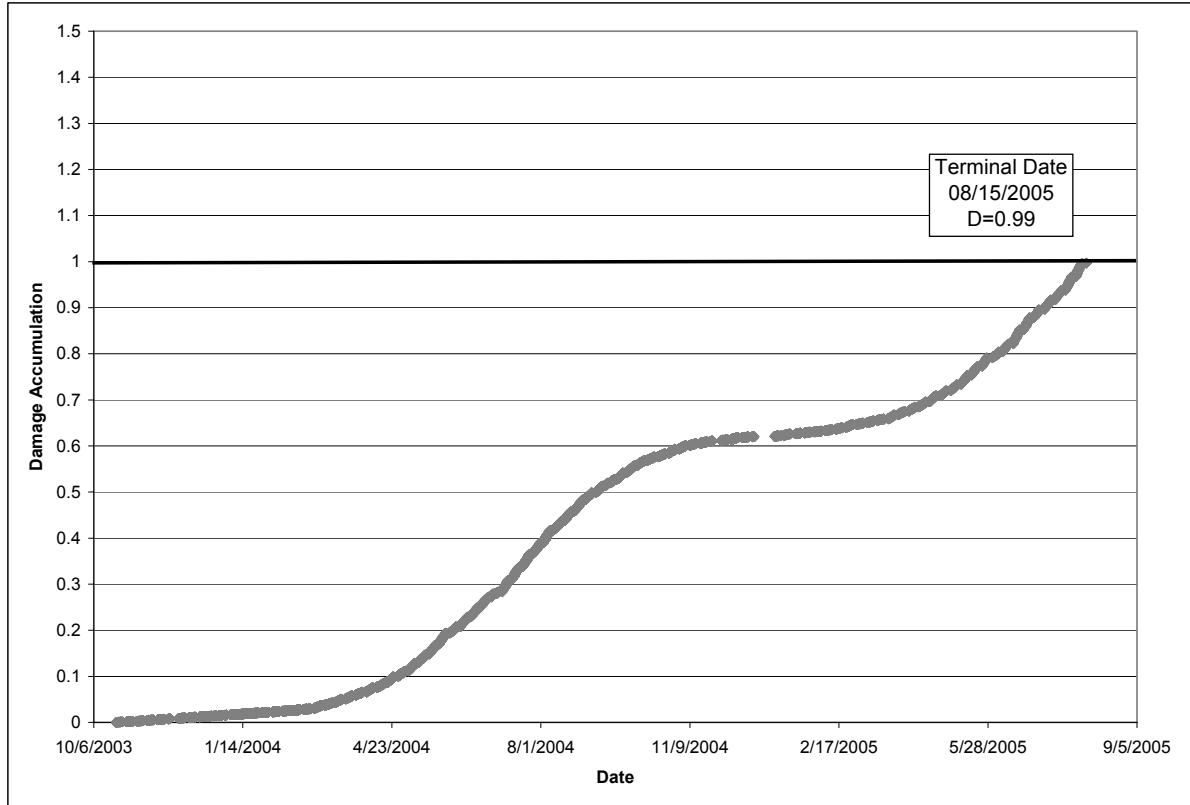


Figure 6.5 Damage Accumulation for Section N8.

The response and performance of section N8 warrants further discussion. Recall from Chapter 5, the stiffness of section N8 is approximately the same as the other sections. However the strain values, from Figure 5.10, were relatively low until they began to increase around November 2005, when cracking was observed. In fact, the strain values measured in section N8 prior to cracking were closer to the values of the 9 in. sections than the other 7 in. sections. Yet, even with the lower strain values, the section performed poorly compared to the other 7 in. sections. The rich bottom concept hypothesizes that the added asphalt will create a more fatigue resistant bottom layer without compromising the overall strength and stability of the structure in regards to rutting. Recall, that a study conducted by Harvey et al. (1995) investigated the rich bottom concept. They not only predicted an increase in stiffness of the rich layer, which may be reason for the lower strain values found here, they also reported an increase in fatigue life by a factor of 2.18. From this experiment, the rich bottom concept did not hold true considering the performance of N8 versus the control section, N7, which had only small signs of cracking at the time of this report. As discussed above, slippage was found in N8 which contributed to its poor performance (Willis and Timm, 2006). Therefore, it was not necessarily the rich-bottom that caused the premature distress, but rather a construction issue. This should be monitored closely in the future.

Thick Model

In order to calibrate a fatigue model using the data from sections N3-N7, a current damage ratio was assumed. In the calibration of the thin and rich bottom models, the damage was set equal to 1 at the time of failure. In calibration of the thick model, hourly temperature and traffic data until August 2, 2005 were used, and a current damage ratio was assigned to each test section. Section N6 had the highest amounts of cracking and was the only section with areas of interconnected cracks; therefore, it was assigned a damage of 0.7. Section N5 had a small amount of cracking in both wheelpaths, and there were some transverse cracks in section N7; consequently, section N5 and N7 were assigned damage ratio values of 0.4 and 0.5, respectively. The two 9 in. sections (N3 and N4) had no observed cracking prior to August 2, 2005 and were assigned a value of 0.2. Using the data from the five sections and the damage assumptions, the general model developed is given below:

$$N_f = 0.4831 * \left(\frac{1}{\varepsilon_t} \right)^{3.063} * \left(\frac{1}{E} \right)^{0.5992} \quad (6.8)$$

The damage accumulation for section N6 is shown in Figure 6.6 to serve as an example. It, along with the other thick sections, followed the same pattern of section N8 (Figure 6.3). As further comparison, the average daily air temperatures are shown in Figure 6.7. From the two figures, the damage accumulation matches well with the temperature data; the warmer days causing more fatigue damage.

The increase in damage and cracking during the warmer months may contradict some conventional understanding of cracking damage in flexible pavements. For example, temperature-induced surface cracking is a major distress in many areas of the U.S., which occurs during the winter months due to daily temperature fluctuations. This is not the same mechanism that occurs in bottom-up fatigue cracking. Consider Equation 6.8; the driving parameter is the tensile strain at the bottom of the HMA layer, which increases in warmer months due to the decrease in stiffness. The stiffness term included in the equation may counter-balance this change to some degree, but considering the power coefficients, not to the same magnitude. In fact, it should be clarified that the stiffness term was originally included in fatigue models to distinguish between different mixes rather than characterize seasonal variation of one mix. Additionally, in Alabama, there are no spring thaw issues that colder climates must consider. During spring thaw, the underlying layers can become saturated and weakened due to partial thaw conditions. This condition leads to a loss of support which, in turn, causes high tensile strains at the bottom of the HMA layer. In colder climates, the effect of spring thaw would have to be considered in the strain data and fatigue models. For example, temperature alone would not be an accurate predictor of strain during spring thaw conditions.

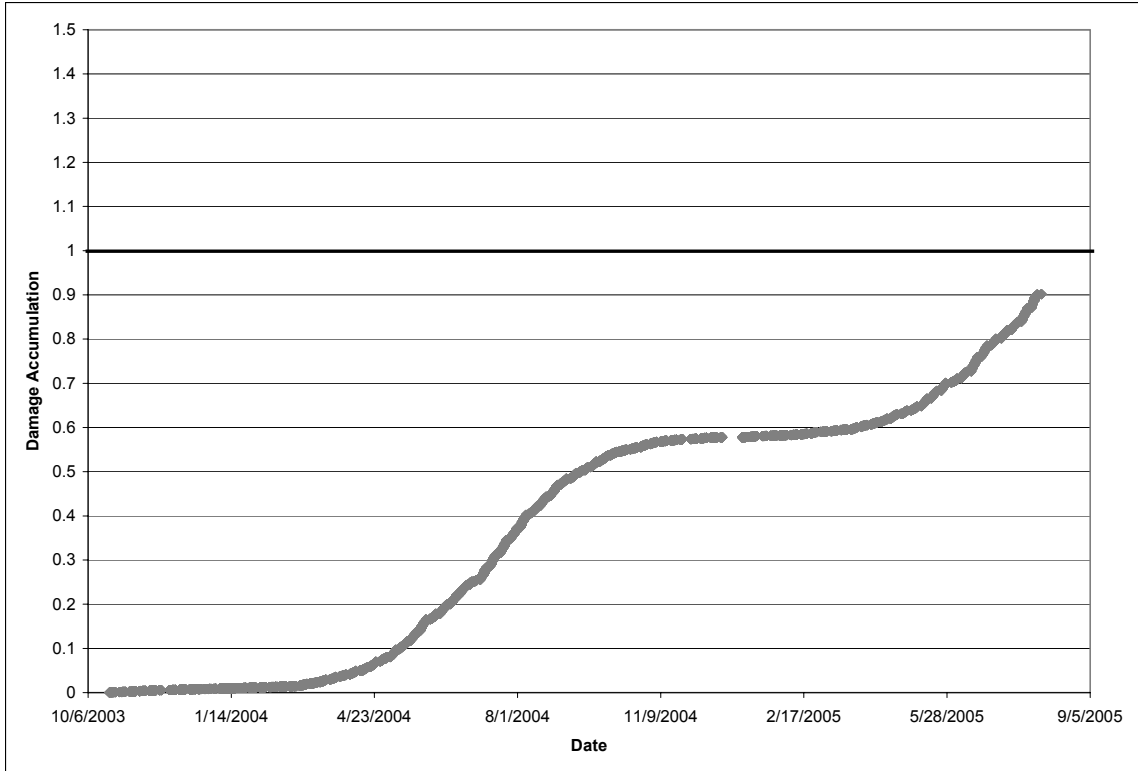


Figure 6.6 Damage Accumulation for Section N6.

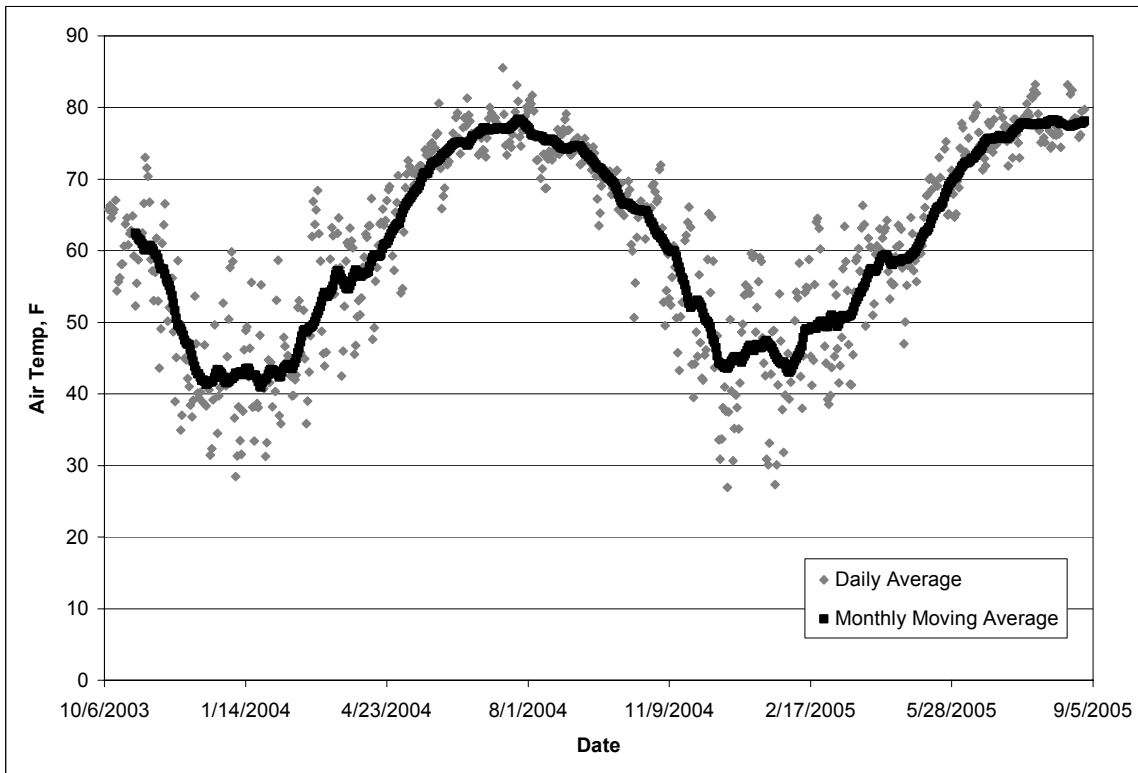


Figure 6.7 Mean Air Temperature.

As mentioned prior, the thick fatigue transfer function (Equation 6.8) is based on assumptions regarding the current state of distress of the test sections. Further improvements should be made as the test sections are further trafficked and show further distress and subsequent failure. The plans for the 2006 Test Track testing cycle include leaving these sections in-place for further traffic and observation. Although the function may be updated, it is predicted that one function can be developed to describe the performance of all five test sections, including both thicknesses (7 and 9 in.).

CONCLUDING REMARKS ON MODEL DEVELOPMENT

The fatigue transfer functions presented here were developed to aid ALDOT and other states in adopting M-E design procedures. The models are applicable to public highway analysis and design for similar conditions of the NCAT Test Track. The test sections were designed using ALDOT materials and specifications; therefore, they are directly applicable to the State of Alabama and other states with similar mixture designs and climatic conditions. Further, two separate models were presented for thick and thin HMA pavements, avoiding any necessary shift factors. The rich bottom model was developed using only one test section, so further investigation is warranted, especially considering the section did not perform as expected.

CHAPTER 7 – CONCLUSIONS AND RECOMMENDATIONS

An accurate fatigue transfer function is the critical link in M-E flexible pavement design. The model relates the conditions of the pavement structure to the expected performance or life of the pavement. The conclusions of this research, including the developed methodology and transfer functions, are presented below. Following the conclusions, a few recommendations on testing procedure and data collection for future testing cycles are presented. Further, this component of M-E design is probably the most deficient; thus, it warrants further attention and improvements. The recommendations based on this study for additional improvements and research are also given.

CONCLUSIONS

Regarding the dynamic instrumentation and test facility, the following conclusions can be stated:

1. The strain gauge array was sufficient for the experiment. It successfully captured the wheel wander and maximum strain response along with providing adequate redundancy to account for gauge loss.
2. The strain quantification used in this research is unique to what others have done in the past, and it is well suited for the conditions at the Test Track. The developed strain amplitude algorithm accurately describes an entire vehicle strain trace and captures the dynamic effects of truck loading.
3. Dynamic response data are highly variable and must be investigated thoroughly. The dynamic data processing procedure developed at NCAT is both interactive and efficient. Further, it can be adapted to further testing cycles and/or other facilities.

Below are the conclusions regarding the methodology and parameter characterization presented in this report:

1. It is not necessary to collect and process continuous dynamic response data. The task would be overwhelming, especially for a project of this size. Stiffness – temperature and strain – temperature relationships should be established and used to predict the response for the pavement for the given condition. Further, dynamic response data should be collected at regular intervals through the test cycle to monitor the test sections.
2. The five triple-trailer trucks should be considered duplicates of one test vehicle in regards to the strain characterization. Further, the wheel wander at the NCAT Test Track is representative of open-access facilities.
3. The maximum registered strain response within the gauge array is considered the best hit of a tire over the gauge. Further, three passes of each testing vehicle should be collected to gather the full range of variability.

The conclusions regarding the performance of the test sections and the developed fatigue models are given below:

1. Both 5 in. sections, N1 and N2, exceeded their design life of 1.1 million ESAL. The first signs of fatigue cracking was observed at 1.6 and 2.5 million ESAL for section N1 and N2, respectively. Based on the very limited data of these two sections, the

unmodified PG 67-22 test section N1 performed slightly better than its modified counterpart, N2. Although, it can be argued that the two sections were basically the same in terms of fatigue performance.

2. All of the 7 in. test sections outlived their design life of 2.9 million ESAL. Of the four 7 in. test sections, only N8 had progressive fatigue cracking and reached the failure criteria by the date of this report. The first signs of cracking in N8 were noticed after approximately 3.4 million ESAL of traffic. Based on the limited test sections, the rich bottom layer did not produce a more fatigue-resistant structure. However, this may be attributed to slippage rather than a defect within the rich-bottom itself.
3. No fatigue cracking was observed in the two 9 in. test sections at the time of this report.
4. The fatigue transfer function developed for thin asphalt pavement sections (less than 5 in.) based on the data of sections N1 and N2 was found to be:

$$N_f = 0.4875 * \left(\frac{1}{\epsilon_t} \right)^{3.031} * \left(\frac{1}{E} \right)^{0.6529}$$

5. The preliminary fatigue transfer function developed for thicker asphalt pavement sections based on the data from sections N3-N7 was found to be:

$$N_f = 0.4831 * \left(\frac{1}{\epsilon_t} \right)^{3.063} * \left(\frac{1}{E} \right)^{0.5992}$$

6. Lastly, the fatigue transfer function developed from the rich bottom section, N8, is presented below:

$$N_f = 0.4814 * \left(\frac{1}{\epsilon_t} \right)^{3.007} * \left(\frac{1}{E} \right)^{0.6911}$$

Recall that this function was developed from data from only one test section.

RECOMMENDATIONS

Based on this research the following recommendations can be made regarding full-scale testing, instrumentation and methodology. Further research opportunities are also explored.

1. The test sections should be designed to ensure failure during the testing cycle. In addition, if the test sections reach their terminal life, they should be repaired and maintained. This may involve an overlay or other rehabilitation techniques. In that way, the maintenance technique can be observed and mechanistically evaluated.
2. A more extensive data collection effort should be performed at the beginning of the testing cycle prior to any pavement damage. This includes dynamic data collection as well as FWD testing at a variety of testing temperatures. In this way, accurate prediction models can be developed on the intact pavement structure.
3. It is recommended that the intact test sections (N3-N7) be left in place for the next round of testing at the NCAT Test Track for further observation. As the sections deteriorate, a more accurate thick fatigue model can be developed. Additionally, the model presented here can be used to predict the life of the remaining test sections.

The model may also need revised calibration coefficients to more accurately represent the actual performance of these test sections.

4. Further investigation is warranted into the rich bottom layer concept, both in the laboratory and the field. Further, the rich bottom transfer function developed here may need further verification because it was based on data from only one test section.
5. The effect of binder type and binder modification on fatigue performance should be further investigated because the data were limited to one comparison set (N1 and N2). As recommended above, the other sections should be further trafficked in order to draw more substantial conclusions.
6. Additional cross sections should be tested in later research cycles including different base and subgrade materials.

REFERENCES

1. *AASHTO Guide for Design of Pavement Structures*. Washington D.C.: American Association of State and Highway Transportation Officials, 1993.
2. About Minnesota Road Research. Minnesota Department of Transportation (MnDOT). 3 October 2005 <
http://www.mrr.dot.state.mn.us/research/MnROAD_Project/mnroadproject.asp>.
3. Ali, Hesham A. and Shiraz D. Tayabji. "Evaluation of Mechanistic-Empirical Performance Prediction Models for Flexible Pavements." *Transportation Research Record No. 1629*, Washington, D.C.: Transportation Research Board, 1998, pp.169-80.
4. Al-Qadi, I. L., A. Loulizi, M. Elseifi and S. Lahouar. "The Virginia Smart Road : The Impact of Pavement Instrumentation on Understanding Pavement Performance." *The Journal of Association of Asphalt Paving Technologists* Vol. 83, 2004, pp. 427-66.
5. Alvarez, C. and M.R. Thompson. "Mechanistic-Empirical Evaluation of the Mn/Road Mainline Flexible Pavement Sections," Project IHR-535, Illinois Cooperative Highway and Transportation Research Program, University of Illinois, Urbana, IL, 1998.
6. Beer, Michael G., Greg Johnson and Dave Van Deusen. "Performance of Mn/Road Load Response and Subsurface Instrumentation," Staff Paper, Office of Minnesota Road Research, Maplewood, MN: Minnesota Department of Transportation, 1996.
7. Cooper, K.E. and P.S. Pell. "The Effect of Mix Variables on the Fatigue Strength of Bituminous Materials," LR 663, UK: Transport and Road Research Laboratory, 1974.
8. El-Basyouny, Mohammed and Matthew Witzak, "Development of the Fatigue Cracking Models for the 2002 Design Guide," *Transportation Research Record* 1919, Transportation Research Board, 2005, pp. 77-86.
9. --- "Calibration of the Alligator Fatigue Cracking Model for the 2002 Design Guide." *Transportation Research Board 84th Annual Meeting Compendium of Papers*. CD-ROM. Washington, D.C., 2005.
10. Epps, J.A., A. Hand, S. Seeds, T. Schulz, S. Alavi, C. Ashmore, C.L. Monismith, J.A. Deacon, J.T. Harvey and R. Leahy, "Recommended Performance-Related Specification for Hot-Mix Asphalt Construction: Results of the Westrack Project," NCHRP Report 455, Washington D.C.: Transportation Research Board, National Research Council, 2002.
11. Eres Consultants Division. "Guide For Mechanistic-Empirical Pavement Design of New and Rehabilitated Pavement Structures," Final Report, NCHRP 1-37A, 2004.
12. Finn, F., C. Saraf, R. Kulkarni, K. Nair, W. Smith and A. Abdullah. "The Use of Distress Prediction Subsystems for the Design of Pavement Structures." *Proceedings, Fourth International Conference Structural Design of Asphalt Pavements*, Vol. 1, University of Michigan, 1997.
13. Hajj, E. Y., P. E. Sebaalay, and D. Weitzel. "Fatigue Characteristics of Superpave and Hveem Mixtures." *Journal of Transportation Engineering*, ASCE , 2005, pp. 302-10.

14. Hallin, John. "Implementation of the 2002 Design Guide." 11 Jan 2004. Report, ERES Consultants. 13 Oct 2005 < http://www.webs1.uidaho.edu/bayomy/trb/afd60/TRB2004/Design%20Guide%20workshop/Hallin_Research%20Team%20Implementation%20Ideas.pdf>.
15. Harvey, John T., John A. Deacon, Bor-Wen Tsai and Carl L. Monismith. "Fatigue Performance of Asphalt Concrete Mixes and Its Relationship to Asphalt Concrete Performance in California," Report No. RTA-65W485-2, Berkeley: California Department of Transportation, 1995.
16. Huang, Yang H. *Pavement Analysis and Design* New Jersey: Prentice Hall, 1993.
17. Ioannides, Anastasios M. "Mechanistic Performance Modeling: A Contradiction of Terms." Proceedings, 7th International Conference on Asphalt Pavements, Vol. 2, Nottingham, England, 1992, pp. 165-79.
18. Jameson, G.W., K.G. Sharp and N.J. Vertessy. "Full-depth Asphalt Pavement Fatigue Under Accelerated Loading." Proceedings, 7th International Conference on Asphalt Pavements, Vol. 2, Nottingham, England, 1992, pp. 180-200.
19. Mateos, Angel and Mark B. Snyder. "Validation of Flexible Pavement Structural Response Models with Data from the Minnesota Road Research Project." *Transportation Research Record No. 1806*, Washington D.C.: Transportation Research Board, 2002, pp. 19-29.
20. Miller, John S. and William Y. Bellinger. *Distress Identification Manual for the Long-Term Pavement Performance Project*. FHWA-RD-03-031, Washington D.C.: FHWA, 2003.
21. Miner, Milton A. "Estimation of Fatigue Life with Particular Emphasis on Cumulative Damage." *Metal Fatigue*, edited by Sines and Waisman, McGraw Hill, 1959, pp. 278-89.
22. Monismith Carl L. "Analytically Based Asphalt Pavement Design and Rehabilitation: Theory to Practice, 1962-1992." *Transportation Research Record No. 1354*, Washington, D.C.: Transportation Research Board, 1992, pp. 5-26.
23. Monismith, C.L. and J.A. Epps. "Asphalt Mixture Behavior in Repeated Flexure," Transportation and Traffic Engineering, Berkeley, CA: University of California, 1969.
24. Monismith, C.L., J.A. Epps and F.N. Finn. "Improved Asphalt Mix Design," Proceedings, Association of Asphalt Paving Technologists Technical Sessions, San Antonio, Texas, 1985, pp. 347-406.
25. Myre, J. "Fatigue of Asphalt Pavements," Proceedings, Third International Conference on Bearing Capacity of Roads and Airfields, Norwegian Institute of Technology, 1990.
26. Pell, P. S. and K. E. Cooper. "The Effect of Testing and Mix Variables on the Fatigue Performance of Bituminous Materials." Proceedings, Association of Asphalt Paving Technologists Vol. 44, 1975, pp. 1-37.
27. Rauhut, J.B., R.L. Lytton and M.I. Darter. "Pavement Damage Functions for Cost Allocation – Vol. 2 – Descriptions of Detailed Studies," FHWA-RD-84-019, Washington D.C.: FHWA, 1984.

28. *Research and Development of The Asphalt Institute's Thickness Design Manual (MS-1) Ninth Edition*, Research Report No. 82-2, College Park, MD: The Asphalt Institute, 1982.
29. Romero, Pedro, Kevin D. Stuart and Walaa Mogawer. "Fatigue Response of Asphalt Mixtures Tested by the Federal Highway Administration's Accelerated Loading Facility." *Journal of the Asphalt Paving Technologists* Vol. 69, 2000, pp. 212-35.
30. Shook, J.F., F.N. Finn, M.W. Witczak, and C.L. Monismith. "Thickness Design of Asphalt Pavements – The Asphalt Institute Method," Proceedings, 5th International Conference on the Structural Design of Asphalt Pavements, Vol.1, The Netherlands, 1982, pp. 17-44.
31. Tangella, R., J. Craus, J. A. Deacon, and C. L. Monismith. *Summary Report on Fatigue Response of Asphalt Mixtures*. TM-UCB-A-003A-89-3, SHRP Project A-003-A. University of California, Berkeley: Institute of Transportation Studies, 1990.
32. *Thickness Design, Asphalt Pavements for Highways and Streets*. Report MS-1, The Asphalt Institute, 1982.
33. Timm, D.H., Bjorn Birgisson and David E. Newcomb. "Development of Mechanistic-Empirical Design for Minnesota." *Transportation Research Record No. 1629*, Washington, D.C.: Transportation Research Board, 1998, pp. 181-88.
34. Timm, D.H., D.E. Newcomb and B. Birgisson. "Mechanistic-Empirical Flexible Pavement Thickness Design: The Minnesota Method," Staff Paper, MN/RC-P99-10, St. Paul: Minnesota Department of Transportation, 1999.
35. Timm, D.H. and A.L. Priest, "Material Properties of the 2003 NCAT Test Track Structural Study," Report No. 06-01, National Center for Asphalt Technology, Auburn University, 2006.
36. Timm, D.H. and A.L. Priest. "Wheel Wander at the NCAT Test Track," Report No. 05-02, Auburn University: National Center for Asphalt Technology, 2005.
37. Timm, D.H., A.L. Priest and T.V. McEwen. "Design and Instrumentation of the Structural Pavement Experiment at the NCAT Test Track," Report No. 04-01, Auburn University: National Center for Asphalt Technology, 2004.
38. Verstraeten, J., V. Veverka and L. Francken. "Rational and Practical Designs of Asphalt Pavements to Avoid Cracking and Rutting," Proceedings, Fifth International Conference on the Structural Design of Asphalt Pavements, Vol.1, The Netherlands, 1982, pp. 45-58.
39. Virginia's Smart Road Project. Virginia Department of Transportation (VDOT). 3 October 2005 <<http://virginiadot.org/projects/constsal-smartdrdooverview.asp>>.
40. Wolf, P.R. and R.C. Brinker, *Elementary Surveying*, Ninth Edition, HarperCollins College Publishers, New York, 1994.